Faculty of Science and Engineering

Department of Electrical and Computer Engineering

A New Converter Station Topology to Improve the Overall Performance of a Doubly Fed Induction Generator-Based Wind Energy Conversion System

Mahmoud Yousef Khamaira

This thesis is presented for the degree of

Doctor of Philosophy

of

Curtin University

September 2015

DECLARATION

"To the best of my knowledge and belief, this thesis contains no material previously published by any other person except where due acknowledgement has been made. This thesis contains no material which has been accepted for the award of any other degree or diploma in any university"

Signature: ……………………….

Date: ..……………………..

DEDICATION

"To my mother and father for their endless love and support throughout my life, and to my wife who supported me during my study in Australia"

ABSTRACT

Due to the degradation and cost increase of conventional fossil fuels, along with the global trend to decrease the greenhouse effect, clean energy production from renewable sources has been given much focus over the last few decades. Among renewable energy sources, wind energy conversion systems have received the most attention due to their many advantages. More than 35 GW of new wind power capacity was brought globally online in 2013, and by the year 2020, wind power is estimated to produce approximately 10% of global electricity.

During the early stages of wind turbine implementation, disconnection of wind turbines during various grid faults was permitted, in order to protect the turbine from being damaged. However, due to the significant portion of load that wind farms now contribute, Transmission Line Operators currently require the wind turbine to remain connected during grid disturbance events. This has led to the establishment of strict grid codes, which wind turbine generators must meet, to maintain connection to the grid during fault conditions.

To achieve these requirements, researchers have given concern to modulate reactive power during fault events by connecting a flexible ac transmission system device such as STATCOM to the point of common coupling of the wind turbine generator and the grid. To modulate active and reactive powers during fault conditions, devices such as superconducting magnetic energy storage unit or unified power flow controller have to be connected to the point of common coupling. These devices, however, are very costly, and electric utilities are reluctant to adopt them.

This thesis presents a reliable and cost effective technique that calls for reconfiguration of the existing converters of a typical Doubly Fed Induction Generator to include a coil of low internal resistance. A coil within the DC link is the only hardware component required to implement this technique. With a proper control scheme, activated during fault conditions, this coil can provide the same degree of performance as a superconducting magnetic energy storage unit during fault conditions. It will smoothly, rapidly and independently modulate both active and reactive power at the point of common coupling in four-quadrant operational mode, and enable the wind turbine generator to meet all grid codes whilst maintaining its connection to the grid during various fault conditions.

ACKNOWLEDGMENTS

I praise and glorify the name of Allah the Almighty who has always protected, sustained and helped me, and my family, and also created pleasant opportunities for me to capitalise on.

I would like to express my deepest gratitude to my supervisor Dr. Ahmed Abu-Siada for this invaluable support and excellent supervision during my PhD study at Curtin University. Also, many thanks for my core supervisor Professor Syed Islam.

I would also like to sincerely thank all the staff of the Electrical and Computer Engineering department for their support.

I would like to acknowledge the support of all my PhD's colleagues. Thank you for the fruitful discussions and friendships, which made my academic life easy and enjoyable.

Many thanks to my Libyan friends, who made my stay in Perth stress-free while I was far away from my family.

Last but not the least; I would like to thank my respected and beloved mother and father for their unconditional love and prayers for me. Heart felt grateful to my beloved wife for her encouragement, invaluable support, and her patience while looking after our daughter alone in my absence.

Perth, Western Australia, September 2015
Mahmoud Yousef Khamaira

LIST OF PUBLICATIONS

Most of the research results presented in this thesis have been published (or are accepted) in the journals and conference papers listed below.

International Journals

[1]   **M. Y. Khamaira**, A. Abu-Siada, S. Islam, and M. A. S. Masoum, "Improved Topology of Doubly Fed Induction Generator based Wind Energy Conversion System," AJEEE, Australian Journal of Electrical & Electronics Engineering, 2014.

[2]   **M. Y. Khamaira,** A. Abu-Siada, S. Islam, and M. A. S. Masoum, "A new topology for doubly fed induction generator to improve the overall performance of wind energy conversion system," *Elixir, Electrical Engineering Online Journal, ,* vol. 73, pp. 26432-26435, 2014.

[3]   **M. Y. Khamaira** and A. Abu-Siada, "DFIG PERFORMANCE IMPROVEMENT DURING FIRE-THROUGH FAULT WITHIN ROTOR SIDE CONVERTER SWITCES " *International Journal of Advances in Engineering and Technology,* p. 8, 2015.

[4]   **M. Y. Khamaira** and A. Abu-Siada, "Application of HTSC to Improve the Dynamic Performance of DFIG-based WECS during Fire-Through fault " *Elixir International Journal,* p. 6, 2015.

International Conferences

[1]   **M. Y. Khamaira,** A. M. Shiddiq Yunus, and A. Abu-Siada, "Improvement of DFIG-based WECS performance using SMES unit," in *Power Engineering Conference (AUPEC), 2013 Australasian Universities*, Hobart, TAS, Australia, 2013, pp. 1-5.

[2]   **M. Y. Khamaira,** A. Abu-Siada, S. Islam, and M. A. S. Masoum, "Application of SMES unit to improve the overall performance of DFIG-based WECS," in *PES General Meeting | Conference & Exposition, 2014 IEEE*, Washington, 2014, pp. 1-5.

[3]   **M. Y. Khamaira,** A. Abu-Siada, S. Islam, and M. A. S. Masoum, "A new control approach to improve the overall performance of DFIG-based WECS," in *Power Engineering Conference (AUPEC), 2014 Australasian Universities*, Perth, Australia, 2014, pp. 1-5.

[4]   **M. Y. Khamaira**, A. Abu-Siada, and S. Islam, "DFIG-based WECS fault ride through complying with Australian grid codes," in *Power Engineering Conference (AUPEC), 2014 Australasian Universities*, Perth, Australia, 2014, pp. 1-5.

[5]   **M. Y. Khamaira,** A. Abu-Siada, and S. Islam, "Application of High Temperature Superconductor to Improve the Dynamic Performance of WECS," presented at the Power and Energy Society General Meeting, Denver, Colorado, 2015.

[6]   **M. Y. Khamaira** and A. Abu-Siada, "Improvement of DFIG Dynamic Performance during Intermittent Fire-Through Fault," presented at the The 24th IEEE International Symposium on Industrial Electronics, Brazil, 2015.

[7]   **M. Y. Khamaira,** A. Abu-Siada, and Yasser M. Alharbi "A New Converter Topology for Wind Energy Conversion System," accepted at the IEEE PES Asia-Pacific Power and Energy Engineering Conference Brisbane, Australia, 2015.

LIST OF CONTENTS

LIST OF FIGURES

LIST OF TABLES

LIST OF ABBREVIATIONS

GWEC   Global wind energy council

WECS   Wind Energy Conversion Systems

SCIG   Squirrel-cage induction generator

DFIG   Doubly fed induction generator

PCC   Point of common coupling

FRT   Fault ride through

FACTS   Flexible AC transmission system

STATCOM   Static Synchronous Compensator

SSSC   Static Synchronous Series Compensator

TCSC   Thyristor Controlled Series Compensator

UPFC   Unified Power Flow Controller

SMES   Superconducting magnetic energy storage

SVC   Static Var Compensator

EWEA   European wind energy association

VAWTs   Vertical axis wind turbines

HAWTs   Horizontal axis wind turbines

MPPT   Maximum power point tracking

PMSGs   Permanent-magnet synchronous generators

WRSGs   Wound-rotor synchronous generators

WRIGs   Wound-rotor induction generators

VSC   Voltage source converter

RSC   Rotor side converter

GSC   Grid side converter

SG   Synchronous generator

RSI   Rotor side inverter

GSI   Grid side inverter

IGBT   Insulated-gate bipolar transistor

CSC   Current source converter

PM   Permanent-magnet

HVDC   High voltage direct current

THD   Harmonic distortion

TLOs   Transmission Line Operators

VRT	Voltage Ride through
LVRT	Low Voltage Ride Through
HVRT	High Voltage Ride Through
NEM	National Electricity Market
IGBT	Insulated Gate Bipolar Transistor
PWM	Pulse-width modulation
AI	Artificial Intelligent
FL	Fuzzy Logic
FLC	Fuzzy Logic Controller
D	Duty Cycle
MF	Membership Function
2L-G	Double Line to Ground Intermittent Fault
rms	root mean square
3Φ-G	Three Phase to Ground
PI	Proportional Integral

LIST OF SYMBOLS

Subscripts

"s", "r' refer to stator and rotor

"a", "b", "c" refer to grid phases

α, β Two-axis static reference frame

d-q   Two-axis direct and quadrature rotating reference frame

Superscripts

"s", "r' space vector

Parameters

P_m	Mechanical power
ρ	Air density (kg/m3)
v_w	Wind speed (m/s)
A	Turbine swept area (m2)
C_p	Coefficient of wind turbine performance
v	Voltage
i	Current
Φ	Flux
L	Inductance
L_m	Magnetizing inductance
L_σ	Leakage inductance
E	Induced electromagnetic force
R	Resistance
X_σ	Leakage impedance
f	Frequency
R_r	Rotor radius
λ	Tip speed ratio
w_r	Rotor speed
T_m	Wind turbine mechanical torque
β	Pitch angle

H_t	Inertia constants of the turbine
w_t	Turbine speed
T_m	Mechanical torque applied to the turbine
D_t	Damping coefficients of the turbine
D_{tg}	Damping coefficient of the flexible coupling masses
w_r	Rotor speed
T_{tg}	Internal torque of the model
H_g	Inertia constants of generator
D_g	Damping coefficients of the generator
K_{tg}	Shaft stiffness
w_m	Rotational speed of the lumped-mass system
D_m	Damping of the lumped system
T_e	Electrical torque of the generator
P	Active power
Q	Reactive power
r	Transformer resistance
i_{r_dc}	The DC current
i_{G_dc}	DC current that crosses from the DC link capacitor to the grid
i_R	The resistance current
β_d	Desired pitch angles

Chapter One

Introduction

1.1   Thesis Background

Electrical power is the backbone for the continual growth of human civilisation. Since the beginning of the industrial rebellion, around two centuries ago, the world's electrical power usage has grown extensively to advance quality of life, mainly in developed countries. At present, conventional fossil fuels or non-renewable resources (comprising of natural gas, nuclear, oil and coal) represent the core resources used to generate electricity worldwide. Statistics show energy generated by these non-renewable supplies (mainly oil and natural gas) represent nearly three quarters of the demand for energy across the world [1].

Since the binge of the industrial revolution, the burning of fossil fuel has continued to increase rapidly causing gas emissions to also rise. In the 1990s, gas emission increased by around 0.7% per year, and during the period 1999 to 2005, annual gas emission rose from 6.5 to 7.8 GT of carbon. This increase creates harmful greenhouse gases in the Earth's atmosphere and directly influences the average temperature of the Earth's surface. Since the late eighteenth century, the world's normal temperature has risen between 0.7 to 1.4 degrees Fahrenheit [2]. If the portion of greenhouse gases in the atmosphere continues to rise, the Earth's average temperature is expected to increase by 2.5 to 10.4 degrees Fahrenheit by 2100, bringing with it the threat of climate change.

Furthermore, fossil fuel supplies are limited. It is, therefore, essential to invest in the development of alternative clean and renewable energy resources [3]. China, which possesses the world's largest electric power system, and is the main emitter of carbon dioxide and other types of greenhouse gases, aims to meet 10% of their domestic energy demand with renewable energy resources by 2020 [4].

The availability of natural resources means more, energy can be produced closer to load centres, reducing the cost of transmitting electrical power over long distances [5]. Out of all available renewable energy resources, solar and wind energy are the

most widely used worldwide and are expected to play a vital role in the 21st century [4]. The use of solar energy is still limited to small to medium-scale energy applications, such as for small industry and residential areas, although some solar farms are equipped by 50 MW solar systems [5].

Wind power technologies have become one of the fastest developing alternative energy supply worldwide, and several nations encourage wind power technology through domestic incentive programs [5, 6]. According to Global Wind Energy Council (GWEC) statistics, more than 35 GW of new wind power turbines were installed in 2013. This represents a cumulative market increase of more than 12.5% [1]. According to GWEC, global power generation by wind turbine is expected to reach 493 GW by the year 2016 [7].

The use of wind power for generating electricity began at the end of 19th century with the implementation of a 12 kW DC windmill generator [8]. However, it is only since the recent revolution in power electronics and electrical machinery technologies, that a wind energy conversion system (WECS) has become viable. WECSs can now be run at a much lower cost; they are more efficient and reliable, and capacities have increased from a few kilowatts to several megawatts [6].

WECSs can be categorised into two main groups: (1) fixed-speed WECSs and variable-speed WECSs. A fixed-speed WECS - or (type A) - utilises a squirrel-cage induction generator (SCIG) and has the advantage of simplicity, as well as a low manufacturing cost. A fixed-speed WECS does, however, have some drawbacks, such as high mechanical stress factors and unstable output power. Furthermore, since the rotor speed is constant, a fixed-speed WECS has restricted controllability [6].

Variable-speed WECS require electronic power to interface the induction generator with the grids. In comparison to a fixed-speed WECS, a variable-speed WECS is superior in terms of the amount of energy it can capture, and its provision of stable energy to the grid. A variable-speed WECS also incurs less mechanical gearbox stress than a fixed-speed WECS, and is capable of reducing power fluctuations [9, 10].

There are three different types of variable-speed WECSs:

1. Partly variable-speed WECSs - or (type B) - that use a wound-rotor induction generator, with dynamic rotor resistance, directly connected to the grid.

2. Variable-speed WECSs - or (type C) - that use a doubly fed induction generator (DFIG) and are partly connected to the electric system.

3. Variable-speed WECSs - or (type D) - that use a synchronous or induction generator and are fully connected to the electric system.

Doubly Fed Induction Generators (DFIGs) are currently used for variable-speed WECSs above 1 MW [11]. In 2004, a WECS-based DFIG accounted for 55% of the total number of installed WECSs worldwide [12]. DFIG-based WECSs are gaining popularity due to their superior features, including: (1) active and reactive power control; (2) a low cost, low converter rating; (3) reduced losses; and (4) high efficiency [13].

DFIG-based WECSs are equipped with a (AC-DC-AC) voltage source converter, which can maintain both the voltage level and power frequency at the point of common coupling (PCC). The stator winding of the DFIG is connected to the grid via a coupling transformer, whereas a rotor winding is fed through a back-to-back converter station measured at only 30% of the total rated DFIG power [14].

The main drawback of the DFIG is its sensitivity to grid disturbances, which may cause voltage fluctuation at the PCC. Voltage deviation at the PCC leads to high currents in the stator and rotor windings affecting the performance of the AC-DC-AC converter. If an adequate protection scheme is not adopted, damage can be caused

Crowbar resistors are used in most cases to protect the DFIG power converter during grid fault durations and also to isolate the wind turbine from the grid [15-17]. Transmission Line Operators recently set grid codes to be fulfilled when maintaining the connection of the wind turbine to the grid during intermittent fault conditions [18, 19]. To achieve these codes, researchers proposed the use of several flexible AC transmission system (FACTS) devices, along with different control algorithms, such as the static var compensator [20-22] and the static synchronous compensator [11, 23-28]. This method proposes to alleviate the voltage dip of the DFIG-based WECS so the DFIG can ride through the faults.

Additionally, a dynamic voltage restorer [29-33] is used to improve the fault ride through (FRT) of DFIG-based WECSs due to grid faults. In [12, 13, 34-38], the superconducting magnetic energy storage (SMES) unit is introduced to improve the FRT capability and alleviate power fluctuation of the WECS-based DFIG during grid turbulences. This is achieved through the independent control of both active and reactive power in a four-quadrant operation at the PCC. However, apart from the aforementioned advantages of the SMES unit, which make it unique among all FACTS devices, it is still an expensive solution.

This thesis aims to develop a new control technique for the DFIG converters, which possesses the same advantages of a SMES unit but is more cost effective. The new technique will rely on the reconfiguration of the DFIG converters to include a coil activated only during fault conditions. With a suitable control technique, both active and reactive power at the PCC can be modulated smoothly, rapidly and independently in a four-quadrant operational mode. This will also allow the wind turbine generator to meet all required codes and maintain its connection to the grid during various grid faults. The new technique does not call for additional power converters, as it will use the existing converters of the DFIG. The additional coil will be superconductive or a normal coil of low resistance.

1.2 Thesis Objectives

The key objectives of this thesis are:
- To develop a new topology for DFIG converters in order to enhance the FRT of a DFIG-based WECS during fault conditions.
- To develop a new control algorithm for the DFIG converters in order to modulate active and reactive power at the PCC during intermittent fault conditions. This will eliminate the need for additional FACTS devices.
- To investigate the impact of internal converter faults (such as fire-through and misfire faults) on the overall performance of the WECS with and without the new proposed topology.

1.3 Thesis Contribution

This thesis proposes a new topology for DFIG converters by integrating a coil within the DC link. The coil will be disconnected during normal operating conditions and reconnected as soon as a fault takes place within the system. Through a proper

control algorithm, both active and reactive power at the PCC can be modulated in order to improve the performance of the system and maintain the connection of the wind turbine during fault conditions. At present, there is no such technique. The proposed technique in this thesis will open the gate for further improvements to the DFIG converters topology eliminating the need for external FACTS during fault conditions.

1.4   Thesis Layout

This thesis is organised into six chapters, as below:

- **Chapter One**

    This chapter covers the thesis background and objectives.

- **Chapter Two**

    Chapter two describes wind basic theory, and the history and basic technical concepts of WECS. Also presented are the different types of wind turbine towers, wind farm connection, and the effects of a wind farm on power system operations.

- **Chapter Three**

    In this chapter, typical DFIG topologies and modeling are explained. The control systems, including grid side converters, rotor side converters, pitch angles, and terminal voltage, are also described

- **Chapter Four:**

    The proposed new topology of the DFIG converters is detailed in this chapter. The proposed control algorithm is also presented.

- **Chapter Five:**

    Here, the thesis investigates the assessment of the proposed topology / controllers. Various fault scenarios are introduced to the system under study, and the performance of the WECS is investigated with and without the proposed controller.

- **Chapter Six:**

    This chapter summarises the main conclusions and key findings of the thesis. It also presents recommendations for future research options, which can build on the research idea presented in the thesis.

Chapter Two

Wind Energy Conversion System

2.1   Introduction

Due to growing costs, limited reserves, and the harmful effect of fossil fuels on the environment, global installed wind energy capacity has significantly increased from just 6 GW in 1996 to 318 GW by the end of 2013 (as shown in figure 2.1 [39]). This trend is expected to continue, with projections that 10% of the world's power demand will be generated by wind energy by the year 2030 [39, 40].
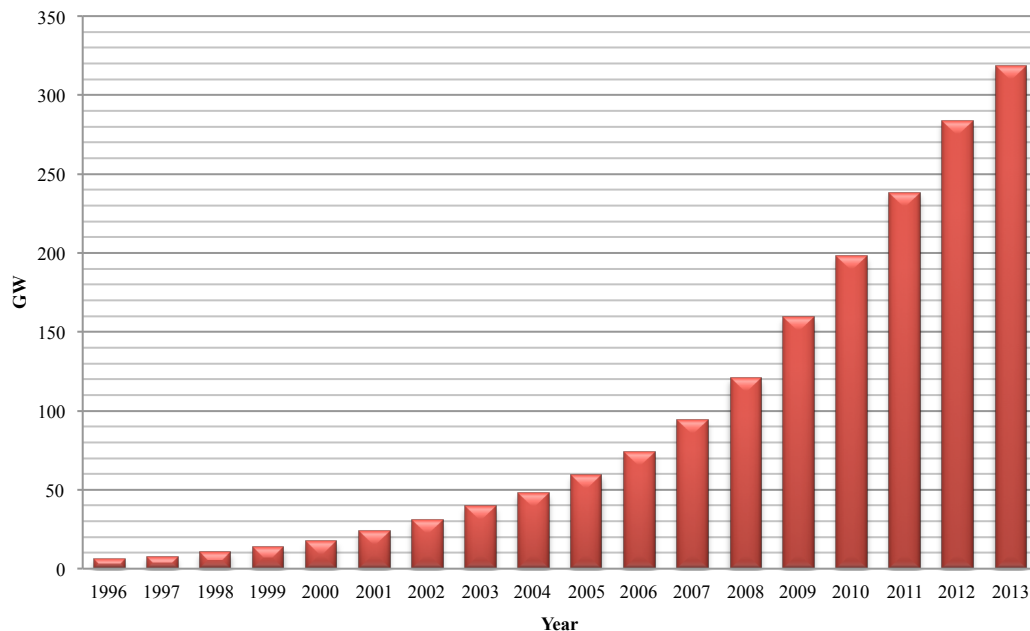
Figure 2.1 Global cumulative installed wind capacity 1996-2013 [40]

Figure 2.2 shows the cumulative installed wind energy capacity of the top ten nations in the world as of 2013 [40]. With a wind energy generation of about 91 GW, China is the largest producer of wind energy, followed by the United States, which produces approximately 61 GW. In the European Union, a total of 121 GW of wind power has been installed, representing approximately 8% of total power demand across the continent [40, 41]. The European Wind Energy Association (EWEA) projects that total wind power generation in Europe will reach 230 GW by the year 2020 and 400 GW by the year 2030 [7].
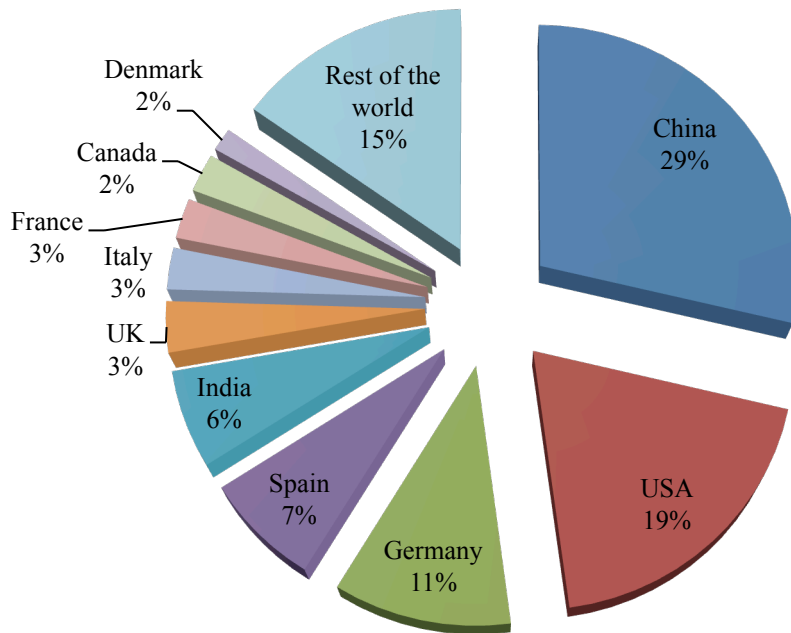
Figure 2.2 Top 10 Cumulative capacity December 2013 [40]

In Australia, following the completion of the largest wind farm in the southern hemisphere in 2013, wind power generation now produces 3,239 MW of the country's electricity. By the year 2020, Australia aims to generate 20% of the total electricity demand from renewable energy resources [40]. The growth of total installed wind capacity in Australia during the period 2001-2013 is shown in figure 2.3, and the installed wind capacity - by state - is shown in figures 2.4 [40].

	2001	2002	2003	2004	2005	2006	2007	2008	2009	2010	2011	2012	2013
MW	73	105	198	380	708	817	824	1306	1712	1990	2226	2584	3239
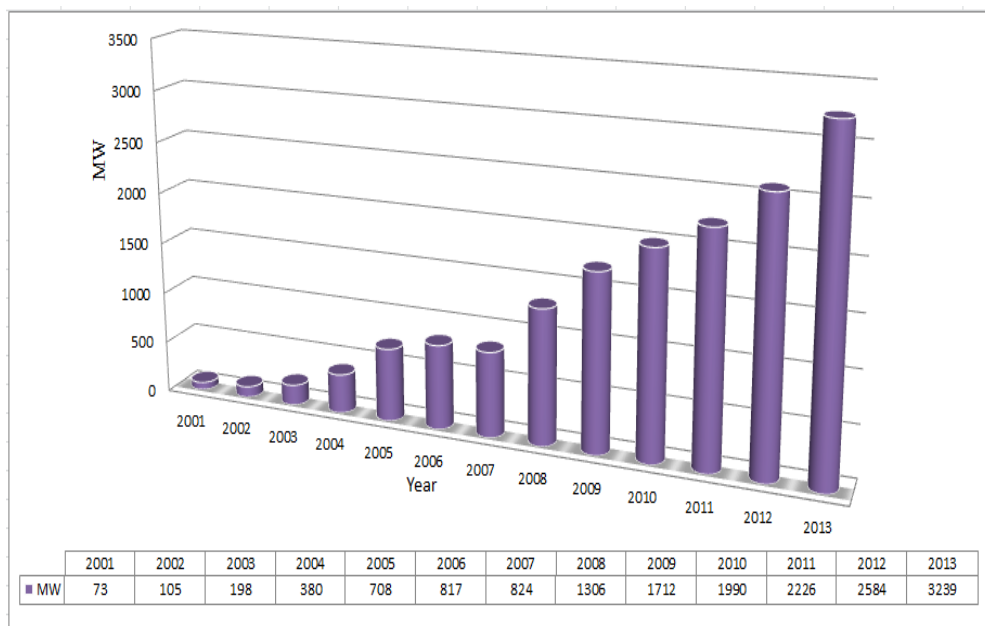
Figure 2.3 The growth of installed wind power generation (peak capacity) in Australia [40]
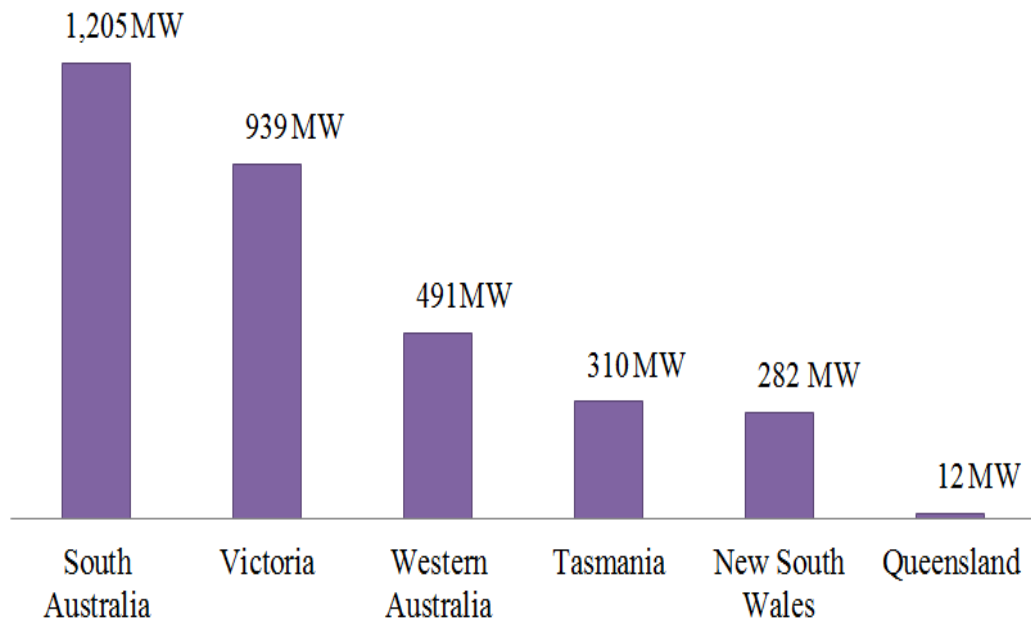
Figure 2.4 The 2013-installed capacity of wind power generation in Australia by state [40]

2.2   Background of Wind Turbine

Depending on the direction of rotation, wind turbines are categorised into two main types: (1) Vertical Axis Wind Turbines (VAWTs) or Horizontal Axis Wind Turbines (HAWTs). Due to the ease of implementation, VAWTs have been more widely used in the past. However, HAWTs with three blades are now more commonly used [6, 42]. The typical arrangement of an offshore HAWT is shown in figure 2.5. The rotor bearing, gearbox and generator, along with other supplementary equipment, are located within a nacelle on the top of the wind turbine tower. The coupling transformer, which connects the turbine generator with the grid, is usually located at the bottom of the wind tower or in an isolated building close to the tower [41, 42]. Wind turbine generators are usually rated at a low voltage of 690 V, and the coupling transformer is used to step-up the generated voltage to the level of the transmission grid [41]. Large blades are necessary to deliver mechanical power at a low speed and high torque, while the gearbox is used to transform the lower speed to the rated speed of the generator [42].
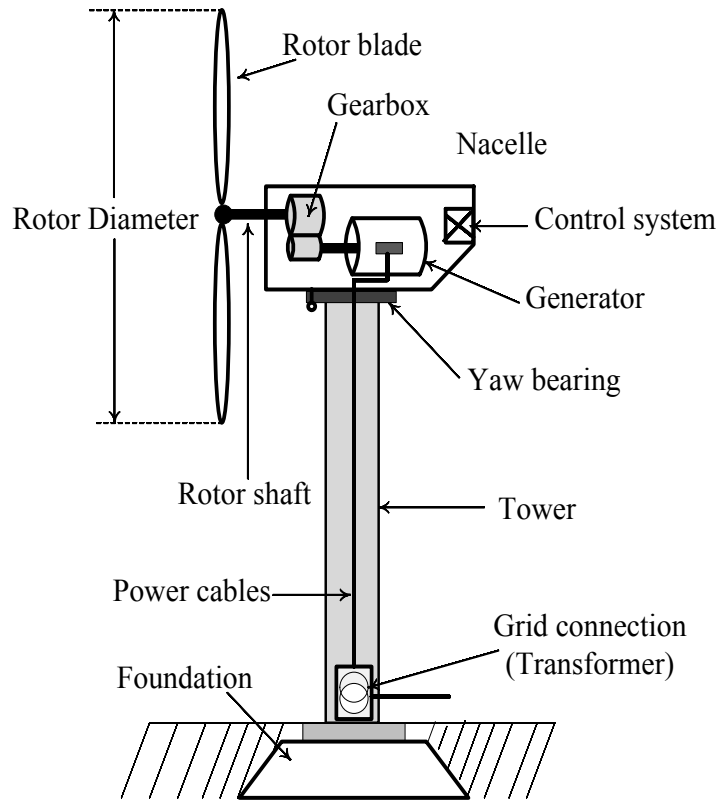
Figure 2.5. Typical configuration of an offshore horizontal-axis wind turbine [42]
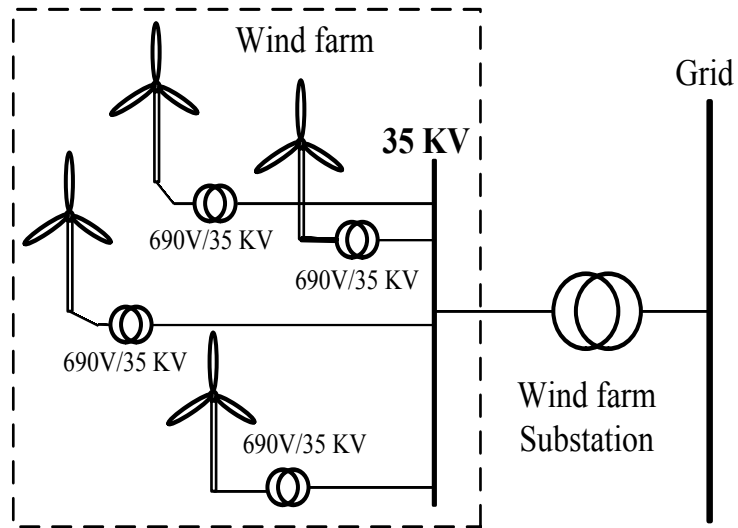
Figure 2.6 Wind farm connected to a grid

The mechanical wind power extracted by the blades of the wind turbine can be expressed as [42, 43]:

$$P_m = \frac{1}{2}\,\rho\,A\,v_w^3 C_p \tag{2.1}$$

The turbine performance coefficient C_p is the ratio of power extracted by the rotor to the wind power, and is a function of blades number and rotational speed [8, 44]. Figure 2.7 shows the correlation between C_p and the tip speed ratio λ, which is non-dimensional quantity representing the ratio of the rotor tip speed to the wind speed v_w. To capture maximum power, the wind turbine should be controlled to track the maximum power point (as shown in figure. 2.7) [42, 43].
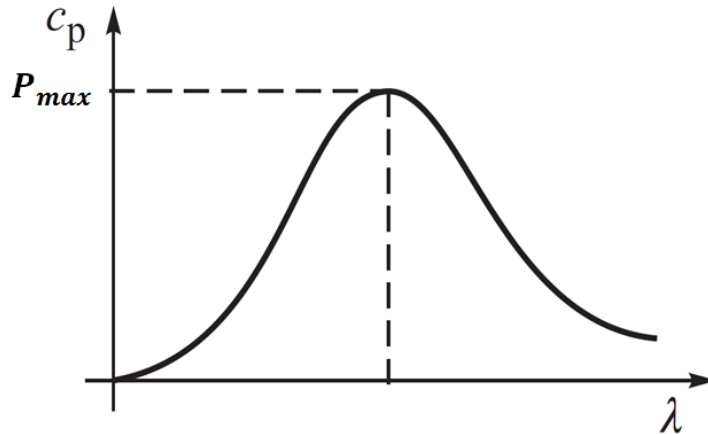
Figure 2.7 Typical Cp/λ curve for a wind turbine [42, 43]

Figure 2.8 shows the power generation of a wind turbine at a particular C_p value.
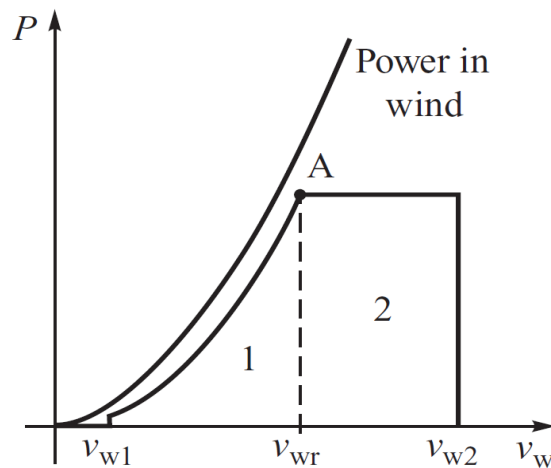
Figure 2.8 Power generation of wind turbine as a function of wind speed: v_{w1}, cut-in wind speed; v_{wr}, rated wind speed, v_{w2}, shutdown wind speed [42, 43].

As shown in figure 2.8, a wind turbine at very low wind speed will generate very little power. The turbine will start functioning only when the wind speed is above the cut-in speed v_{w1}, which is about 3-4 m/s. Above v_{w1}, the turbine generated power increases exponentially until it reaches the limited rated power that

corresponds to the limited wind speed v_{w2}. This rated power will be maintained regardless of any further increment in wind speed. However, if wind speed reaches the shutdown speed, $v_{w2,}$ the wind turbine should be disconnected to avoid possible damage to the turbine [42, 45].

By investigating Eq. 2.1, the generation power of a wind turbine can be increased by enhancing the power coefficient of the turbine (C_p) through the adoption of more aerodynamic approaches, such as (1) increasing the turbine swept area (A), (2) increasing the rotor diameter of the blades and (3) installing wind turbines in specific locations subject to steady and high average wind speed (v_w) e.g. offshore [42, 43].

2.3   Classification of Wind Energy Conversion System

Wind turbines are generally categorised as either a fixed- or variable-speed Wind Energy Conversion Systems (WECSs). A fixed-speed WECS is directly coupled to the electric system and does not require power converter equipment. A variable-speed WECSs, on the other hand, interfaces with the electricity grid through power electronic converters in order to facilitate the variable-speed operation. Direct-drive wind turbines utilise Synchronous Generators (SGs), which are interfaced to the grid by a full-capacity power converter is necessary. Indirect-drive wind turbines use a Doubly-Fed Induction Generator (DFIG), or a Wound-Rotor Induction Generator (WRIG), with controlled rotor resistance. The DFIG is interfaced to the grid via partial capacity converters [9, 41, 42, 45].

2.3.1   Fixed-Speed WECS (Type A)

The Squirrel Cage Induction Generator (SCIG)-based fixed-speed WECS was widely used in the early stages of implementing wind turbines [8]. This was due to its simple configuration and low cost. A typical arrangement for a fixed-speed WECS system is shown in figure 2.9. A three-phase soft starter is used to facilitate a smooth start-up and dampen the undesired inrush current of the SCIG. As the induction generator consumes reactive power, reactive power compensation is usually connected at generator terminals. A coupling transformer links the fixed-speed WECS to the grid [42]. Although the generation of power from a SCIG is limited, due to its constant speed, a fixed-speed WECS is still preferred in particular locations, especially for offshore applications [8, 44].
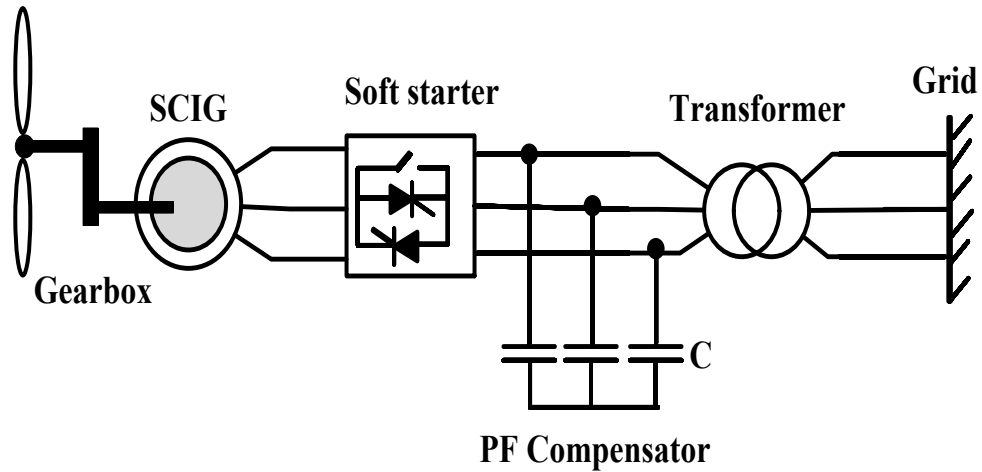
Figure 2.9 WECS equipped with a Squirrel-Cage Induction Generator

The power generated by a SCIG can be improved by changing its magnetic poles through reconfiguration of the stator winding [8, 42].

2.3.2 Variable-Speed WECS

A variable-speed-based WECS currently dominates the wind energy industry because of its many advantages over a fixed speed wind turbine. The variable-speed is achieved through a power converter interface, which permits either a partial or full isolation of the generator and the grid. A variable-speed WECS facilitates the decoupled control of both reactive and active power. Compared to a fixed-speed WECS, variable-speed operation has two key advantages: (1) more energy can be captured, and (2) it produces less mechanical stress on the shaft and gearbox. However, due to the use of power electronic converters, the total cost of the system is 7% more than a fixed speed WECS [9].

2.3.2.1 Partly Variable-Speed WECS (Type B)

Figure 2.10 shows the basic configuration for a partly variable-speed WECS. It is similar to the fixed-speed configuration, except that the induction generator used here is of a wound-rotor type [41, 42]. A Wound-Rotor Induction Generator (WRIG) is equipped with external rotor resistance, in order to facilitate the control of generator slip and rotational speed. By varying the internal rotor resistance, the turbine speed range can be increased (up to 10% over the synchronous speed), offering more flexibility in the system. This configuration, however, has limited speed variety, and inadequate reactive power control [42].
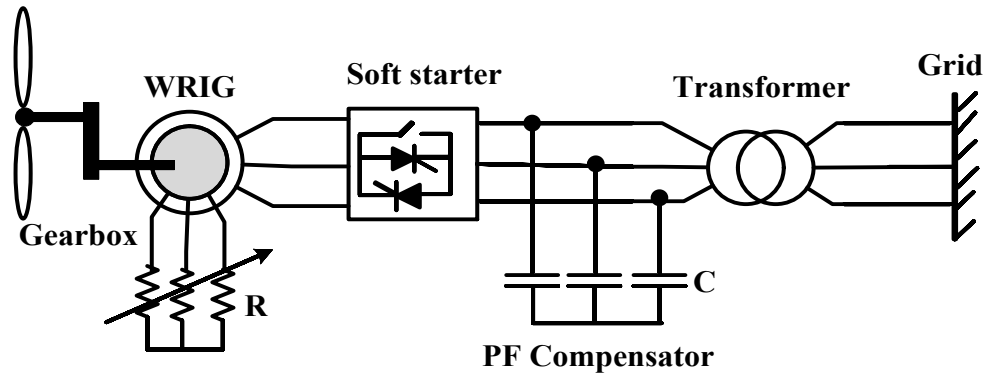
Figure 2.10 WECS equipped with Wound-Rotor Induction Generator

2.3.2.2 Variable-Speed WECS Equipped with Doubly-Fed Induction Generator (Type C)

Variable speed wind turbines equipped with a Doubly-Fed Induction Generator (DFIG) have become very popular and represented 55% of the total installed wind turbines worldwide in 2010 [12]. A DFIG-based WECS is gaining popularity because of its superior advantages, such as reduced converter rating, low cost, reduced losses, easy implementation of power factor correction schemes, variable speed operation and the four quadrants active and reactive power control capabilities compared to other wind turbine generator concepts [46]. The DFIG is basically a wound-rotor machine, which has the capability to control the rotor circuit - by an external electronic device - to achieve variable speed operation. A typical configuration of the DFIG-based WECS is illustrated in figure 2.11. The stator windings of the DFIG are directly connected to the grid through a coupling transformer, while the rotor windings are connected to the grid via (AC-DC-AC) Voltage Source Converter (VSC).
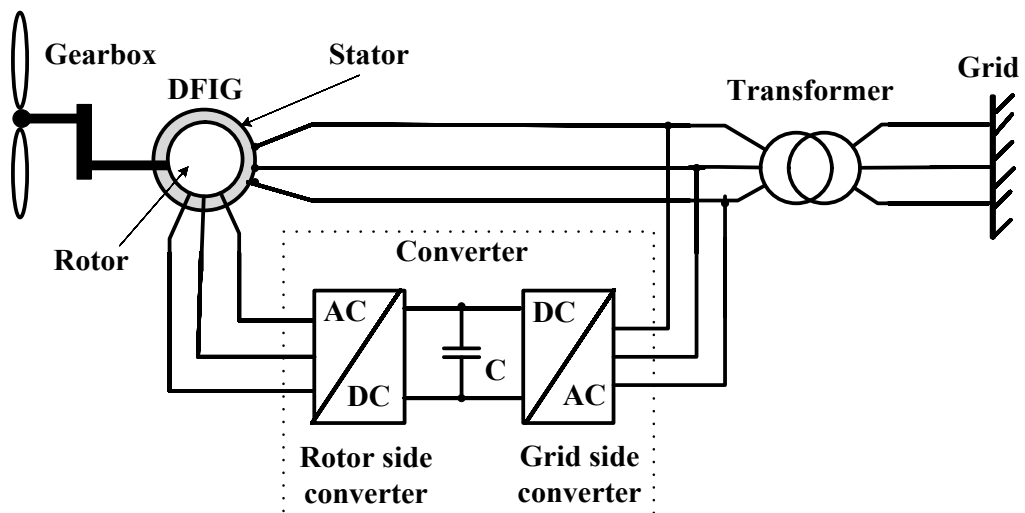
Figure 2.11 WECS equipped with Doubly-Fed Induction Generator

2.3.2.3 Variable-Speed WECS Equipped with SCIG with Full- Capacity Power Converter (Type D)

A full-converter WECS - or Type D - is a variable-speed WECS that employs a SCIG or Synchronous Generator (SG), along with a fully rated power converter to facilitate wide speed variation and to allow full control of the generated active and reactive power. Fully variable-speed WECSs can be employed via either a SCIG or SG. A typical configuration for a variable-speed wind turbine equipped with a SCIG and full-capacity Voltage Source Converter (VSC) is displayed in figure 2.12 [42]. The full capacity converters consist of a Rotor-Side Converter (RSC) and Grid-Side Converter (GSC), and are implemented by an Insulated-Gate Bipolar Transistor (IGBT) and linked by a DC-link capacitor. The RSC is used to regulate the speed of the generator, while the GSC is used to maintain the voltage across the DC link capacitor at a constant level and hence controlling the reactive power at the PCC [8]. Due to the use of full rated converters, the cost of this type is relatively high. However, a Current Source Converter (CSC) can be used instead of a VSC to reduce the converter cost [42].
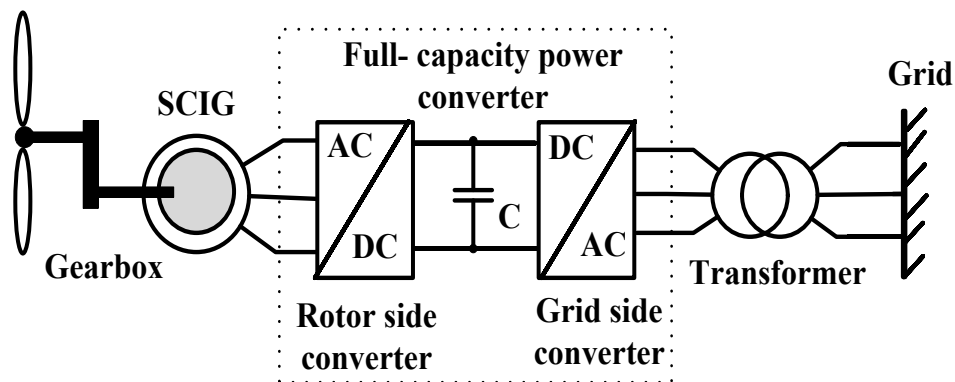
Figure 2.12 Variable-speed WECS equipped with a SCIG with full-capacity power converter

2.3.2.4 Variable-Speed WECS Equipped with a Synchronous Generator with Full- Capacity Power Converter

A typical configuration for a WECS-based Synchronous Generator (SG) of wound-rotor or permanent magnet with full-rated power converters are shown in figures 2.13 and 2.14 respectively. Permanent Magnet Synchronous Generators (PMSGs) have a typical efficiency in the range of 90%. The gearbox can be eliminated in some SG wind turbines, which leads to a cost reduction. The main

drawback of a PMSG is the complexity and costly power electronic converters that interface the generator with the grid [8, 42].
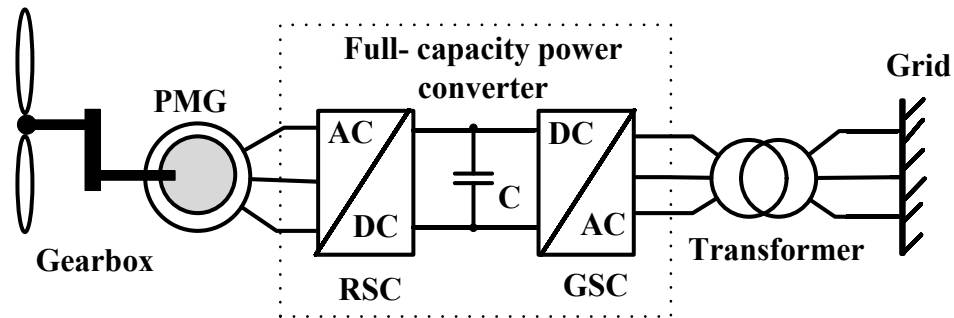
Figure 2.13 Variable speed WECS equipped by PMG with full-capacity power converter
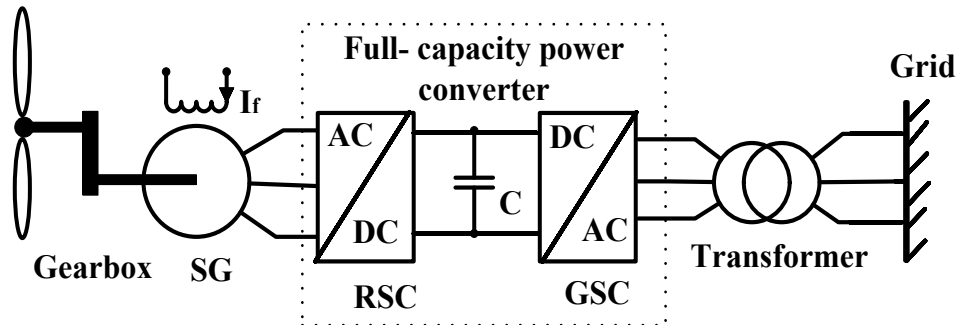
Figure 2.14 Variable speed WECS equipped by SG with full-capacity power converter

A Wound-Rotor Synchronous Generator (WRSG) has the advantage of magnetic field controllability to control the field current. This reduces the mechanical stresses, which may result from the induced electromagnetic forces. The total cost of this type is still expensive because a full rated converter is required [8, 42].

2.4   Connection of Wind Farms

Wind turbines can be installed onshore or offshore; the latter has recently been more widely used, due to its many advantages over those turbines installed on land. [42]. However, offshore wind turbines are located many kilometers away from the shore, and generated power, therefore, needs to be transmitted to an onshore substation through overhead transmission lines, or DC or AC submarine cables. This increases the cost of such an installation [42, 47]. Furthermore, when AC cables are used, the cable length is restricted to 100-150 km with a maximum rating of 200 MW at 145 kV. This is due to cable distribution capacitances [42]. The three possible ways of transmitting generated power from an offshore wind turbine are shown in figure 2.15 (a-c).

AC connection between an offshore wind turbine and the grid can be conducted through an AC cable of medium voltage level (1KV to 50KV) and an onshore transformer as shown in figure 2.15(a). This method eliminates the use of an offshore transformer but the cable length is limited (as mentioned above) and the transmission losses are considerably high. Multiple cables are utilised for a large offshore wind farm capacity [42, 47].
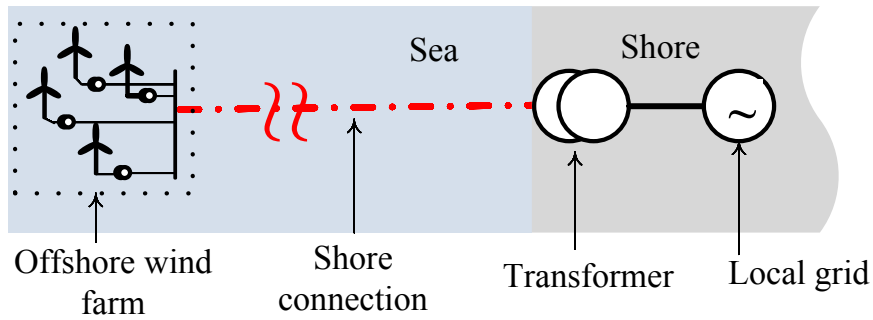
Figure 2.15 (a) AC connection at wind farm voltage level

To reduce transmission losses, an offshore step-up transformer can be used as shown in figure 2.15(b) [47, 48]. In addition to the extra costs this method will incur, with distances of more than 50km, a reactive power compensation technique should also be adopted at the onshore side, especially for weak networks. Usually, the distance is limited to 50 km in such types of connections [47].
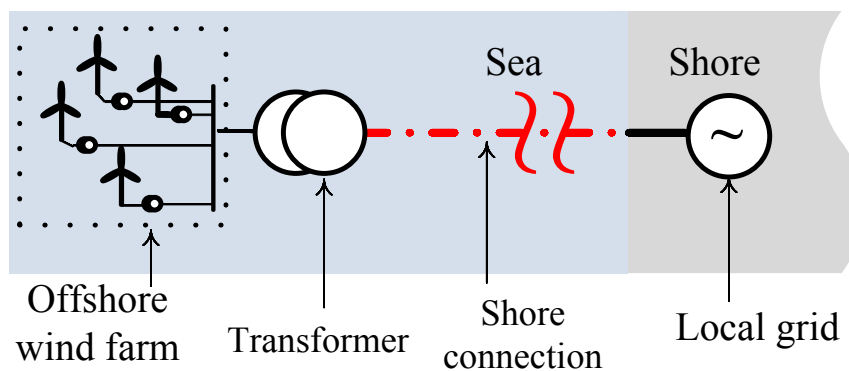
Figure 2.15 (b) High voltage AC connection

A High Voltage Direct Current (HVDC) connection can be used to cover distances more than 100 km [49]. HVDC connection has the following advantages [50]:

- Faults are not transferred between the offshore wind farm and the local grid because they are decoupled by an asynchronous connection
- HVDC connection is not influenced by cable charging currents

- The connection has a high-carrying capacity. A pair of DC cables can carry up to 1200 MW.

- The losses of HVDC connection are lower than an equivalent AC connection scheme.

As seen in figure 2.15 (c), a power converter combined with a step-up transformer is used to enable the HVDC transmission, while another converter and step down transformer are used in the onshore side. This makes the configuration very expensive. [49, 51]. Nowadays, offshore wind farms are being built near to shore to ease the use of AC cables. [50].
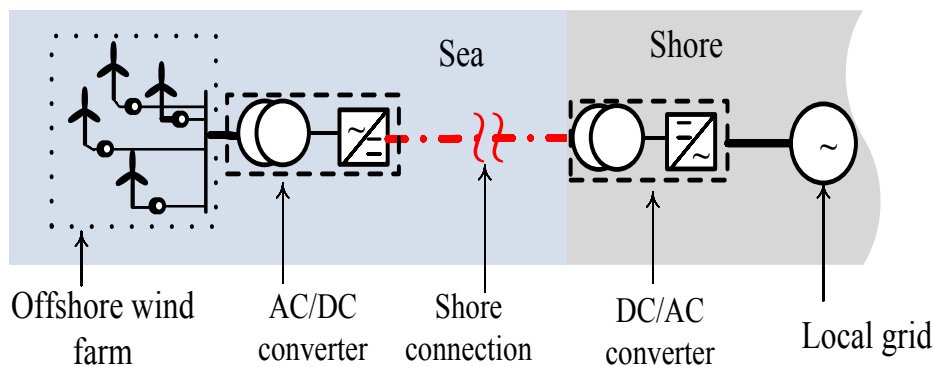
Figure 2.15 (c) High Voltage Direct Current connection

2.5   Effect of Wind Farms on Power System Operation

As wind energy has become the most attractive renewable energy source worldwide, the penetration level of wind farms into existing grids has substantially increased during the last two decades [52]. However, this high penetration level will have a detrimental impact on system stability, reliability and efficiency if no reliable control approaches are adopted [48]. Ref [53] states that voltage and frequency stability are the main issues when connecting wind farms to the electricity grid. [54]. Impacts of wind power generation instability on an electrical system's reliability need to be investigated and analysed before a wind turbine farm is connected to the grid [53]. If power oscillations are caused by the significant penetration of wind turbine farms into the grid, it can have severe impacts on the power quality of an electric system and will cause voltage flickers and frequency deviations. Moreover, the use of a power electronic interface generates harmonic currents, which increase the total harmonic distortion (THD) in the electric system [53-55].

This thesis aims to solve some of these issues through the development of a new topology for the power converters of a DFIG-based WECS. The new topology will

modulate the active and reactive power generation of the DFIG during various fault conditions, and also maintain system stability and reliability.

2.6   Fault Ride Through (FRT) of WECS

In the early stages of wind energy implementation, it was permitted to separate the wind turbine, during various grid faults, to protect it from being damaged. Nowadays, and due to the significant portion of load that wind farms contribute, Transmission Line Operators (TLOs) require wind turbines to remain connected and support the grid during disturbance issues. This has led to the establishment of strict grid codes that wind turbine generators must meet to maintain connection to the grid [56]. The FRT or Voltage Ride Through (VRT) of grid codes can be categorised into two types: (1) Low Voltage Ride Through (LVRT) and (2) High Voltage Ride Through (HVRT). Figure 2.16 shows the LVRT grid codes of the USA, Spain, Mexico, Denmark, Germany, Quebec , UK, and other countries [57, 58].
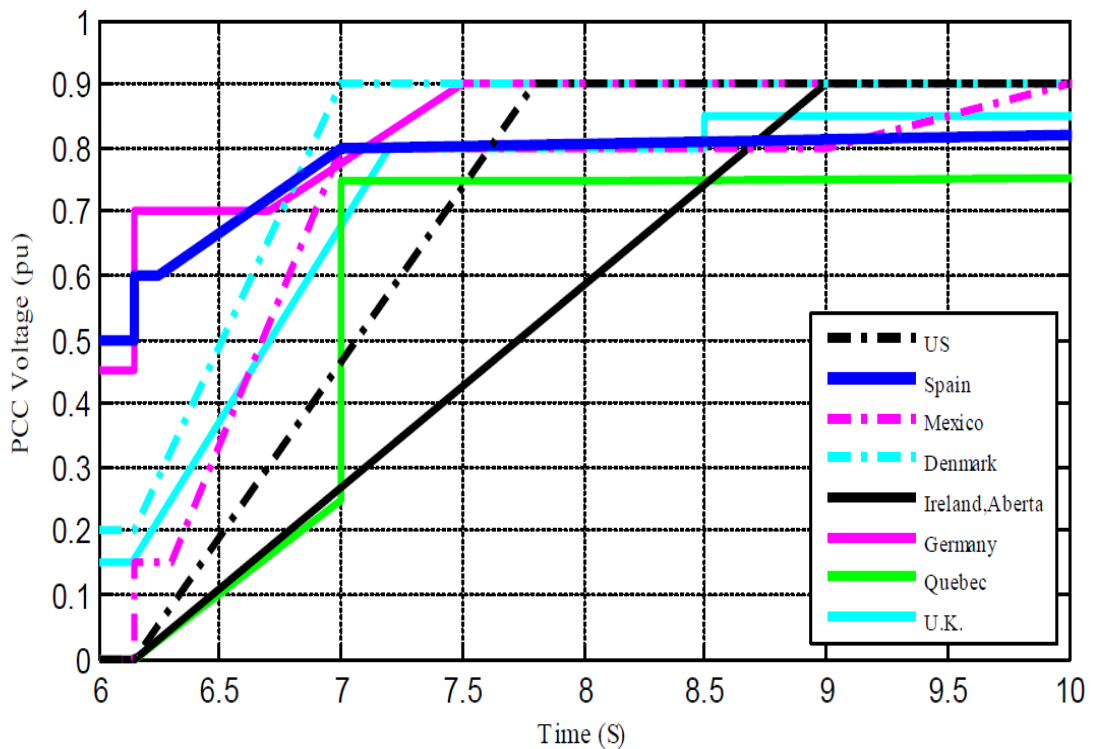
Figure 2.16 LVRT grid codes [56, 57]

In Australia, the connection requirements are predominantly governed by the technical standards specified in the National Electricity Market (NEM) rules, and also local jurisdictional requirements. The regions covered by NEM are Queensland, New South Wales, Victoria, Tasmania and South Australia [59], [60]. The LVRT and HVRT for these regions are shown in Figure 2.17 and Figure 2.18 respectively [61].

For LVRT, the permitted voltage levels are 90% to 110% of normal continuous voltage, 80% to 90% of normal voltage for a period of at least 10 seconds, and 70% to 80% of normal voltage for a period of at least 2 seconds [59]. Western Australia is governed by the Western Power Technical Rules, which are highly stringent (as observed in Figure 2.17) [62]. The HVRT requirement in the Australian Grid Code stipulates that wind turbines must withstand an overvoltage of 1.3 pu for 60 ms after which the HVRT margin ramps [61, 63].
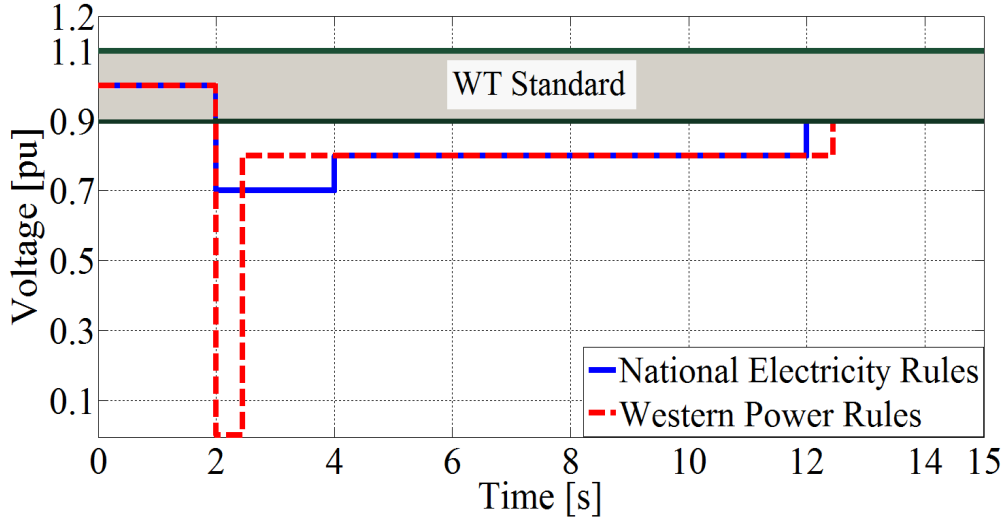
Figure 2.17 LVRT requirements in Australian grid codes [59]
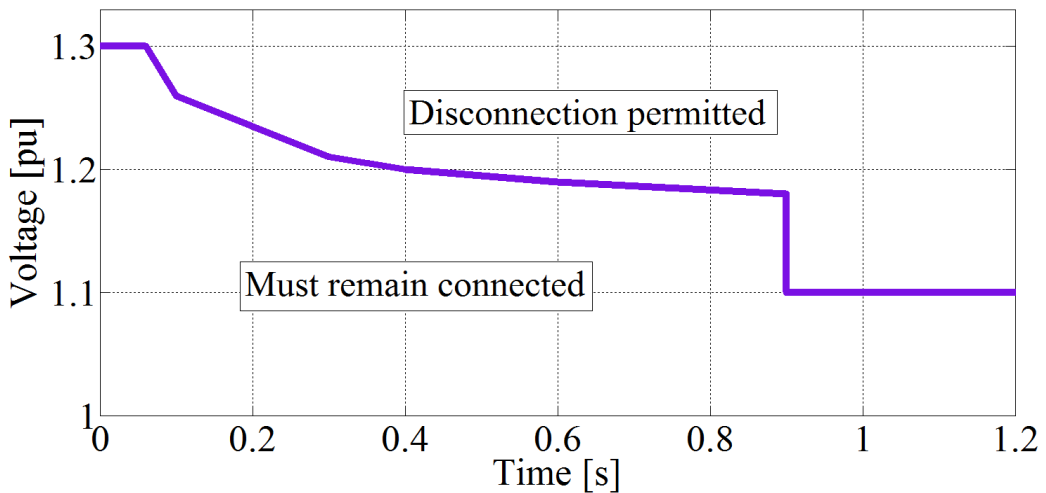
Figure 2.18 HVRT requirements in Australian grid codes [61]

The LVRTs of Spain, Germany and Denmark have been chosen for assessing the effectiveness of the proposed topology, and the following section explains the selected grid codes.

As shown in Figure 2.19 (a), the FRT of Spanish grid codes are classified into three principal zones. The black zone represents the HVRT, where the highest

permissible voltage at PCC is 1.3 and lasts for 0.5 s. The high voltage is then reduced to 1.2 for the next 0.5 s. All voltages at a value higher than those in the black zone will cause the disconnection of the wind turbine from the grid. The light grey zone illustrates the normal situation of the Spanish grid code and is within the range 0.9 to 1.1. All voltages within this zone are defined as a normal condition. Finally, the LVRT of Spain's grid code is shown in the dark grey zone. The lowest voltage falling in this zone is 0.5 and lasts for 0.15 s. This increases to 0.6 until 0.25s. The low voltage limitation then ramps to 0.8 at 1 s, reaching normal operation at 15 s due to fault. The HVRT of Germany's grid code is displayed in Figure 2.19(b). The maximum permissible HVRT is 1.20 for 0.1 s (shown in the black zone). The normal condition, which is represented by the light gray zone, is similar to Spain grid code. As shown in the dark gray zone, the LVRT is allowed to touch 45%, lasts for 0.15 s and has to be at least 70% until 0.7 s. Then the voltage margin ramps to 85% at 1.5 s. The FRT for the Danish grid code is shown in Figure 2.19 (c). The LVRT is permitted to reach 25%, last for 0.5 s and has to be at least 90% until 1.5 s. After that, the voltage level extends to normal zone, which is within the range 90% to 100%.
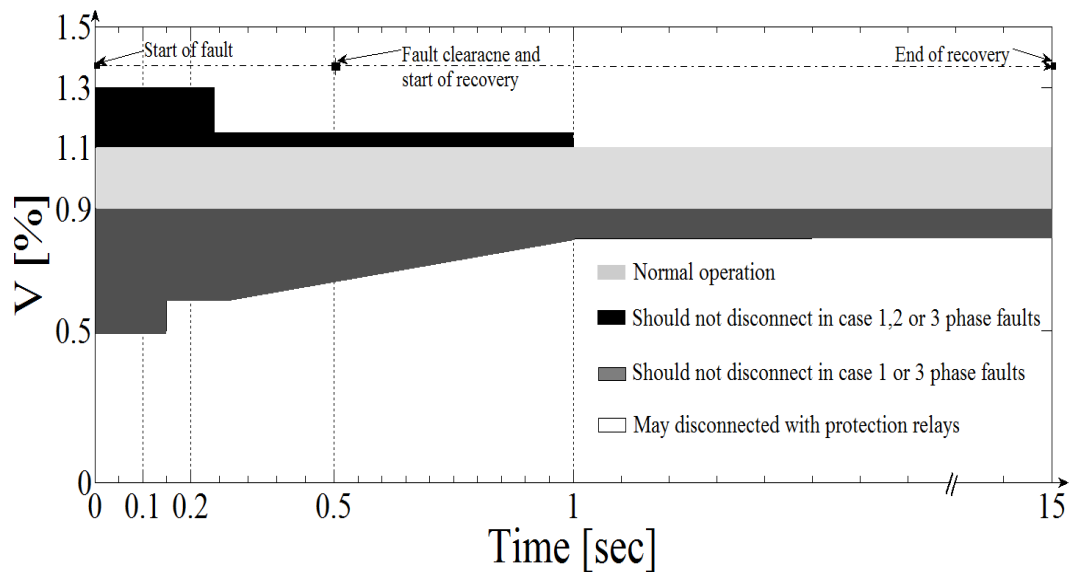
Figure 2.19 (a) Spain FRT grid codes [18, 19]
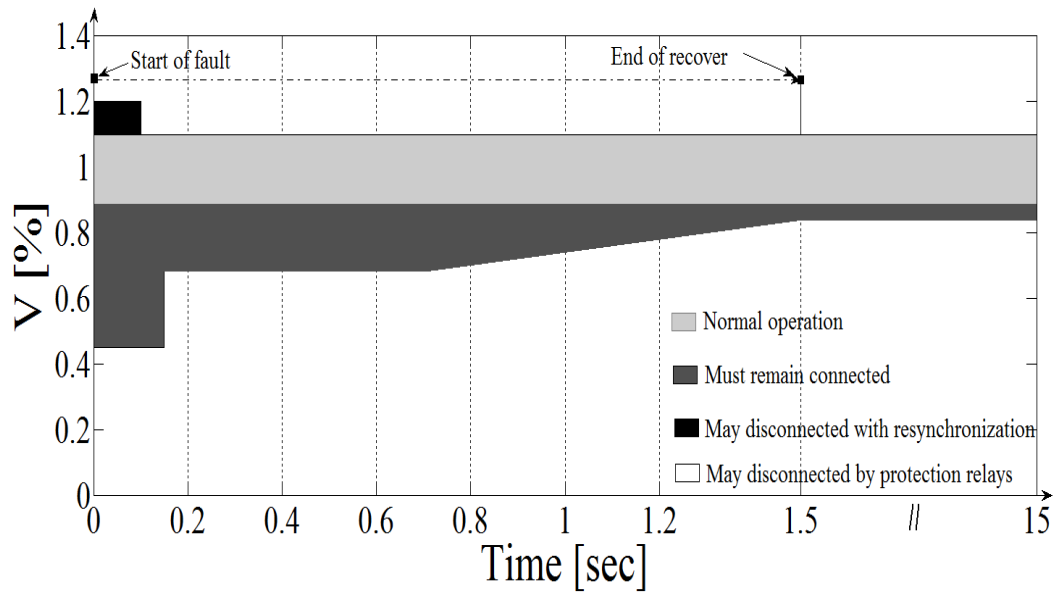
Figure 2.19 (b) German FRT grid codes [18, 19]
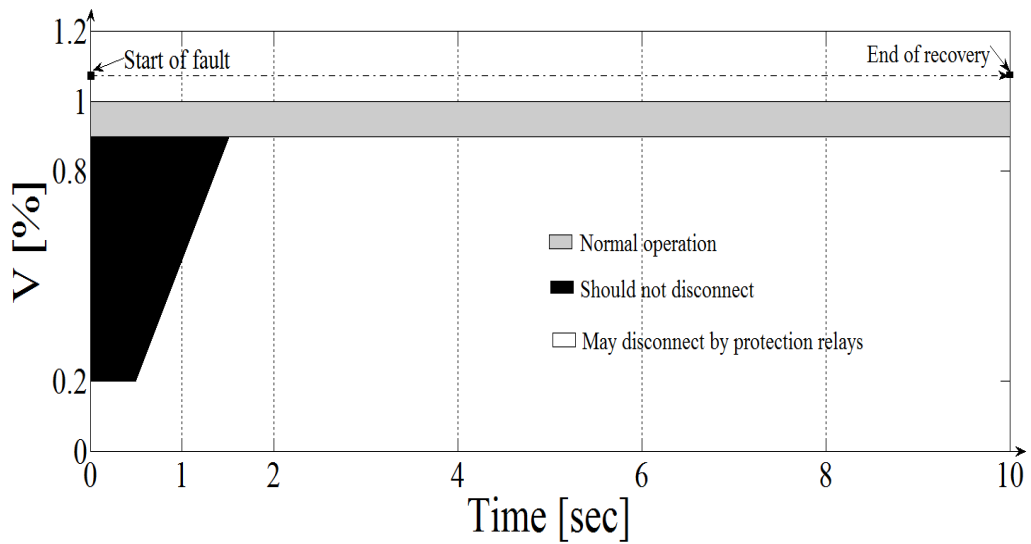
Figure 2.19 (c) Denmark FRT grid codes [18, 19]

Chapter Three

Typical Topology of Doubly Fed Induction Generator

3.1 Introduction

Variable-speed wind turbines equipped with a Doubly Fed Induction Generator (DFIG) are gaining popularity due to their superiority over other wind turbine generator concepts. A DFIG is basically a wound-rotor machine, which is capable of controlling the rotor circuit using external devices and facilitating variable-speed operation. A typical configuration of the DFIG-based WECS is illustrated in Figure 3.1. The stator windings of the DFIG are directly connected to the grid through a coupling transformer, while the windings of the rotor are connected to the electric system via a back-to-back Voltage Source Converter (VSC), harmonic filters, and the coupling transformer. The Rotor Side Converter (RSC) and Grid Side Converter (GSC) use forced-commutated power electronic switches, such as the Insulated Gate Bipolar Transistor (IGBT), to convert AC to DC (and vice versa). A capacitor, connected to the DC-link of the converter, acts as a DC voltage source. The major role of the RSC is to regulate the active and reactive power of the generator, whereas the GSC controls the DC-link voltage and hence the voltage at the point of common coupling (PCC) [14, 42].

The power is supplied to the grid by the stator circuit at all time is unidirectional, whereas the power flow within the rotor circuit is bidirectional. This is because real power is transferred to the grid when the machine is in super-synchronous speed mode (negative slip); real power will only reverse its direction when the machine is in sub-synchronous speed mode (positive slip) [41]. In the two aforementioned modes of operation, the power of the rotor circuit is proportional to the slip, and since the VSCs have only to deal with the rotor power, its capacity is partially rated from the generator's nominal power [41]. A speed variation of ± 25-30% around the synchronous speed can be achieved with a power converter rated at 25-30% of the generator's rated power [14].

The main drawback of the DFIG is its sensitivity to grid disturbances. A crowbar resistive circuit is used to block the VSCs during various disturbances, but

may short the rotor circuit and cause the DFIG to behave like a Squirrel Cage Induction Generator (SCIG) [42, 44].
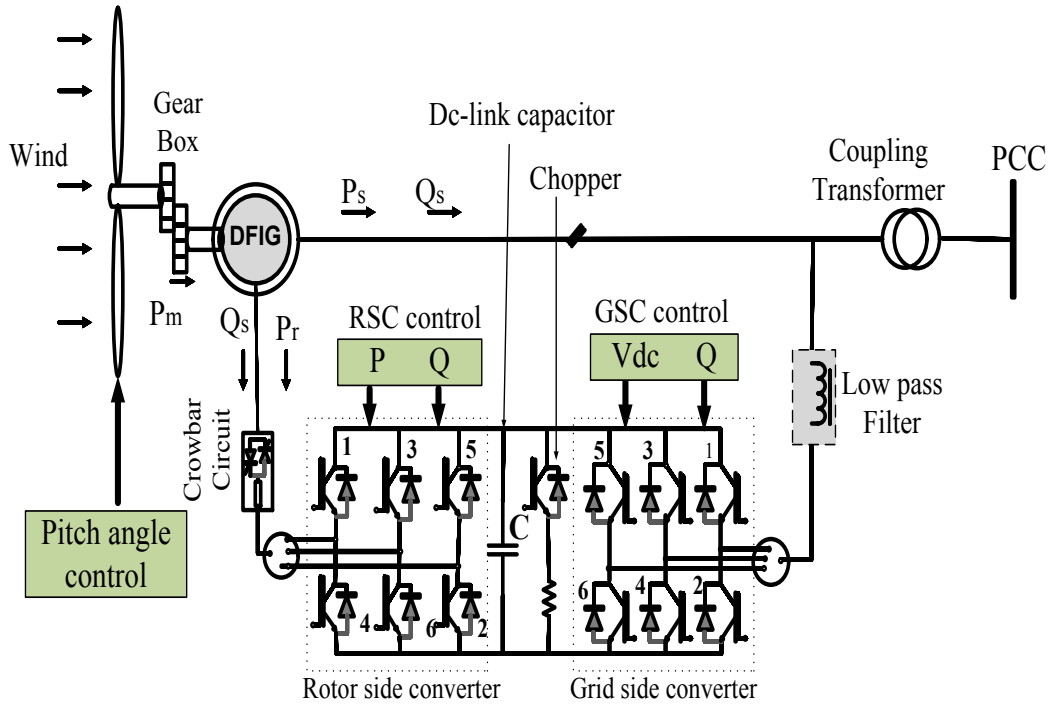
Figure 3.1 A typical topology of the DFIG wind energy conversion system [14, 41, 64]

3.2   Principles of the DFIG

This section briefly explains the fundamentals and concepts of the DFIG.

3.2.1   Steady-State Equivalent Circuit

Based on the explanation in section 3.1, the steady-state equivalent of the DFIG's electric circuit - with different stator and rotor frequencies - can be simplified [14]. As shown in Figure 3.2, both the one-phase of the stator and the rotor are connected in the star configuration. Also, the stator is supplied by the grid at a constant frequency, and the rotor is supplied at a frequency independent from the stator (e.g. through a back-to-back voltage source converter) [14, 41].

By analysing the stator and rotor independently, the stator and rotor steady-state electric equations can be written as follows:

$$V_s - E_s = (R_s + X_{\sigma s})i_s \qquad at\ f_s \qquad\qquad (3.1)$$

$$V_r - E_{rs} = (R_r + X_{\sigma r})i_r \qquad at\ f_r \qquad\qquad (3.2)$$
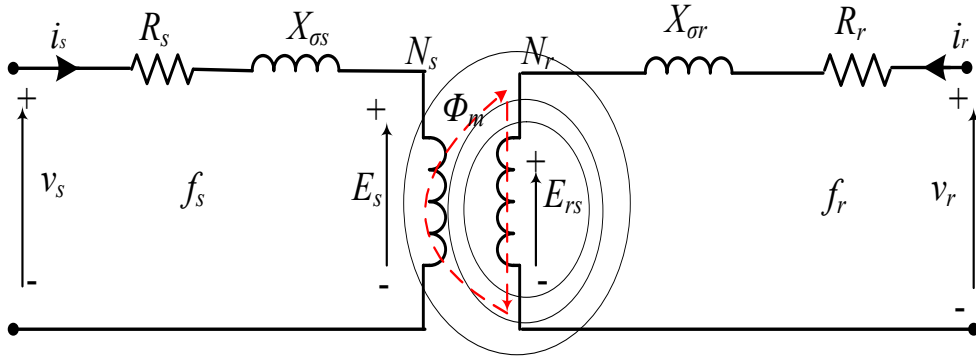
Figure 3.2 One-phase steady-state equivalent electric circuit of the DFIG [14]

3.2.2 Super- and Sub-synchronous Operation of the DFIG

Depending on the wind speed, the DFIG can run at two speeds: (1) super-synchronous speed (n_{sup}), in which the generator's rotor speed is higher than the synchronous speed, and (2) sub-synchronous speed (n_{sub}), in which the rotor speed is lower than the synchronous speed. The value of n_{sup} and n_{sub} can be calculated as follows:

$$n_{sup} = \frac{120}{p} (f_s + f_r) \tag{3.3}$$

$$n_{sub} = \frac{120}{p} (f_s - f_r) \tag{3.4}$$

Using a proper VSC control algorithm, rotor speed can be regulated to an optimum value, from which maximum wind power can be extracted.

Figure 3.3 (a-b) shows the power flow in a DFIG-based WECS. Power is transferred from the grid to the rotor circuit in sub-synchronous mode (as shown in Figure 3.3 (a)), while in super-synchronous mode, power is transferred from the rotor circuit to the grid through the VSC (as shown in Figure 3.3 (b)). In both cases, the stator is injecting real power into the grid. In Figure 3.3, losses in the generator and converters are neglected [14, 41, 42, 65].
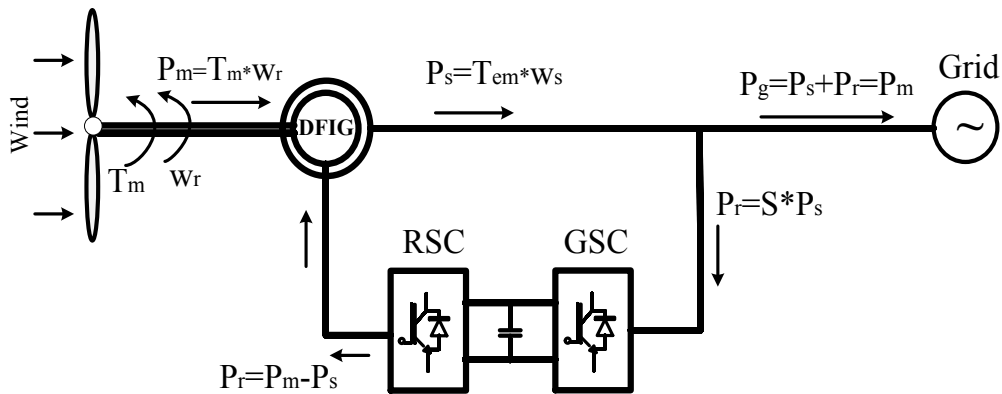
(a) Sub-synchronous mode
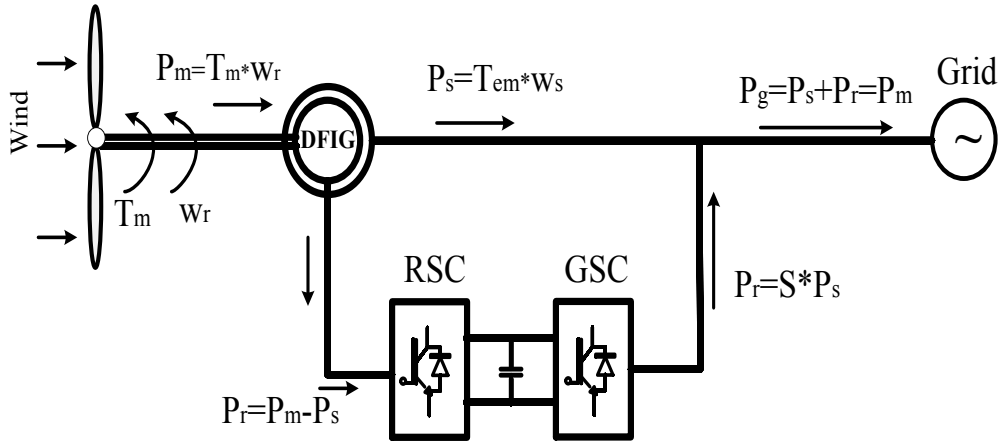
(b) Super-synchronous mode

Figure 3.3 Power flow in DFIG wind energy conversion system [14, 41]

3.3 DFIG Models

In this section, a brief overview of the modelling is presented, as well as the conventional vector control of the DFIG-based WECS [66-71].

3.3.1 Wind Aerodynamic Model

The wind aerodynamic model can be defined by the following equations [44, 72]:

$$P_m = \frac{\rho}{2}\,\pi\,R_r^2 C_p(\lambda,\beta)v_w^3 \tag{3.5}$$

where:

$$\lambda = \frac{w_r}{v_w}\,R_r \tag{3.6}$$

The expression of the wind turbine mechanical torque is [73, 74]:

$$T_w = \frac{1}{2}\frac{\rho}{\lambda}\,\pi\,R_r^2 C_p(\lambda,\beta)v_w^2 \tag{3.7}$$

The power coefficient C_p is a function of the tip speed ratio λ and the pitch angle β, for which the numerical approximation in [70] can be used:

$$C_p(\lambda,\beta) = 0.22\left(\frac{116}{\lambda+0.08\beta} - \frac{25.52}{\beta^3+1} - 0.4\beta - 5\right)e^{-12.5\left(\frac{1}{\lambda+0.08\beta} - \frac{0.035}{\beta^3+1}\right)} \tag{3.8}$$

3.3.2 Mechanical Drive Train Model

The mechanical drive train of the DFIG system can be explained through the two-mass spring dashpot system shown in Figure 3.4 [72, 75, 76]. In this model, a

gearbox is used to magnify the low speed of the wind turbine. The rotating element is modelled as a lumped mass, and each shaft segment is modelled as a mass-less rotational spring with stiffness measured by the spring constant. Viscous damping of each mass is also represented. The equations of the model, expressed per unit, are [77, 78] as follows:

$$2H_t \frac{d}{dt} w_t = T_m - D_t w_t - D_{tg}(w_t - w_r) - T_{tg} \qquad (3.9)$$

$$2H_g \frac{d}{dt} w_r = T_{tg} + D_{tg}(w_t - w_r) - D_g w_r - T_e \qquad (3.10)$$

$$\frac{d}{dt} T_{tg} = K_{tg}(w_t - w_r) \qquad (3.11)$$

The shaft system is represented as a single lumped-mass system, with the lumped inertia constant H_m, defined as [68, 79, 80]:

$$H_m = H_t + H_g \qquad (3.12)$$

The electromechanical dynamic equation is then given by [78]:

$$2H_m p w_m = T_m - T_e - D_m w_m \qquad (3.13)$$
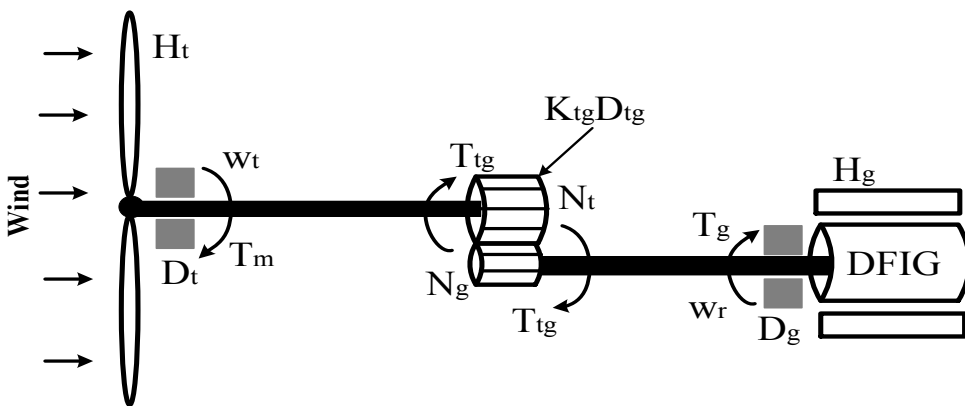
Figure 3.4 DFIG wind turbine shaft system represented by a two-mass model [78]

3.3.3 Induction Generator Modeling

As seen in Figure 3.5, a simplified model of an induction machine can be represented as three windings in the stator side and three windings in the rotor side [14].
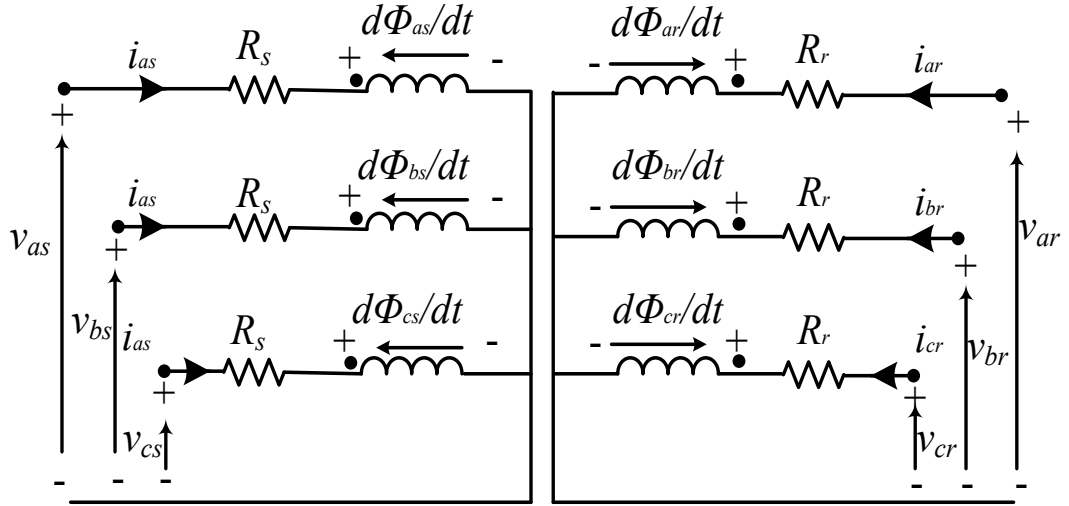
Figure 3.5 DFIG electric equivalent circuit [14]

The instantaneous stator and rotor voltages, currents and fluxes can be given by [14, 41, 42, 81]:

$$v_{as}(t) = \frac{d\Phi_{as}(t)}{dt} + i_{as}(t)R_s \tag{3.14}$$

$$v_{bs}(t) = \frac{d\Phi_{bs}(t)}{dt} + i_{bs}(t)R_s \tag{3.15}$$

$$v_{cs}(t) = \frac{d\Phi_{cs}(t)}{dt} + i_{cs}(t)R_s \tag{3.16}$$

$$v_{ar}(t) = \frac{d\Phi_{ar}(t)}{dt} + i_{ar}(t)R_r \tag{3.17}$$

$$v_{br}(t) = \frac{d\Phi_{br}(t)}{dt} + i_{ar}(t)R_r \tag{3.18}$$

$$v_{cr}(t) = \frac{d\Phi_{cr}(t)}{dt} + i_{ar}(t)R_r \tag{3.19}$$

3.3.3.1 α , β Model

The differential equations of the stator and rotor voltages and fluxes, in stator and rotor coordinates (α , β reference frame), can be written as follows [14, 68, 80]:

$$v_s^s = \frac{d\Phi_s^s}{dt} + i_s^s R_s \tag{3.20}$$

$$v_r^r = \frac{d\Phi_r^r}{dt} + i_r^r R_r \tag{3.21}$$

$$\Phi_s^s = L_s i_s^s + L_m i_r^s \tag{3.22}$$

$$\Phi_r^r = L_r i_r^r + L_m i_s^r \tag{3.23}$$

L_s and L_r can be calculated as:

$$L_s = L_{\sigma s} + L_m \tag{3.24}$$

$$L_r = L_{\sigma r} + L_m \tag{3.25}$$

By referring the corresponding space vectors to the stator reference frame, the α , β model of the DFIG, in stator coordinates (shown in Figure 3.6), can be written as:

$$v_s^s = \frac{d\Phi_s^s}{dt} + i_s^s \tag{3.26}$$

$$v_r^s = \frac{d\Phi_r^s}{dt} + i_r^s R_r + j w_m \Phi_r^s \tag{3.27}$$

$$\Phi_s^s = L_s i_s^s + L_m i_r^s \tag{3.28}$$

$$\Phi_r^s = L_r i_r^s + L_m i_s^s \tag{3.29}$$

The active and reactive powers, on the stator side (P_s, Q_s) and on the rotor side, are simplified to:

$$P_s = \frac{3}{2} \left(v_{\alpha s} i_{\alpha s} + v_{\beta s} i_{\beta s} \right) \tag{3.30}$$

$$Q_s = \frac{3}{2} \left(v_{\beta s} i_{\alpha s} - v_{\alpha s} i_{\beta s} \right) \tag{3.31}$$

$$P_r = \frac{3}{2} \left(v_{\alpha r} i_{\alpha r} + v_{\beta r} i_{\beta r} \right) \tag{3.32}$$

$$Q_r = \frac{3}{2} \left(v_{\beta r} i_{\alpha r} - v_{\alpha r} i_{\beta r} \right) \tag{3.33}$$

The electromagnetic torque can be calculated by:

$$T_{em} = \frac{3}{2} P \left(\Phi_{\beta r} i_{\alpha r} - \Phi_{\alpha r} i_{\beta r} \right) \tag{3.34}$$
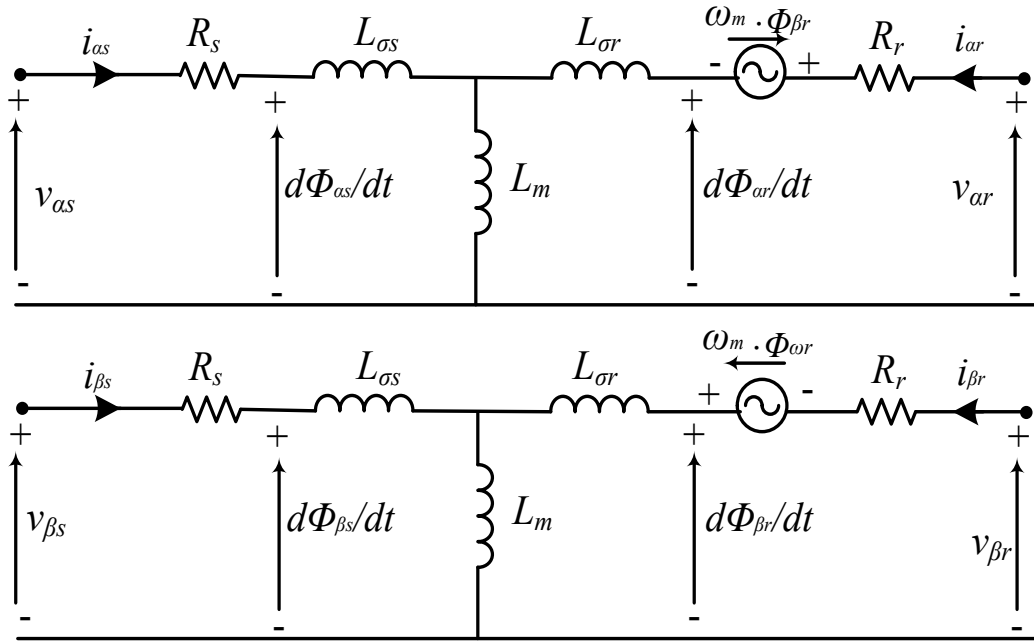
Figure 3.6 α, β DFIG Model in stator coordinates [14, 41]

3.3.3.2 d-q Model

At steady state, the d-q components of the currents, voltages and fluxes will be constant values. This is in contrast to the α , β components, which are sinusoidal magnitudes. The equivalent circuit of the DFIG in the d-q reference frame is shown in Figure 3.7 [82].
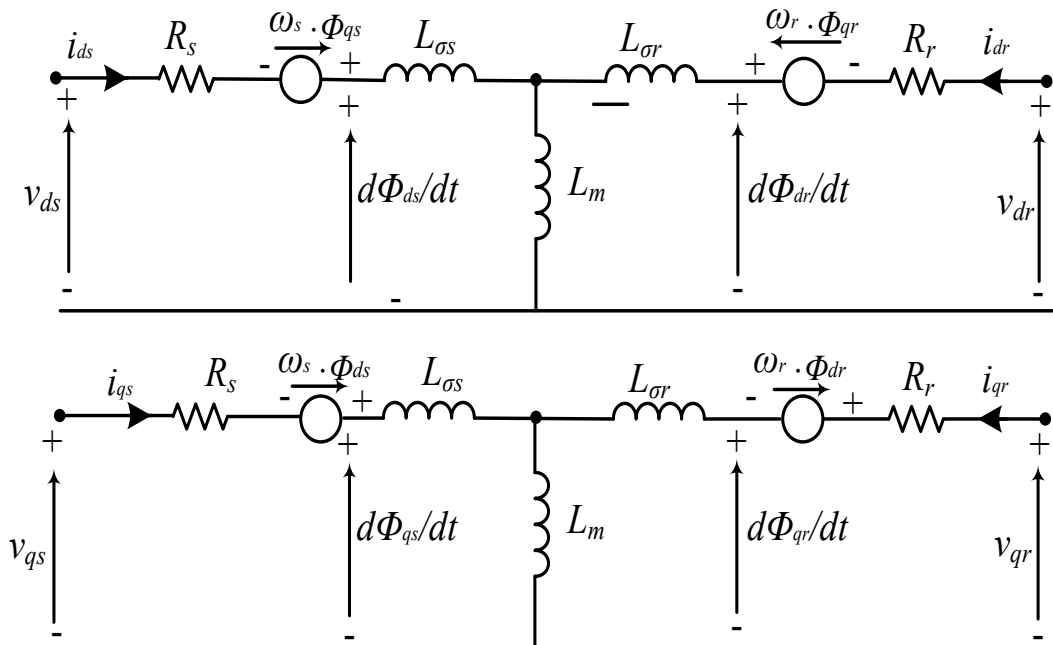
Figure 3.7 d-q DFIM model in synchronous coordinates [14, 41]

The stator and rotor voltages and fluxes, and the active and reactive power expressions in the d-q reference frame, can be written as [83]:

$$v_s^a = \frac{d\Phi_s^a}{dt} + i_s^a R_s + jw_s \Phi_s^a \tag{3.35}$$

$$v_r^a = \frac{d\Phi_r^a}{dt} + i_r^a R_r + jw_r \Phi_r^a \tag{3.36}$$

$$\Phi_s^a = L_m i_r^a + L_s i_s^a \tag{3.37}$$

$$\Phi_r^a = L_m i_s^a + L_r i_r^a \tag{3.38}$$

$$P_s = \frac{3}{2}\left(v_{ds}i_{ds} + v_{qs}i_{qs}\right) \tag{3.39}$$

$$Q_s = \frac{3}{2}\left(v_{qs}i_{ds} - v_{ds}i_{qs}\right) \tag{3.40}$$

$$P_r = \frac{3}{2}\left(v_{dr}i_{dr} + v_{qr}i_{qr}\right) \tag{3.41}$$

$$Q_r = \frac{3}{2}\left(v_{qr}i_{dr} - v_{dr}i_{qr}\right) \tag{3.42}$$

Superscript "a" indicates the space vectors, which refer to a synchronously rotating frame.

The electromagnetic torque of the DFIG in the d-q reference frame can be calculated by [68, 83]:

$$T_{em} = \frac{3L_m}{2L_s}P\left(\Phi_{qs}i_{dr} - \Phi_{ds}i_{qr}\right) \tag{3.43}$$

3.3.4 Modelling of the Variable-Frequency Converter

The DFIG's variable frequency converter enables variable-speed runs via separating the frequency of the grid from the frequency of the rotor. The typical arrangement for a DFIG's variable frequency converter comprises of two back-to-back PWM voltage source converters joined through a DC link [14].

3.3.4.1 Grid Side Converter Modelling

The GSC is modelled through ideal bidirectional switches, which enable power exchange in both directions [14]. The main role of the GSC is to maintain the DC link voltage at a constant level and also to make a path for power exchange between the

rotor windings and the electric system at unity power factor. As a result, the reactive power exchange with the grid is produced totally through the DFIG stator windings.
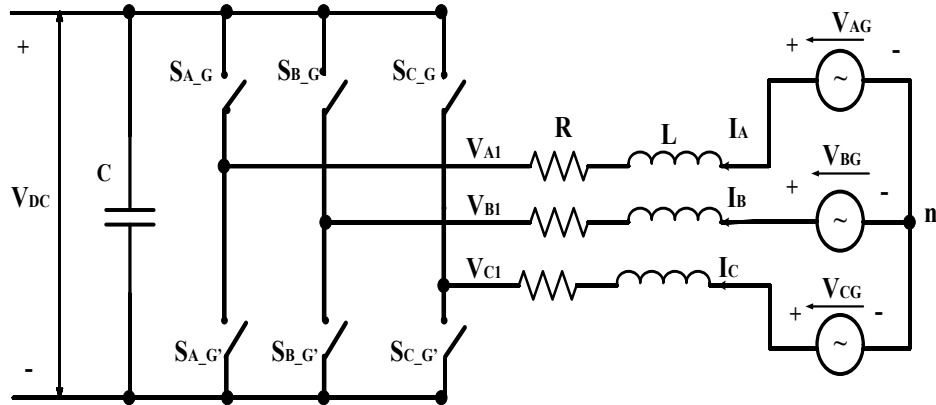
Figure 3.8 Schematic of the DFIG grid-side power converter [14]

A schematic of the GSC is depicted in Figure 3.8, in which the grid-side voltages can be written as [84, 85]:

$$\begin{bmatrix} V_{AG} \\ V_{BG} \\ V_{CG} \end{bmatrix} = r \begin{bmatrix} I_A \\ I_B \\ I_C \end{bmatrix} + L\frac{d}{dt}\begin{bmatrix} I_A \\ I_B \\ I_C \end{bmatrix} + \begin{bmatrix} V_{A1} \\ V_{B1} \\ V_{C1} \end{bmatrix} \tag{3.44}$$

In the d-q reference frame (3.45), the equation can be rewritten as below [84, 85]:

$$\begin{bmatrix} v_d \\ v_q \end{bmatrix} = r \begin{bmatrix} i_d \\ i_q \end{bmatrix} + L\frac{d}{dt}\begin{bmatrix} i_d \\ i_q \end{bmatrix} + \omega_s L \begin{bmatrix} -i_d \\ i_q \end{bmatrix} + \begin{bmatrix} v_{d1} \\ v_{q1} \end{bmatrix} \tag{3.45}$$

The active and reactive power in the d-q reference frame can be expressed as follows [84, 85]:

$$P = v_d i_d + v_q i_q \tag{3.46}$$

$$Q = v_d i_q + v_d i_q \tag{3.47}$$

The alignment between the d-axis and the stator-voltage position v_d is constantly maintained, and therefore, active and reactive power is proportional to i_d and i_q respectively [84]. This is the basic idea for the decoupled d-q control algorithm used for the GSC, where the direct axis current is used to regulate the DC-link voltage, and the quadrature axis current component is used to regulate the reactive power [10-15].

The conventional decoupled d-q controller of the GSC is shown in Figure 3.9. A suitable reference level for the d-axis stator current (i_{dG}^*) is created using the voltage error signal of the DC-link capacitor voltage.It is compared with the measured i_{dG} to create an error signal that is fed to a PI controller. To maintain unity power factor at the PCC, during normal operating condition, i_{qG}^* is adjusted to zero and compared to the measured $i_{qG,}$ which is fed to another PI controller. The output signals of the two PI controllers are converted to the abc reference frame and used as an input to the PWM circuit [84-86].
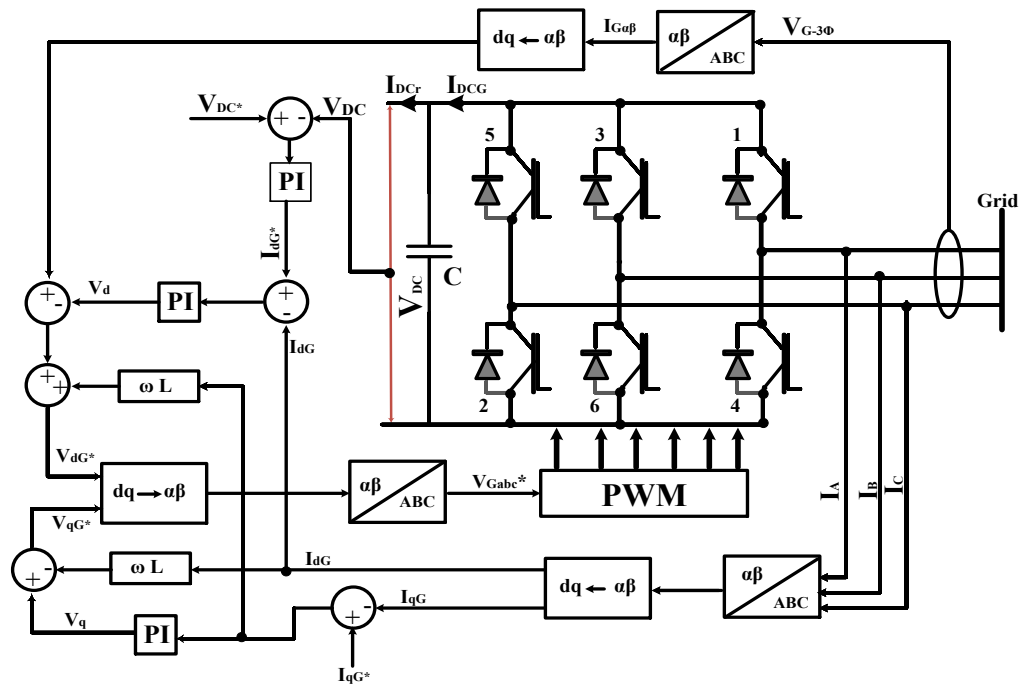
Figure 3.9 Grid-side converter vector control system [85, 86]

3.3.4.3 Rotor Side Converter Modelling (RSC)

Figure 3.10 shows the RSC and the filter, which is located between the rotor winding and the RSC [14, 85].
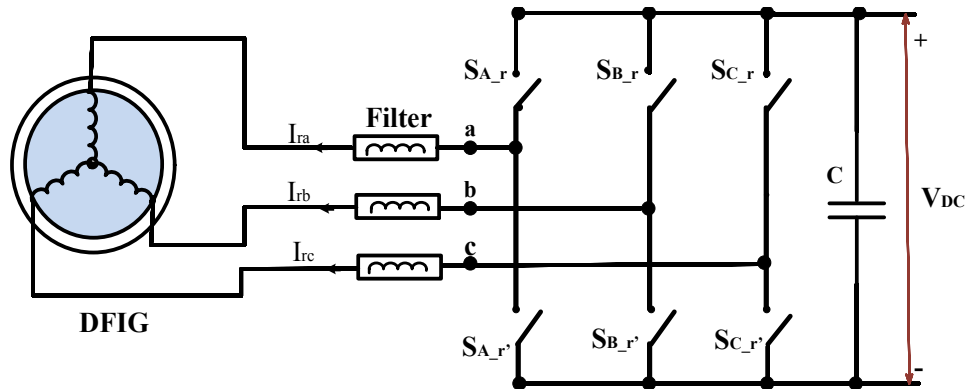
Figure 3.10 Scheme of DFIG rotor-side power converter [14]

The active and reactive powers of the stator windings can be calculated as [84]:

$$P_s = 1.5 v_{sd} i_{ds} = -1.5 v_s \frac{L_m}{L_s} i_{dr} \tag{3.48}$$

$$Q_s = 1.5 v_{sd} \left(i_{qr} + \frac{v_{sd}}{w_s L_m} \right) \tag{3.49}$$

Equations 3.48 and 3.49 indicate that P_s and Q_s can be independently controlled by controlling i_{dr} and i_{qr} respectively. The field-oriented vector control arrangement for the RSC can be configured as shown in Figure 3.11.
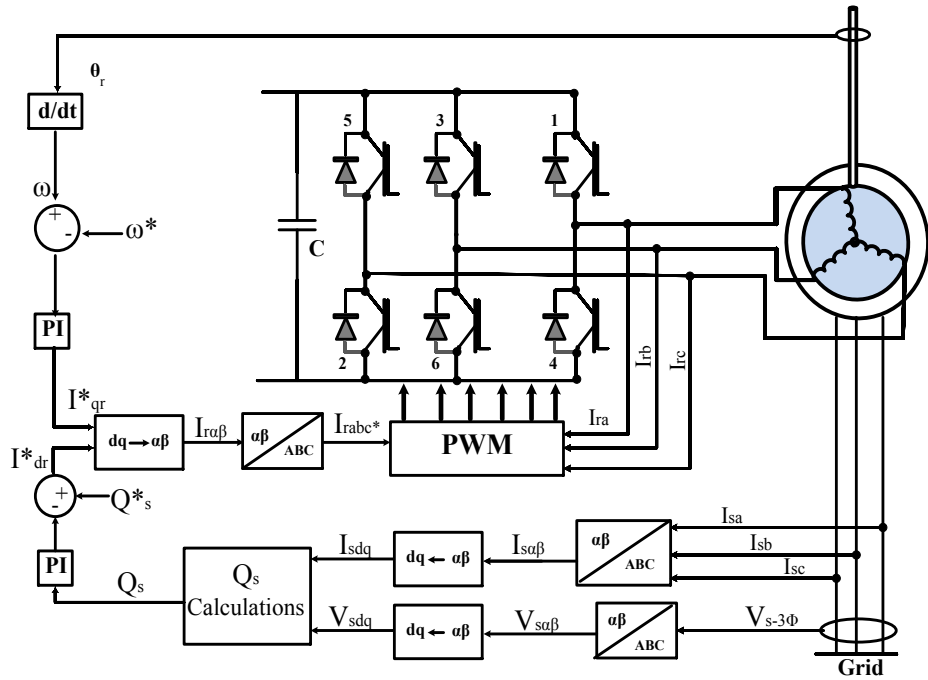
Figure 3.11 Rotor side converter vector control system [86]

As shown in Figure 3.11, "a reference signal (w^*) is selected, based on the wind turbine's characteristics, to track maximum power. It is then compared with the measured rotor speed to create an error signal, which is fed to a PI controller to generate the q-axis rotor current (I_{qr}^*). To achieve unity power factor operation, the reactive power reference (Q_s^*) is set to zero and compared with the measured value. This creates an error signal, which is fed to another PI controller to generate the reference rotor d-axis current (I_{dr}^*). The Clarke-Park transformation is used to convert I_{qr}^* and I_{dr}^* to I_{abc}^*. This is used as input to the RSC PWM circuit - along with I_{abc} - to create appropriate firing pulses for the RSC switches" [86].

3.3.4.3 DC Link of the DFIG converter

The DC link of the DFIG converter consists of a capacitor in parallel with a high resistance as shown in Figure 3.12. [14].
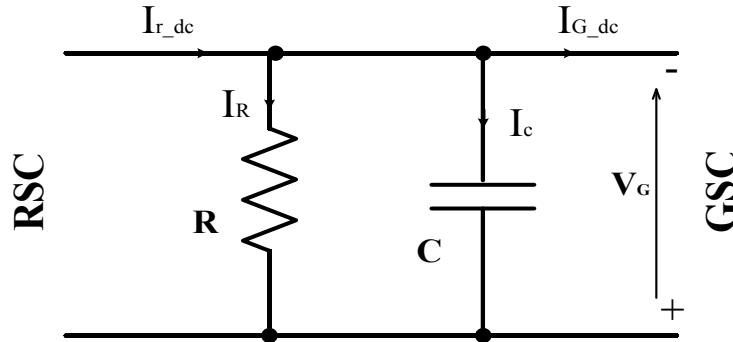
Figure 3.12 DC-link system of DFIG converter [14]

The current through the DC link capacitor i_C can be calculated by

$$i_C = i_{r\_dc} - i_{G\_dc} - i_R \qquad (3.50)$$

3.3.5 Pitch Angle Modelling

The pitch angle controller module is used to maintain the rotor speed within a certain range. It is employed for over-speed protection of the converter switches when high wind speeds may cause the generated power of the wind turbine to increase to dangerous levels [79]. Pitch angle control is also useful when an electric system disturbance takes place in the WECS [87]. During high wind speeds, the blade pitch angle is adjusted to reduce C_p [79]. The pitch angle controller model is shown in Figure 2.13, where the dynamic performance of the pitch is described by [88, 89]:

$$\beta' = -\frac{1}{\tau}\beta + \frac{1}{\tau}\beta_d \qquad (3.51)$$
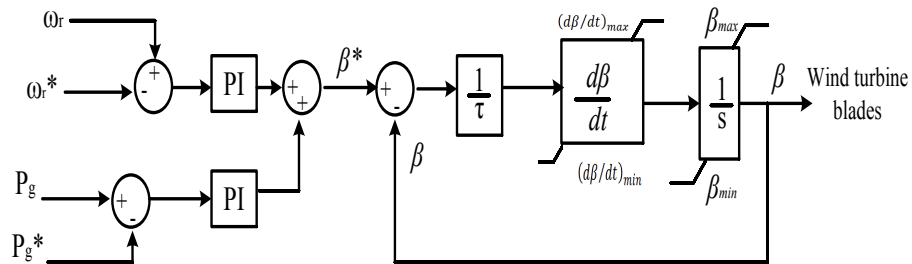
Figure 3.13 Pitch angle controller model [64, 90]

The pitch control block (in Figure 3.13) changes the blade pitch angle - when wind speed is higher than the rated wind speed - and spills excess power. The output power is kept at beneath the rated wind speed, despite wind speed surpassing the rated value. "The reference speed and actual speed are compared and the error drives the upper PI controller. Reference power and actual power are also compared and the error drives the lower PI controller. The PI controller outputs are then summed and hard-limited to generate the reference pitch angle signal, which is compared to the actual pitch angle. The pitch angle signal is active only when wind speed is close to rated. Otherwise, it is fixed at zero" [78].

Chapter Four

Proposed Converter Station Topology for a Doubly Fed Induction Generator-Based Wind Energy Conversion System and Results Discussion

4.1   Introduction

As mentioned in the previous chapter, DFIG-based WECSs have, to date, dominated the wind energy market due to their superior advantages over other wind turbine technologies. The main disadvantage of a DFIG, however, is its sensitivity to external disturbances, which reduce its Fault Ride Through (FRT) capability [91]. Grid disturbances may lead to significant voltage sag at the PCC, making necessary the disconnection of the wind turbine and converters (through a crowbar circuit across the rotor windings) to protect them from being damaged [16, 17, 92]. If the wind turbine supplies a significant portion of the overall demand, the disconnection of the wind turbine during fault conditions may lead to voltage instability and cause a blackout in the electricity grid to which it is connected [93].

Recently, Transmission Line Operators set grid codes to be fulfilled when maintaining the connection of the wind turbine to the grid during various disturbance events [12]. To achieve these codes, researchers proposed the use of an external FACTS device - such as a static synchronous compensator (STATCOM) [21, 26, 27, 56, 94, 95], a static var compensator (SVC) [20, 22, 96-98], a dynamic voltage restorer [29, 30, 33, 99], a static synchronous series compensator (SSSC) [100, 101], a unified power flow controller (UPFC) [59, 102-105], a thyristor controlled series compensator (TCSC) [106], or superconducting magnetic energy storage (SMES) [12, 13, 34-37, 107] - at the PCC. Out of all the proposed FACTS devices, a SMES unit is the most effective technology that can effectively compensate both active and reactive powers at the PCC [12, 13, 34, 107, 108]. This technology, however, has not yet been implemented due to its high cost [12, 34].

This chapter presents a new topology for the DFIG converters, which will provide the same performance of the SMES unit during fault conditions. The new topology relies on the integration of a coil that can either be a high temperature superconductor or of very small internal resistance to reduce the losses within the DC

link of the DFIG's back-to-back converters as shown in Figure 4.1. This coil is deactivated with full charge during normal operating conditions and will be connected to the circuit, as soon as a disturbance occurs within the system. This will enable the smooth, independent and rapid control of both active and reactive power in four-quadrant operation during fault conditions. Apart from the coil and the associated control circuit, this technique does not call for any additional equipment as it utilises the main infrastructure of the DFIG converters. To assess the robustness of the proposed technique, extensive simulation analyses with various fault scenarios were conducted using Simulink/Matlab. These scenarios will be detailed in the following sections.
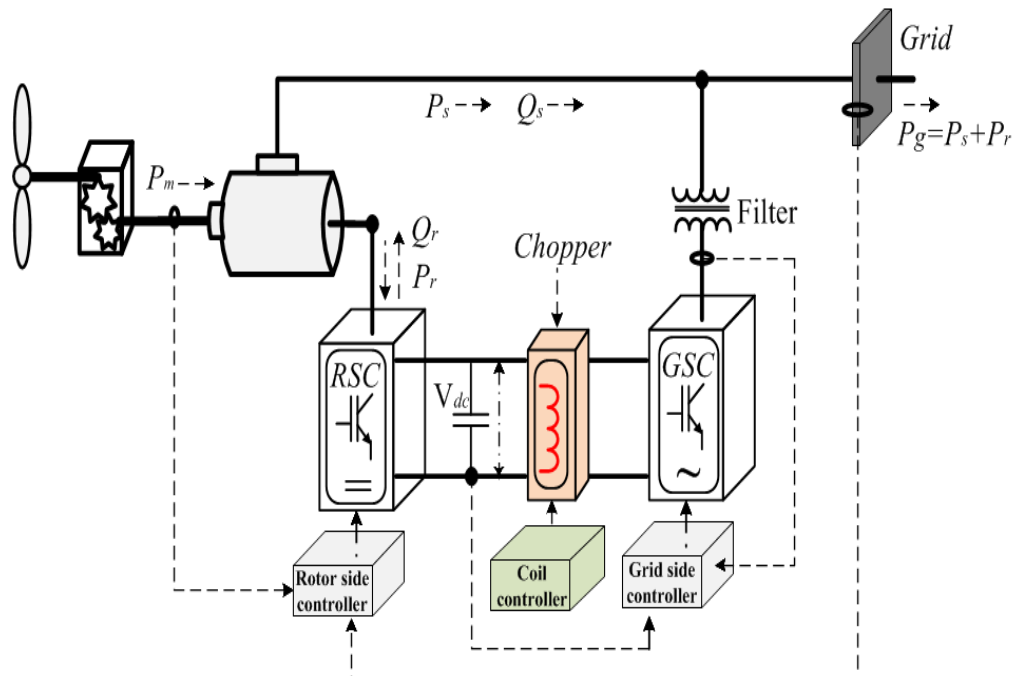
Figure 4.1 The proposed new converter topology of a DFIG-based WECS

4.2 Coil Control Algorithm

The main challenge of the proposed topology is the design of a proper control scheme for the integrated coil, which can handle the system's nonlinear, complex and time-varying parameters. In this regard, an Artificial Intelligent (AI)-based control scheme is investigated. Considered as a logical system, possessing suitable human reasoning abilities, Fuzzy Logic Controller (FLC) has been extensively used in control systems [109, 110]. A general fuzzy inference system is shown in Figure 4.2. The system includes four blocks: (1) Fuzzifier, (2) Defuzzifier, (3) Inference Engine

and (4) Fuzzy Rule Knowledge Base [110]. These blocks will be briefly explained below.
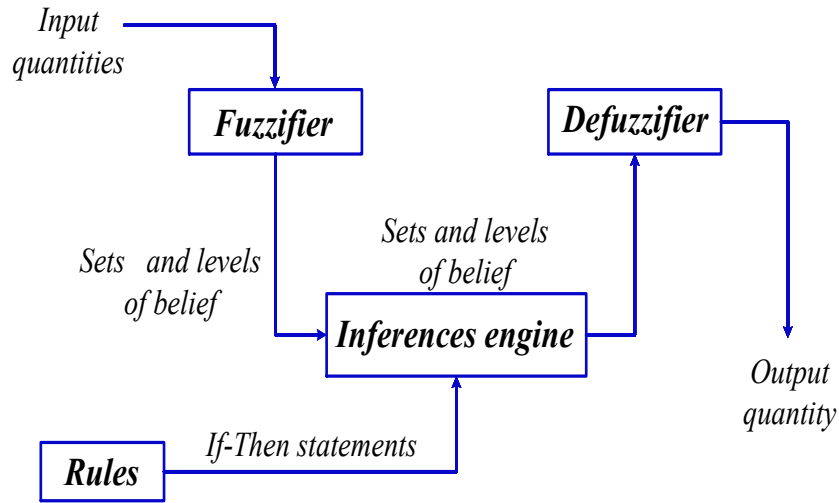
Figure 4.2 Block diagram for a typical fuzzy logic system [110]

To regulate the power exchange between the coil and the grid, a two-quadrant DC-DC chopper is used, and a fuzzy logic-based control scheme is designed to control the duty cycle (D) of the DC chopper. The proposed control scheme of the DC chopper is shown in Figure 4.3. The FLC is established according to the fuzzy inference block diagram depicted in Figure 4.2. As seen in Figure 4.3, the model inputs are power generation of the DFIG (P_g) and current passing through the coil (I_c). The FLC output is the DC chopper duty cycle (D), which controls the amount and direction for energy exchange between the coil and the grid.
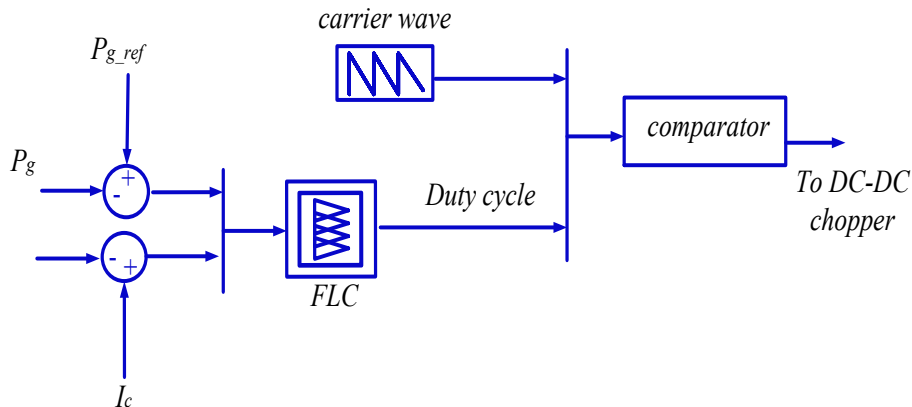
Figure 4.3 Control algorithm of the DC-DC chopper

The relationship between the voltage across the coil V_c and the DC link capacitor voltage V_{dc} can be written as [12]:

$$V_c = (1 - 2D)V_{dc} \tag{4.1}$$

Triangular Membership Functions (MFs) are used to simulate all possible levels of the input parameters. The triangular membership function can be expressed mathematically as [110]:

$$f(x; a, b, c) = \begin{cases} 0, & x \le a \\ \frac{x-a}{b-a}, & a \le x \le b \\ \frac{c-x}{c-b}, & b \le x \le c \\ 0, & d \le x \end{cases} \tag{4.2}$$

As shown in Figures 4.4 and 4.5, the two input variables, DFIG generated real power (P_g) and coil current (I_c), are fuzzified into five sets of Triangular-type membership functions. The MF for the duty cycle (D) is on the scale from 0 to 1 as shown in Figure 4.6.
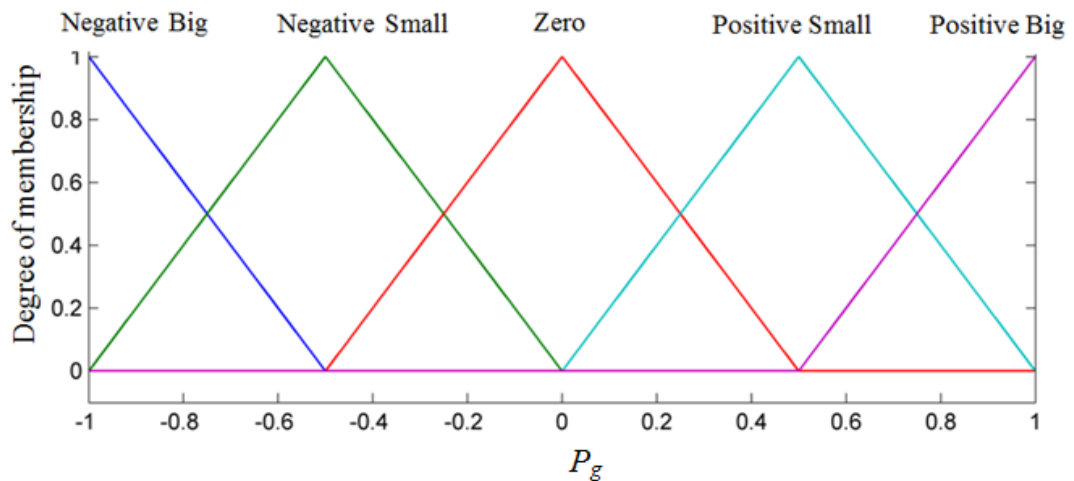
Figure 4.4 Membership function for the power generation Pg (pu)
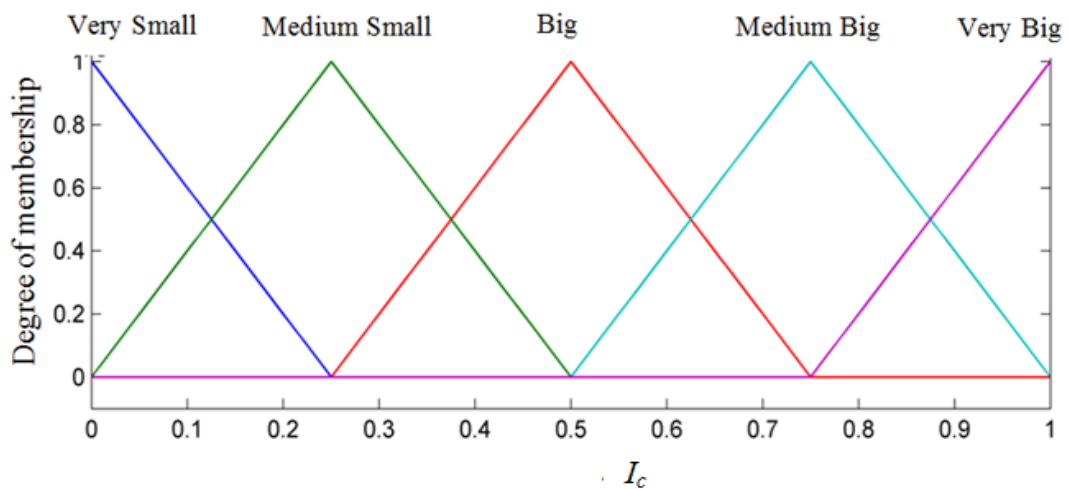
Figure 4.5 Membership function for the coil current Ic (pu)
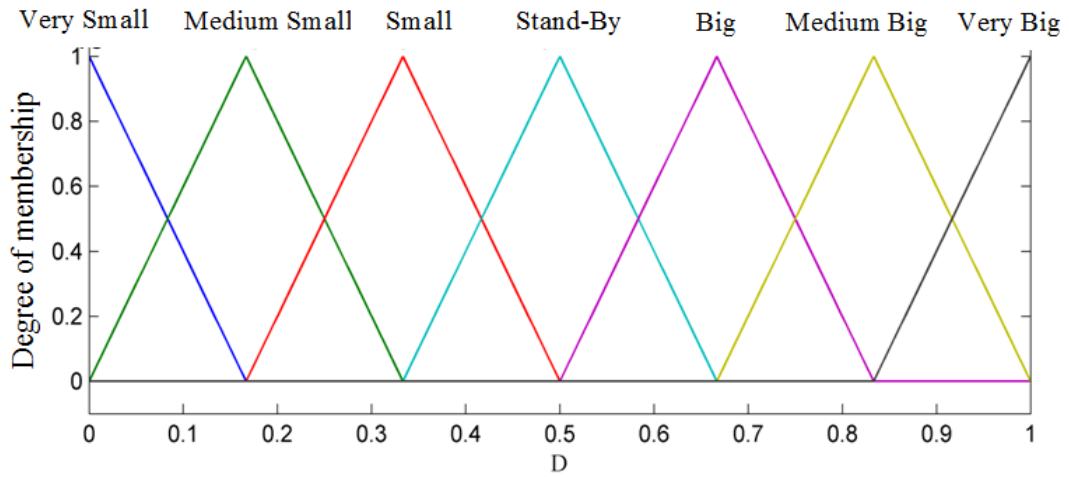
Figure 4.6 Membership function for the duty cycle (*D*)

The Centre-of-Gravity method, widely used in fuzzy logic models, is selected for the defuzzification process, where the desired output, z_0, is calculated as [13]:

$$z_0 = \frac{\int z.\mu_c(z)dz}{\int \mu_c(z)dz} \tag{4.3}$$

A set of fuzzy logic rules, in the form of (IF-AND-THEN) statements relating the input to the output variables, is developed using the graphical user interface tool provided by MATLAB. The model output, D, for any set of the 2 input parameters, Pg and Ic, can be determined using the 3D surface graphs shown in Figure 4.7 or the rules shown in Figure 4.8.
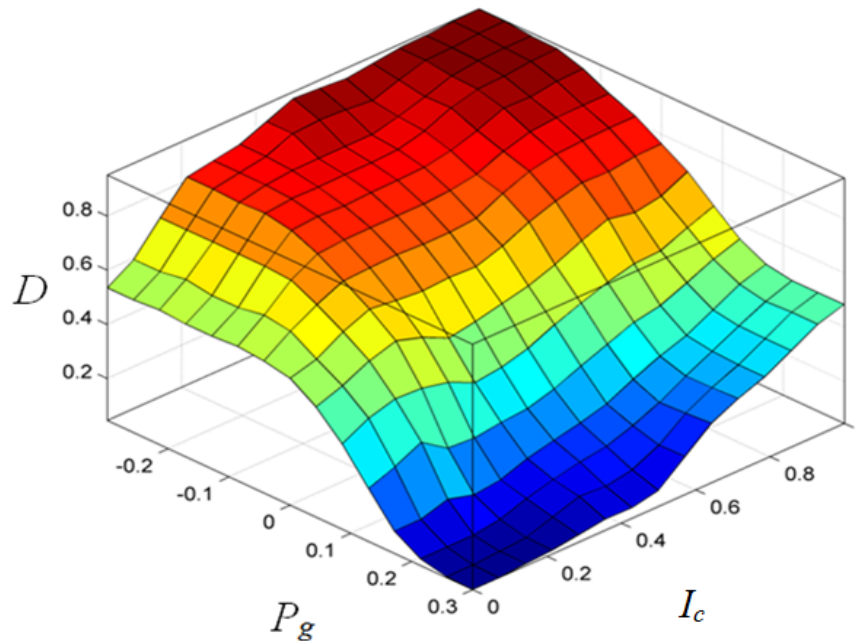
Figure 4.7 Surface graph relating the input parameters with the duty cycle
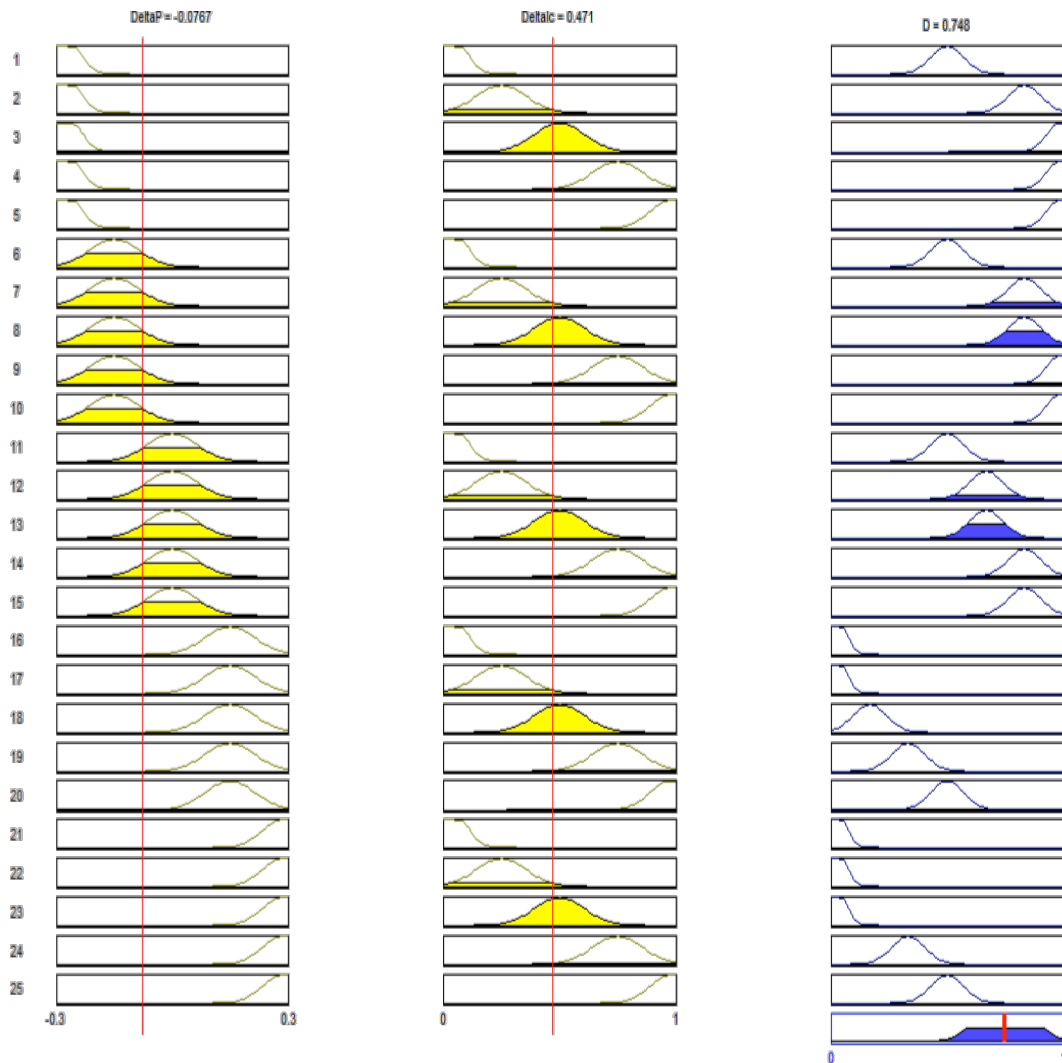
Figure 4.8 Fuzzy logic rules relating the two input parameters with the duty cycle

4.2.1   Coil Operational modes

Based on the system's condition, the proposed coil has three modes of operation. These are described in sections (4.2.1.1) to (4.2.1.3).

4.2.1.1 Freewheeling Mode (Standby)

The standby operational mode of the coil is shown in Figure 4.9. This operating mode takes place at normal condition and after the fault clearance. During standby mode, the value, *D,* is maintained at 0.5, and according to (4.1), voltage across the coil is zero while the coil current is held constant at its rated value. As a result, there is no energy exchange between the coil and the grid, and maximum energy is stored within the coil [12].

4.2.1.2 Discharging Mode

The discharging operational mode of the coil is shown in Figure 4.10. This mode occurs during fault events within the grid, where extra power is needed to maintain system stability. The value of the duty cycle will vary between the range 0 to 0.5, which will result in negative voltage across the coil. Because the current passing through the coil is unidirectional, stored energy in the coil is discharged into the system, and the current (I_c) is reduced, creating a negative slope (*di/dt*). The amount of energy exchanged is determined by the value of the duty cycle. According to FLC rules, the coil is recharged after the fault clearance [13].
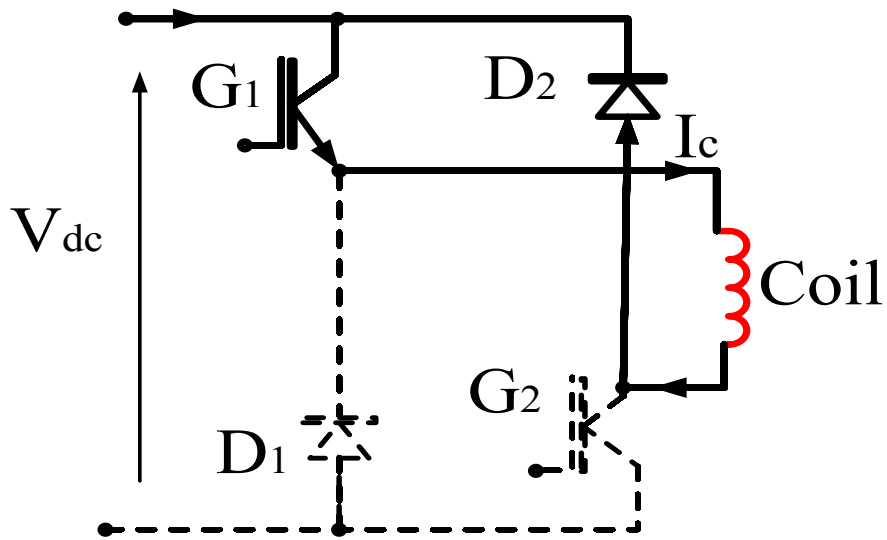
Figure 4.9 Freewheeling mode
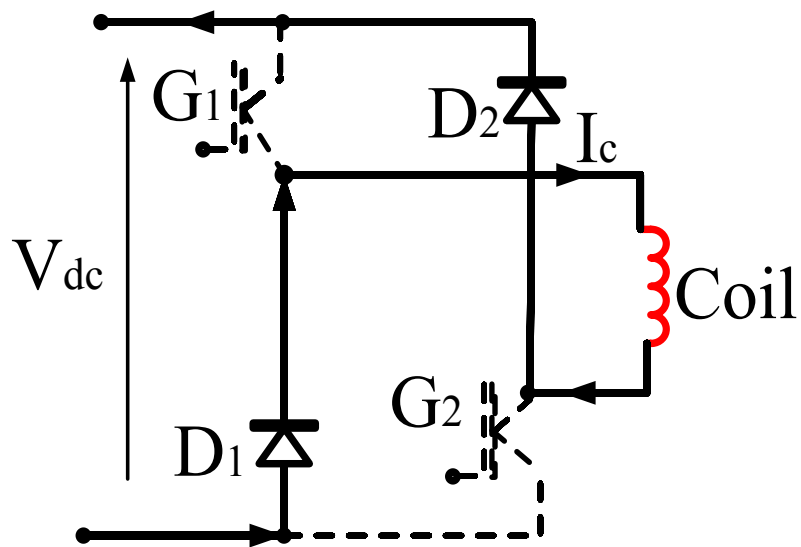
Figure 4.10 Discharging mode

4.2.1.3 Charging Mode

With some grid fault disturbances, such as voltage swell or significant load shedding, a surplus power will flow in the grid. During such events, the coil-charging mode of operation is activated. During this mode, the FLC controls the value of *D* to be within the range 0.5 to 1. The coil current is increased, making a positive slope (*di/dt*), and the voltage across the coil becomes positive to enable power exchange from the grid to the coil (as seen in Figure 4.11) [12].
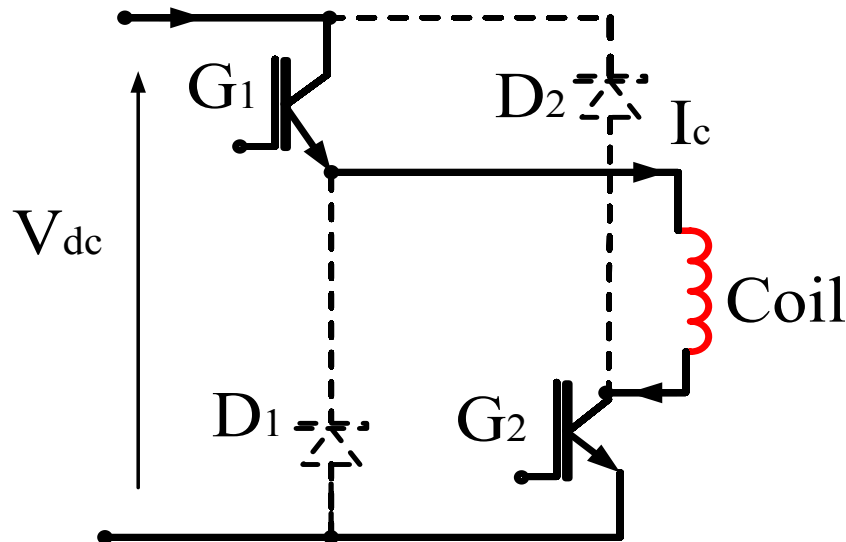
Figure 4.11 Charging mode

4.3   System under Study

Figure 4.12 (a) shows the system under study, which consists of six 1.5-MW DFIGs connected to the AC grid at the PCC. The grid is represented by an ideal three-phase voltage source of constant frequency, and it is connected to the wind turbines via a 30-km transmission line and step-up transformer. During normal operating conditions, reactive power produced by the wind turbines is regulated at zero MVar to maintain unity power factor connection. At an average wind speed of 15 m/s, which is the example wind speed used in this study, the turbine output active power is 1.0 pu and the rotor shaft speed is 1.2 pu. A coil is connected to the DC-link of the DFIG's back-to-back power converters with a DC-DC chopper (as shown in figure 4.1). All parameters of the system under study are given in Appendix A.

4.4   Simulation Results and Discussion

Extensive simulation analyses were carried out to assess the robustness of the new proposed topology, along with the developed control system. Various disturbance

scenarios were simulated on the system under study, and the overall performance of the DFIG - with and without the coil - was investigated and compared. Simulation was carried out using MATLAB/Simulink.
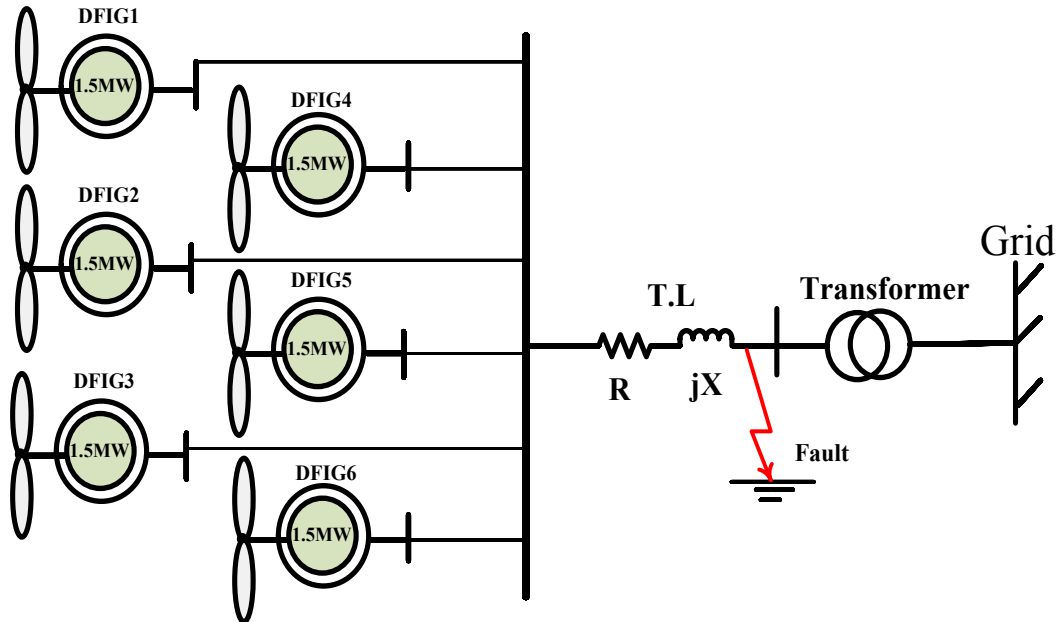
Figure 4.12 System under study

4.4.1 Case Study 1: Double Line to Ground Intermittent Fault (2L-G)

The purpose of this case study is to test the performance of the studied system when a double line (phase A and phase B) to ground (2L-G) fault takes place at the grid side (as shown in Figure 4.12 (a)). The fault starts at t = 3 sec and continues for a duration of 50 msec. Figures 4.13 through 4.20 show the performance of the studied system - with and without the proposed coil - during such an event. Figure 4.13 (a,b) shows the three phase instantaneous voltage at the PCC with and without the coil. Figure 4.13 (c) shows the root mean square (rms) voltage of phase A, indicating the voltage at the PCC drops to 0.4 pu when the proposed coil is not used. By integrating the coil within the DFIG converters, the voltage at the PCC is raised to 0.7 pu. This is due to the extra reactive power support from the coil.

Compared with the Fault Ride Through of Spain and Germany, the LVRT margin of the two grid codes is violated when the coil is not connected (as shown in Figure 4.14). This calls for the disconnection of the wind turbine from the grid using the crowbar protection circuit. However, with the proposed converter station topology, the voltage drop decreases to a safe level within grid connection requirements (Figure

4.14), and wind turbine connection to the grid is maintained.
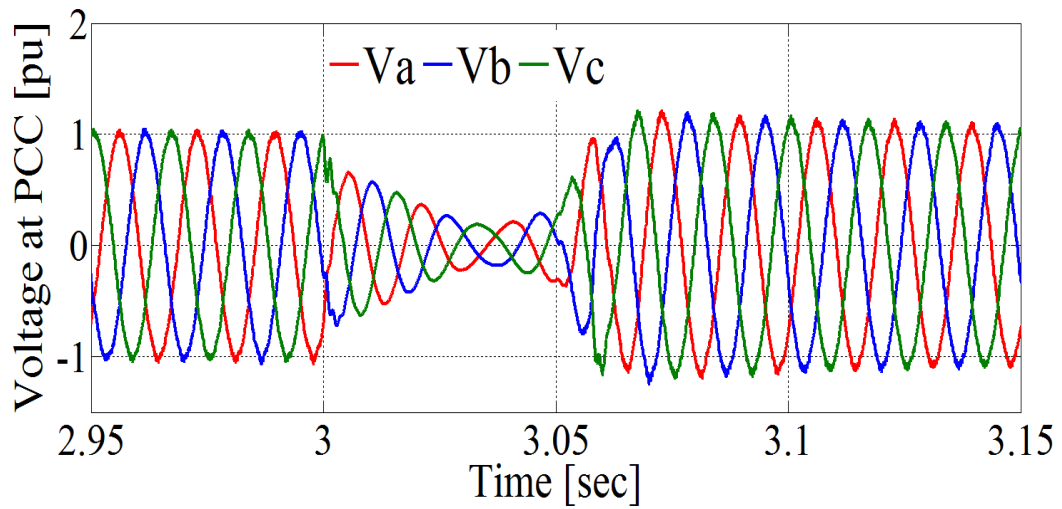
Figure 4.13 (a) Three-phase voltage profile at the PCC without coil
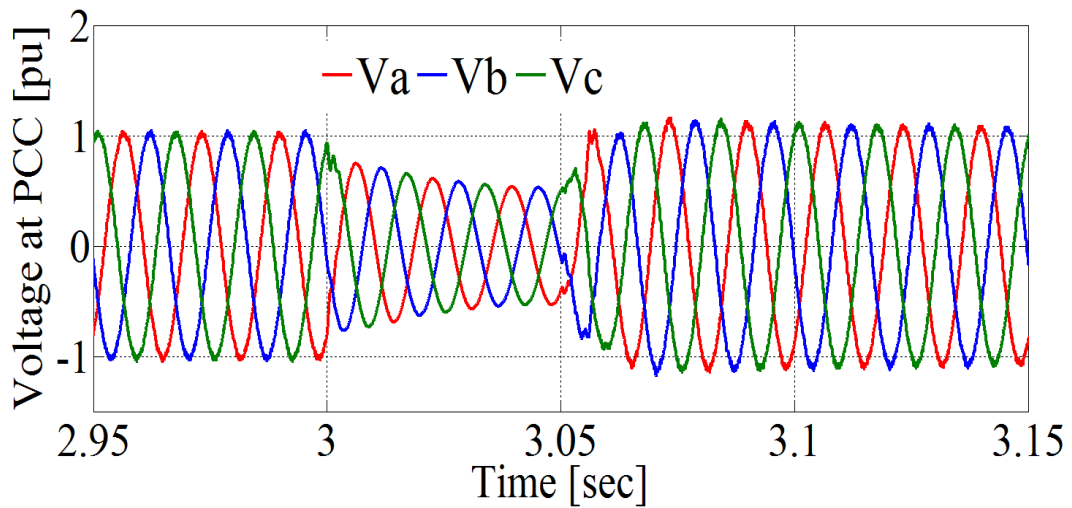
Figure 4.13 (b) Three-phase voltage profile at the PCC with coil
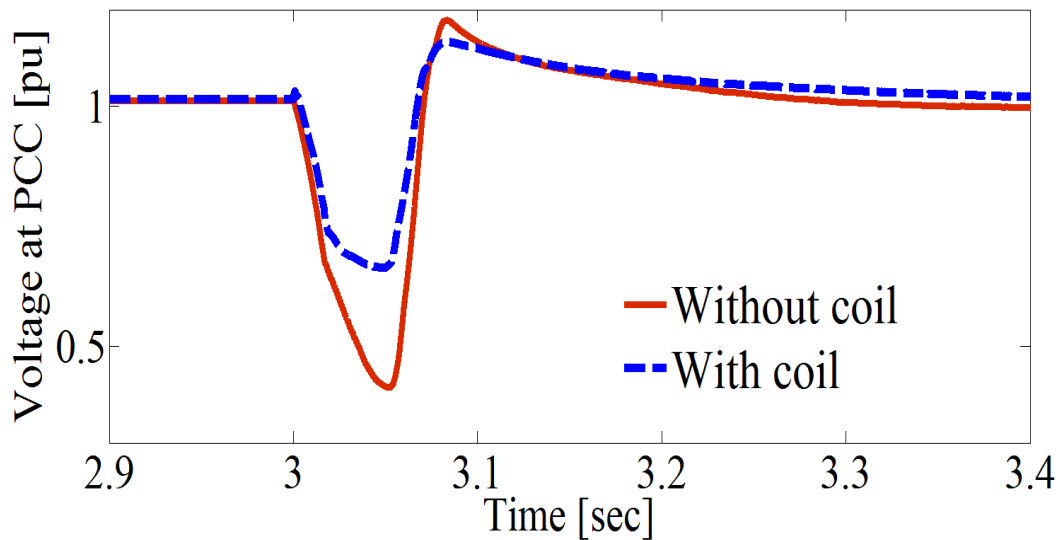
Figure 4.13 (c) RMS voltage of phase A at the PCC
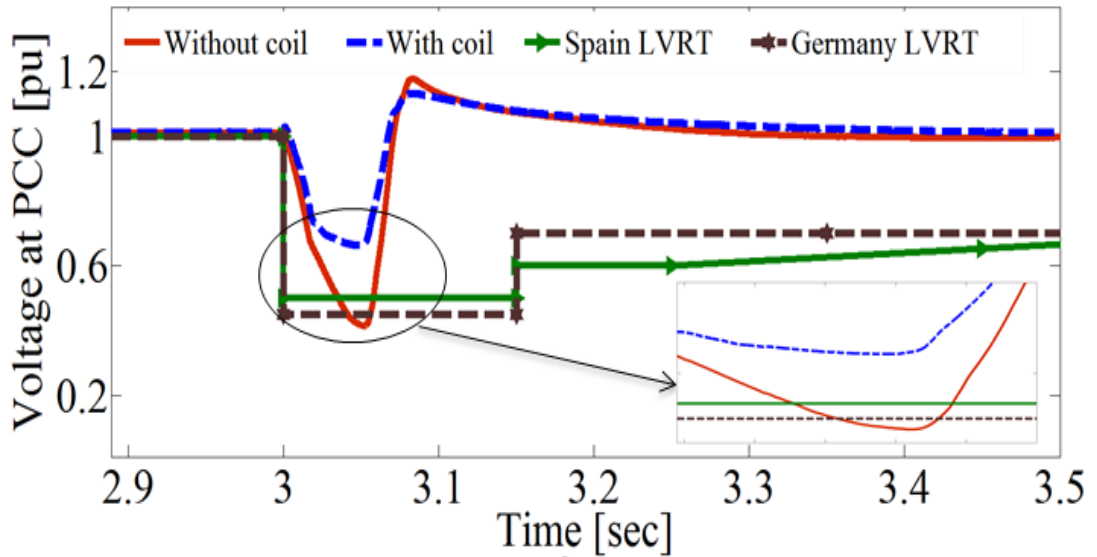
Figure 4.14 PCC voltage compliance with Spain and Germany LVRT

Without connection of the coil in this grid fault scenario, active power at the PCC falls to -0.4 pu. This indicates the DFIG is absorbing active power from the grid and working as a motor (as shown in Figure 4.15). When the coil, however, is integrated within the DFIG converters, the active power at the PCC is modulated to 0.1 pu (as shown in Figure 4.15). Figure 4.16 shows the reactive power at the PCC - with and without the integration of the coil - and also the surplus reactive power, compensated by the coil.
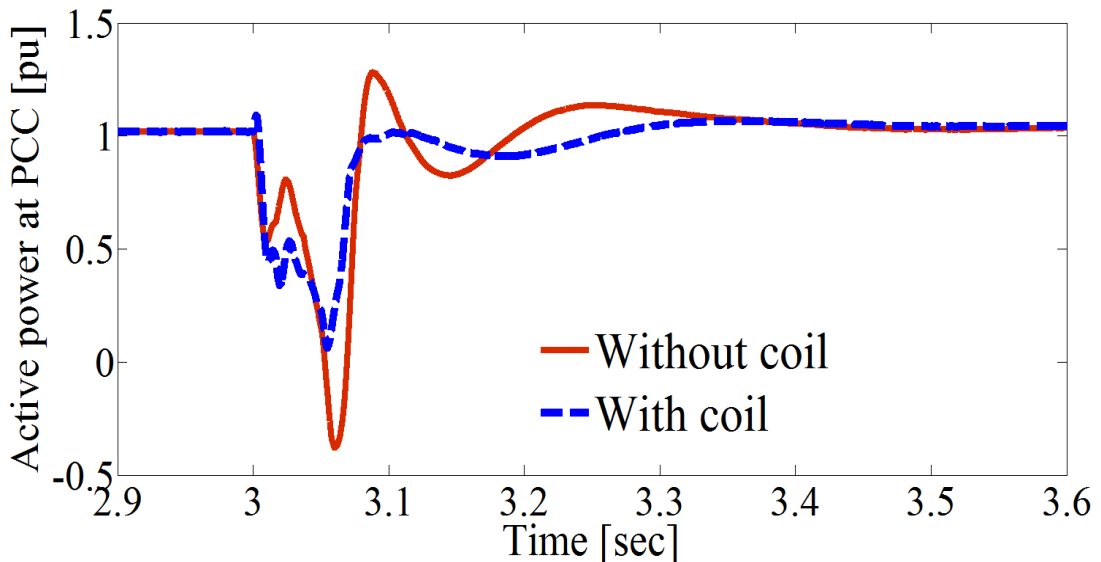
Figure 4.15 Active power at the PCC
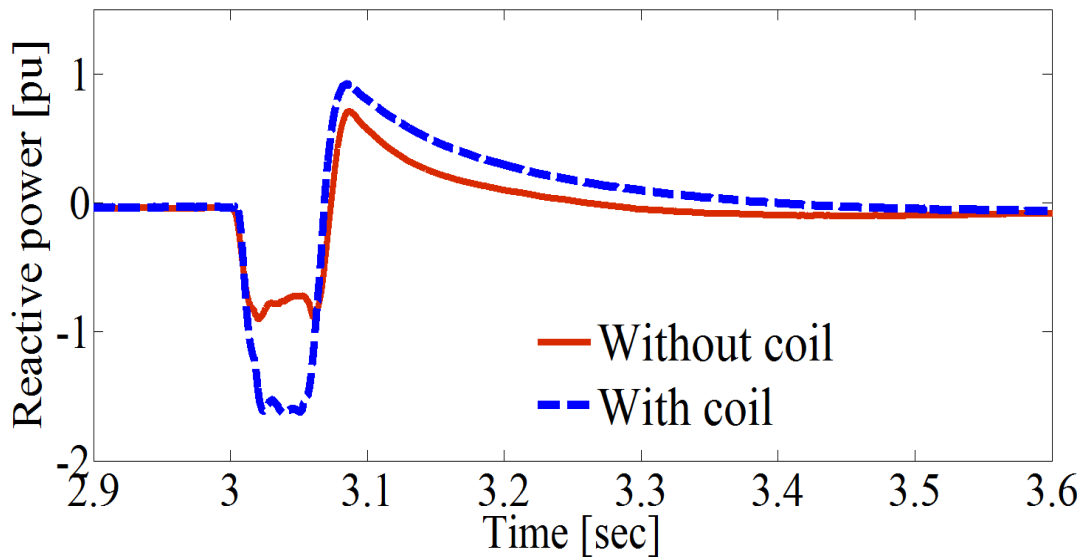
Figure 4.16 Reactive power at the PCC

To compensate for the sudden drop in generated active power within the DFIG, the DFIG's shaft speed accelerates (as shown in Figure 4.17). Figure 4.17 also shows that the generator's shaft speed reaches a crest value of 1.3 pu. When the proposed coil is connected, however, maximum overshooting in the speed is reduced, as well as the settling time (as shown in Figure 4.17). The same trend can be observed in the shaft's mechanical torque (as shown in Figure 4.18).
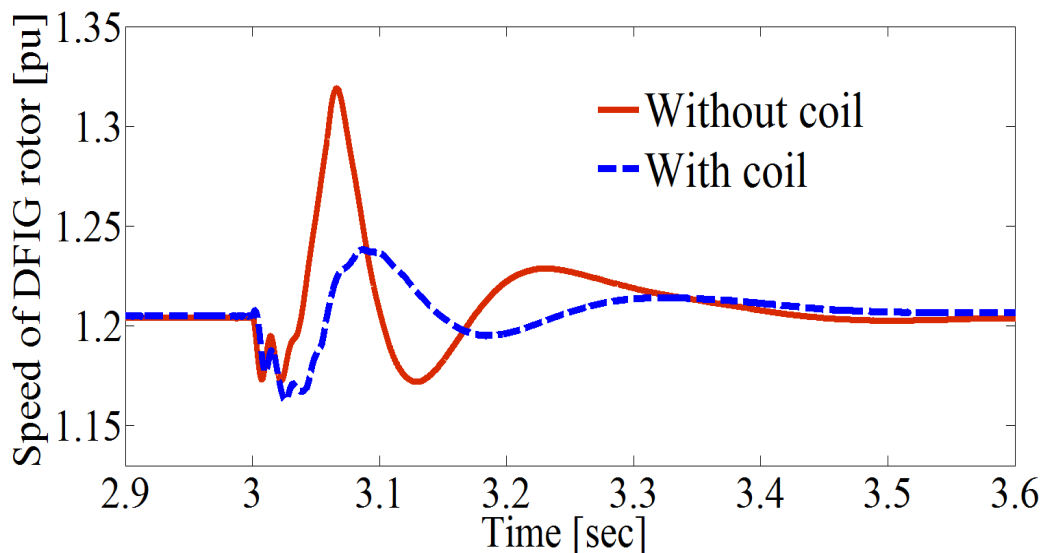
Figure 4.17 Speed of the DFIG rotor

Figure 4.19 (a-c) and Figure 4.20 respectively show the stator current and electromagnetic torque with and without the integration of the coil. As shown in the figures, maximum overshooting and settling time, in both cases, are lessened due to the extra power compensation of the proposed integrated coil.
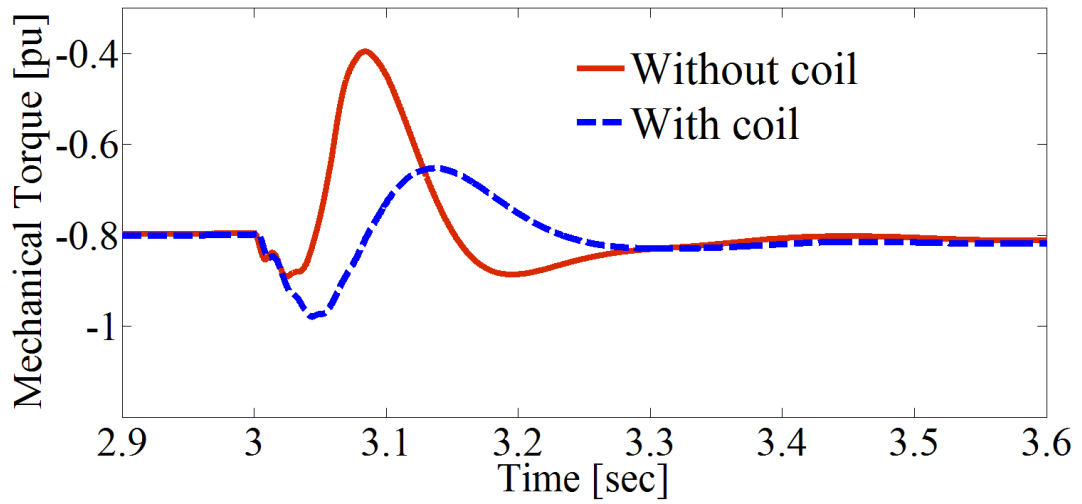
Figure 4.18 Shaft's mechanical torque
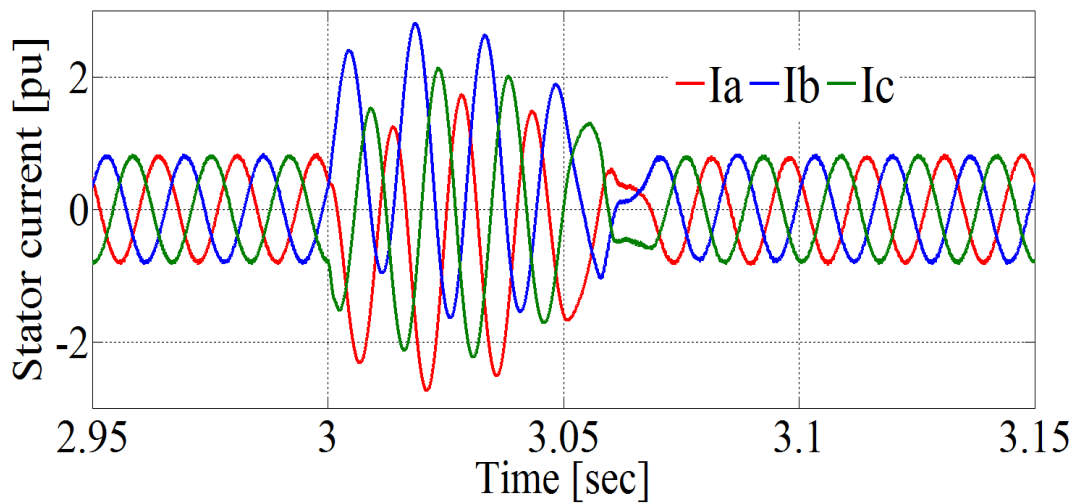
Figure 4.19 (a) Stator three-phase currents without coil
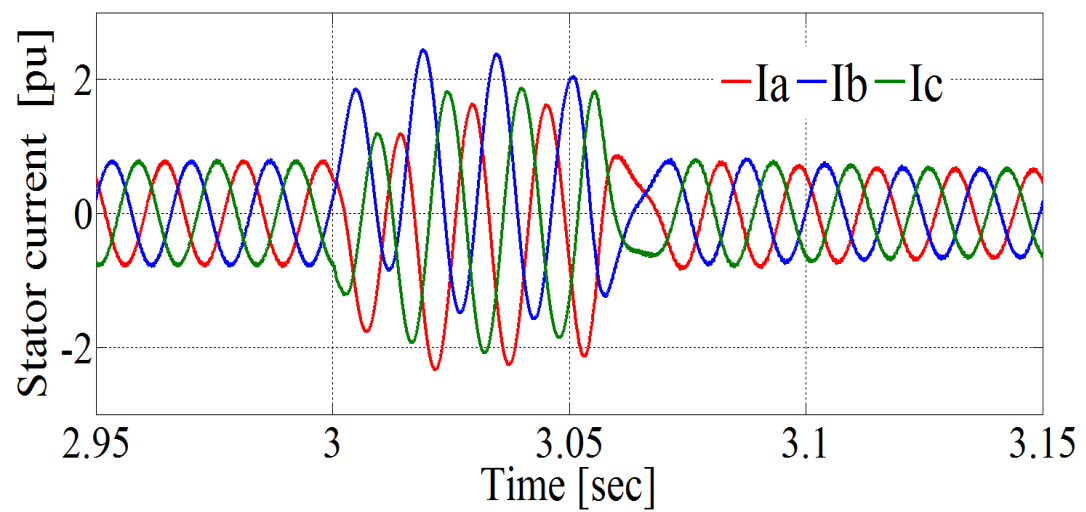
Figure 4.19 (b) Stator three-phase currents with coil
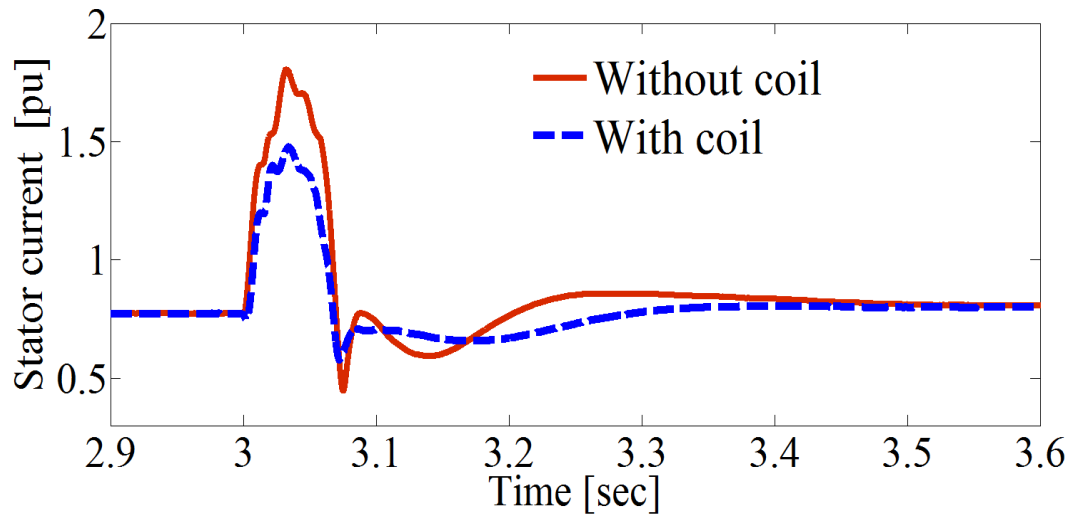
Figure 4.19 (c) Stator Phase A rms current
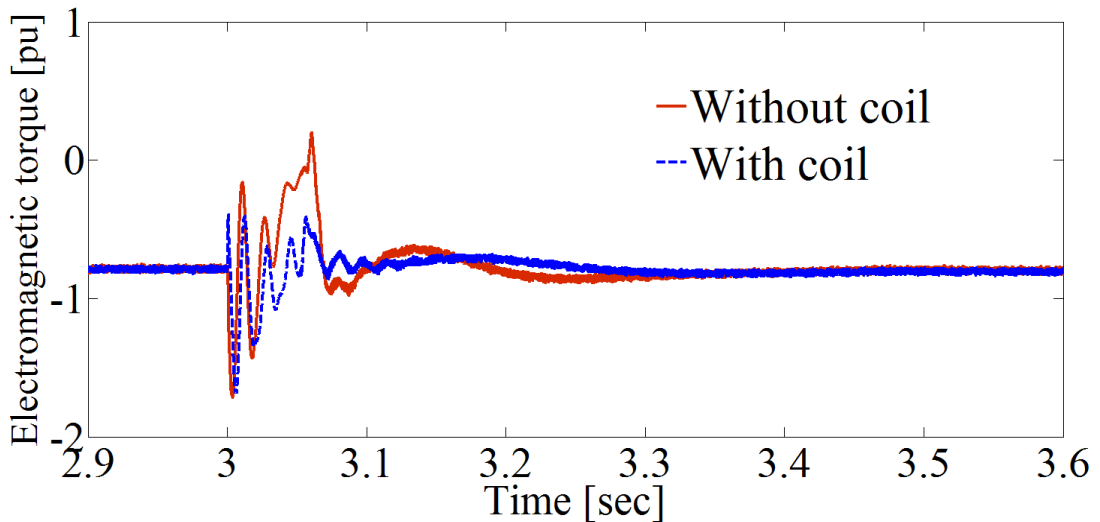
Figure 4.20 DFIG electromagnetic torque

The coil's behaviour during a 2L-G fault is investigated in Figures 4.21 (a-c). The figures display the voltage across the coil (V_c), the coil current (I_c), and the stored energy in the coil ($E_c = 0.5L_cI_c^2$) respectively. Before application of the fault, and during normal operation, the developed fuzzy logic controller maintains the duty cycle, *D,* at 0.5, which leads to zero voltage across the terminals of the coil. The zero voltage level corresponds to both the maximum coil current and the rated stored energy (as seen in Figure 4.21 (c)). After the 2L-G fault occurs, the fuzzy logic controller reduces the duty cycle to a value between 0 and 0.5 (depending on the amount of power required by the grid). Duty cycle (*D*), in this range, creates a negative voltage across the coil, and the unidirectional current exhibits a negative slope, allowing a portion of its stored energy to be delivered to the grid. As the fault is cleared at t=3.05 sec, the fuzzy logic controller retains the *D* level at 0.5.
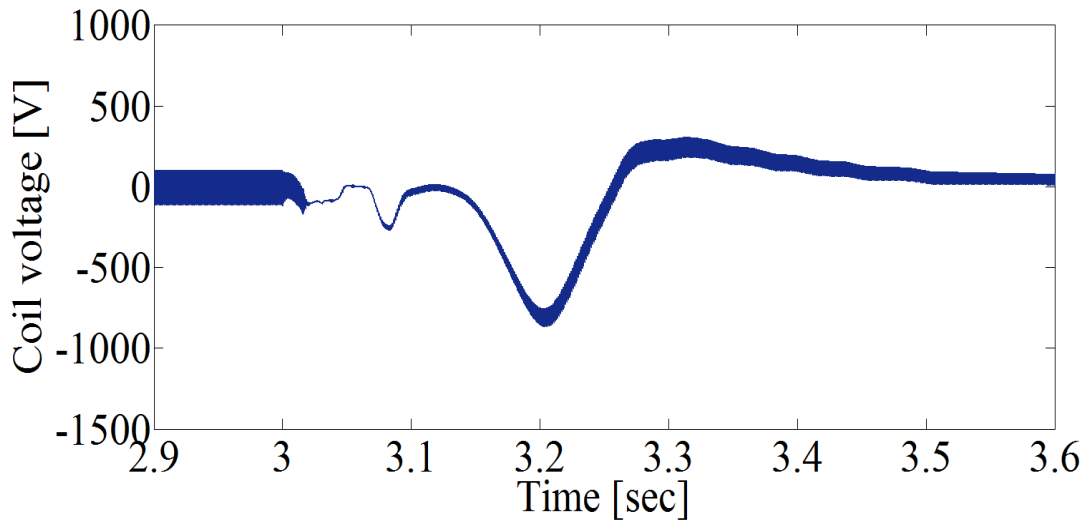
Figure 4.21 (a) Voltage across the coil
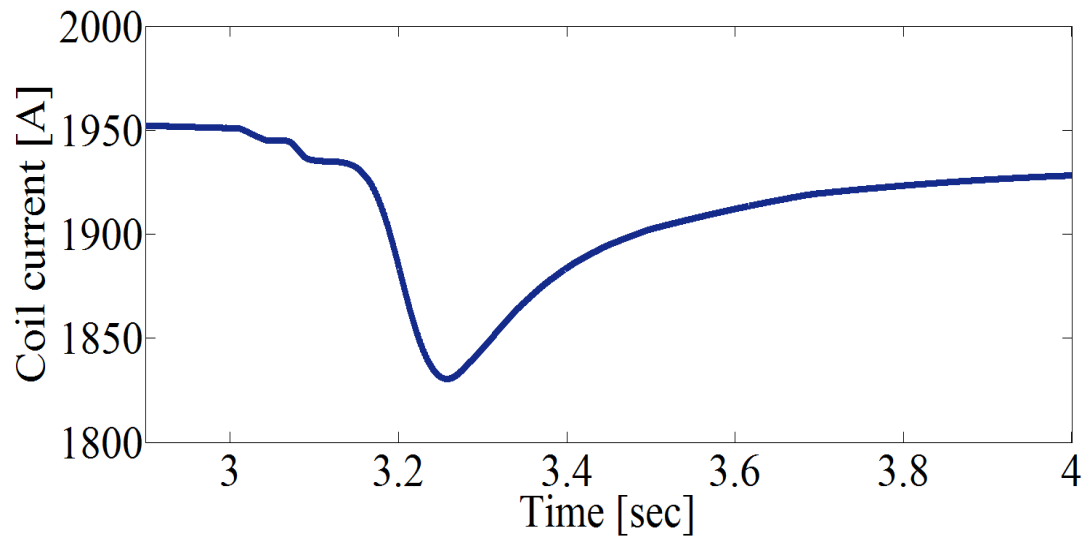
Figure 4.21 (b) Coil current
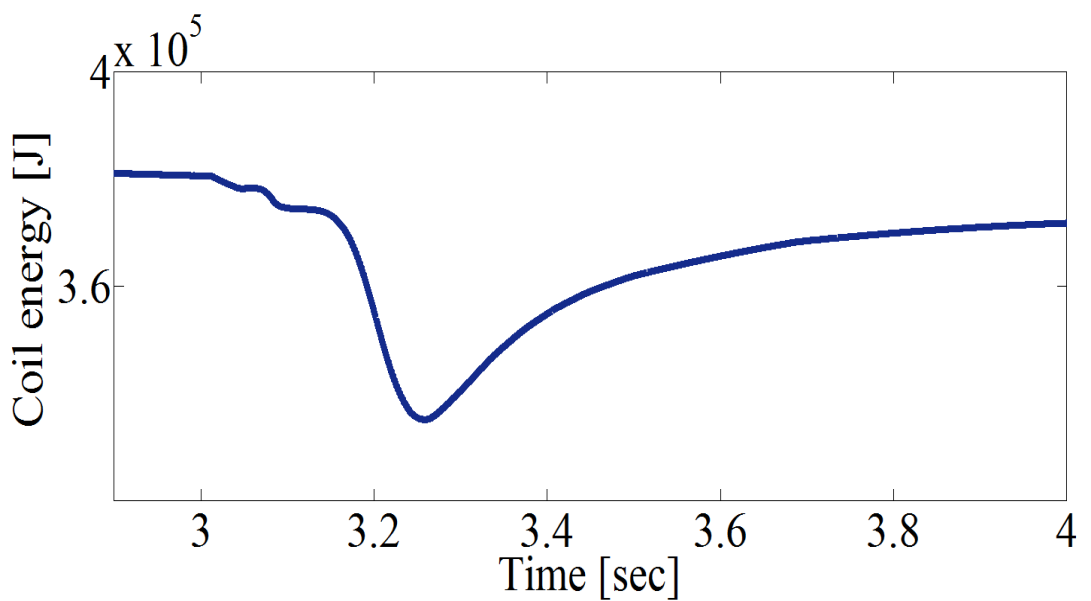
Figure 4.21 (c) Stored energy of the coil

4.4.2   Case Study 2: Voltage Sag

Voltage sag is one of the key issues affecting power system quality, and may occur due to short circuit faults or a sudden increase in the load [13]. Voltage sag is a decrease in the root mean square (rms) value (0.1 to 0.9 pu) for a short duration (0.5 sec to several seconds) [111]. Several studies in the literatures agree that voltage sags cause 92% of defects in electric distribution systems [111, 112]. To investigate the effectiveness of the proposed topology, and to improve the overall performance of the studied system under voltage sag conditions, the voltage sag of 0.2 pu at the grid side, lasting for 3 cycles, starts at t=5.0 sec. Figures 4.22 through 4.27 show the performance of the studied system - with and without the proposed coil - during this disturbance event.

As seen in Figure 4.22, the voltage profile at the PCC, without the use of the proposed coil, drops to 0.36 pu due to the fault. However, by integrating the coil within the DFIG converters, dropped voltage at the PCC is modulated to 0.52 pu. This is due to the extra reactive power support from the coil. Compared to the Fault Ride Through of Germany, the voltage at the PCC violates the LVRT code when the coil is not integrated within the converters (as shown in Figure 4.23). After the coil is connected, however, voltage drop decreases to a safe level within grid connection requirements (Figure 4.23), and wind turbine connection to the grid is maintained.
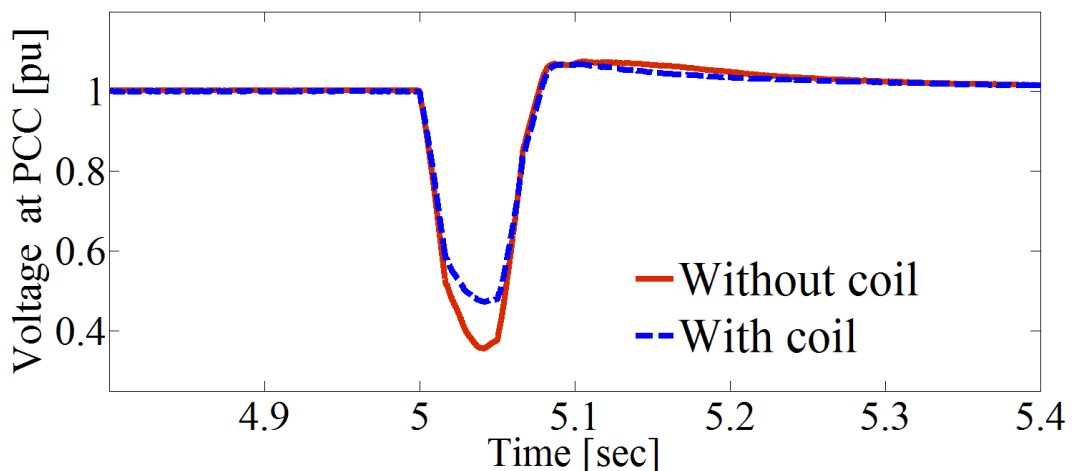
Figure 4.22 Voltage profile at the PCC

Without the connection of the coil in this fault scenario, real power at the PCC decreases to 0.32 pu (as shown in Figure 4.24). When the coil is integrated within the DFIG converters, the active power at the PCC is modulated to 0.69 pu (as shown in

Figure 4.24). Figure 4.25 shows reactive power at the PCC with and without the integration of the coil. With the coil, reactive power at the PCC is almost levelled during the fault application.
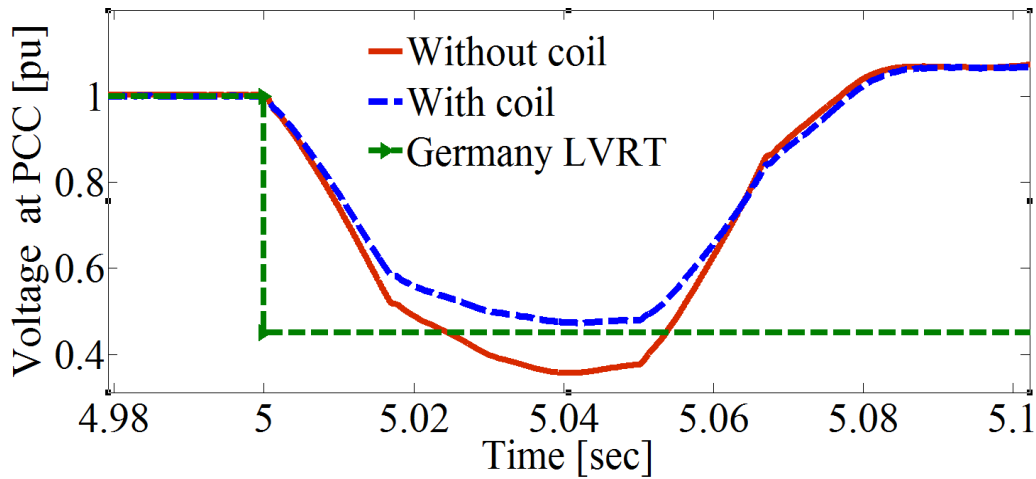
Figure 4.23 PCC voltage compliance with Germany LVRT
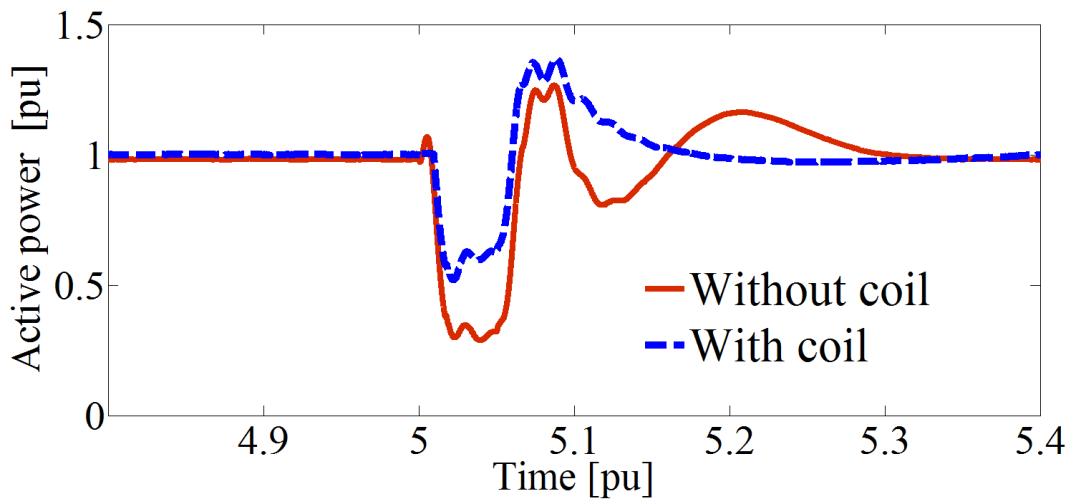
Figure 4.24 Active power at the PCC
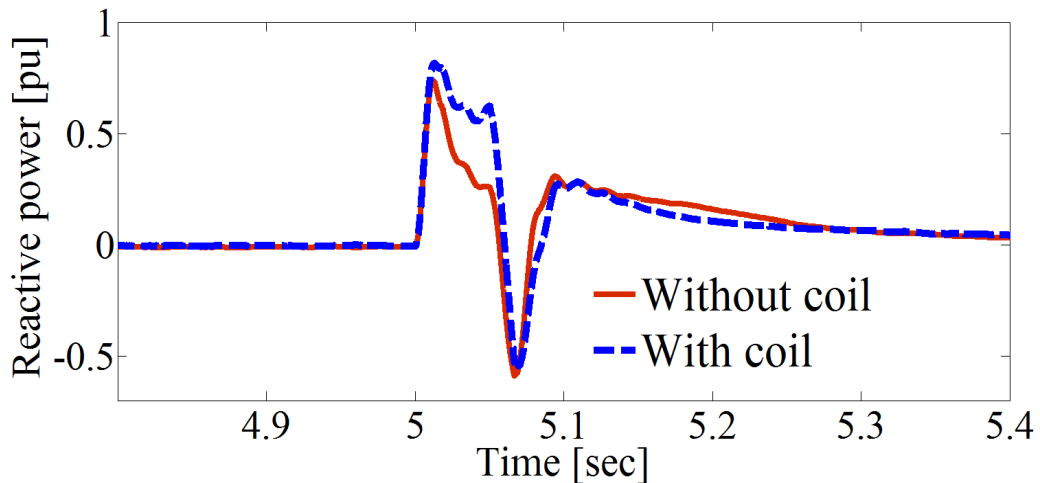
Figure 4.25 Reactive power at the PCC

The drop in DFIG-generated active power causes the speed of the generator to accelerate, compensating for the power imbalance in the system (as presented in Figure 4.26). Figure 4.26 also shows that generator speed accelerates to reach a crest value of 1.31 pu. When the coil is connected, maximum overshooting in the speed, and also the settling time, are substantially reduced (Figure 4.26). The same tendency can be observed in the shaft's mechanical torque (shown in Figure 4.27).
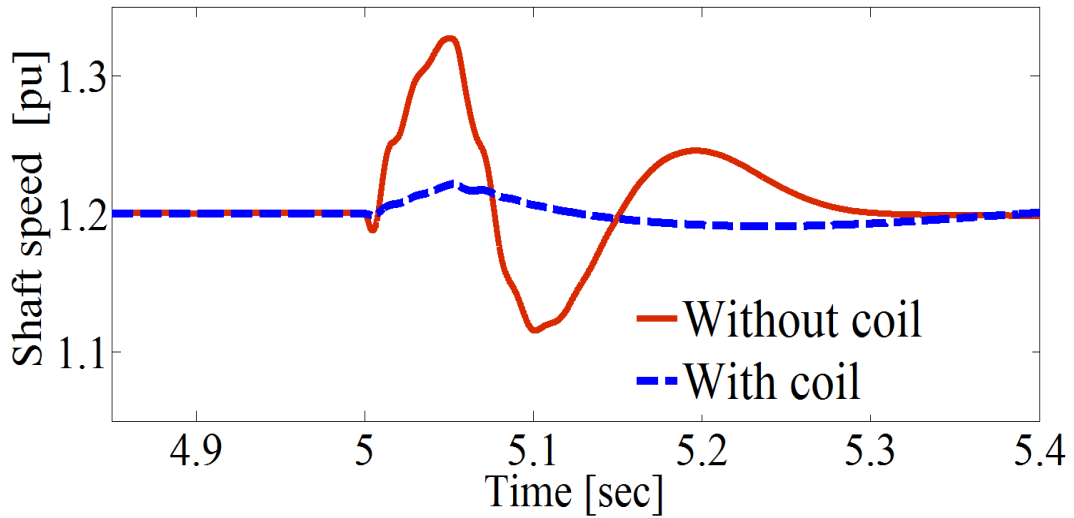
Figure 4.26 DFIG shaft speed
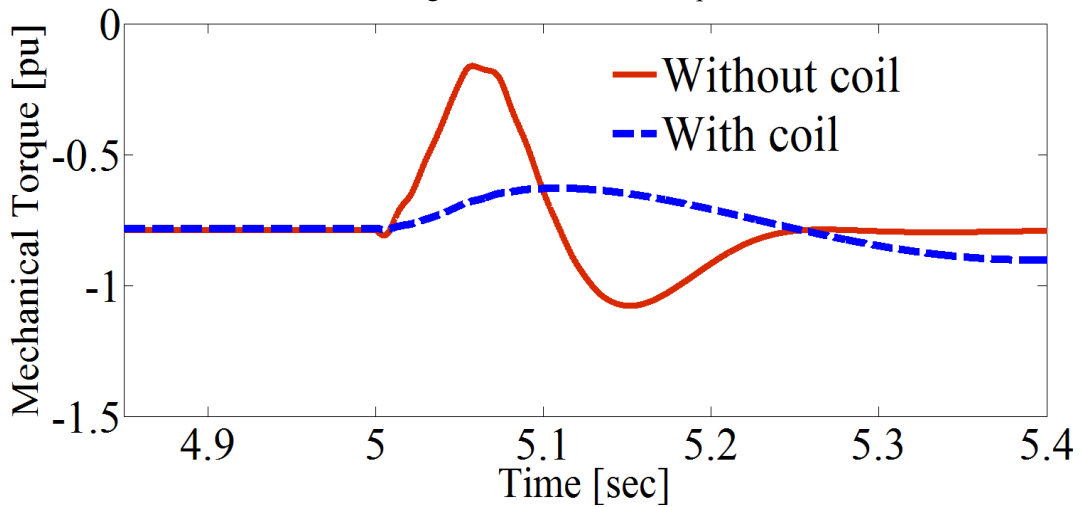
Figure 4.27 Shaft's mechanical torque

The coil's performance during the voltage sag can be observed in Figures 4.28 (a-c). These figures respectively show coil voltage, coil current and the coil's stored energy in three different modes (pre-fault, during fault and post fault). Before the fault application and during normal operating conditions, coil voltage is equal to zero, and coil current is kept constant at the rated coil current. As a result, there is no energy exchange between the coil and the grid (freewheeling mode). When the voltage sag takes place at t=5sec, coil current exhibits a negative slope (*di/dt*), coil voltage

becomes negative, and the stored energy in the coil is transferred to the electric system (discharging mode). After the fault clearance at 5.05 sec, the coil current rises, and coil voltage changes to positive, allowing energy to transfer from the grid to charge the coil (charging mode). It is worth mentioning here that the coil can be of a very low or zero internal resistance (superconductor), which will decrease the time constant to almost zero and produce a rapid charging and discharging process.
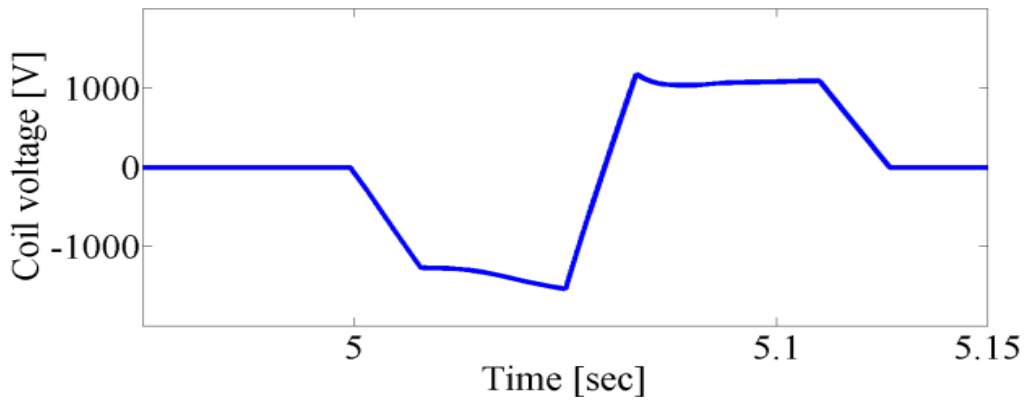
Figure 4.28 (a) Voltage across the coil
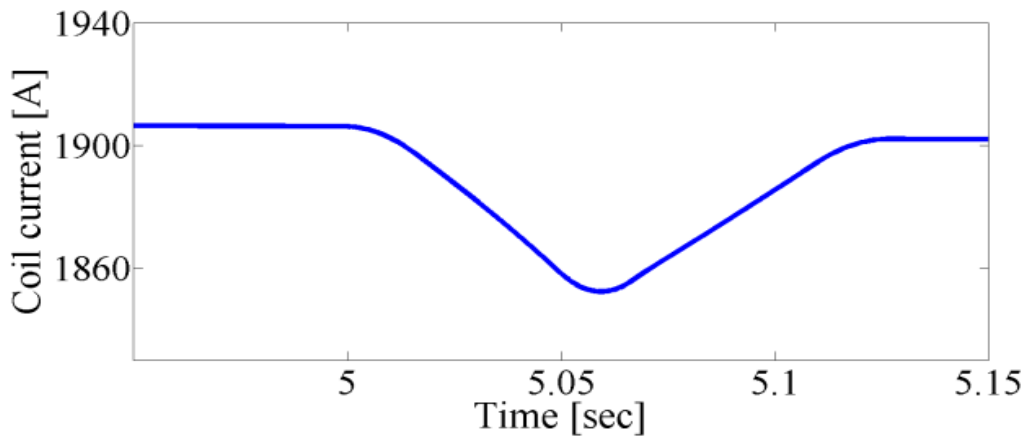
Figure 4.28 (b) Coil current
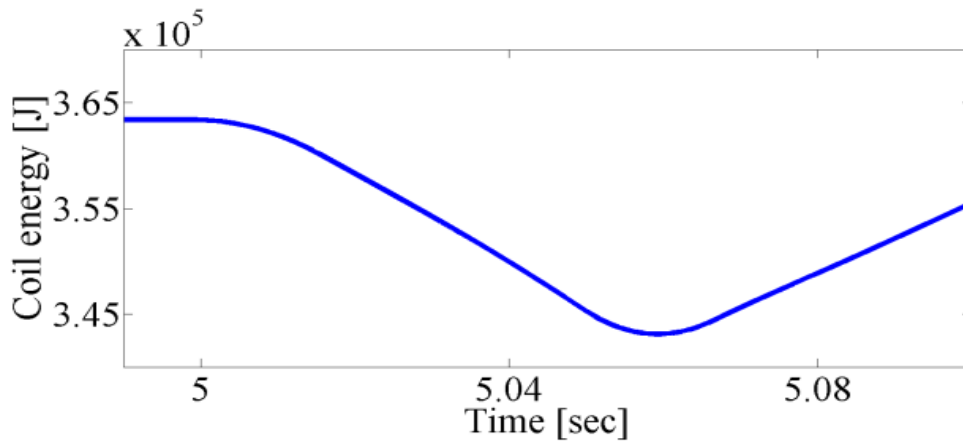
Figure 4.28 (c) Stored energy of the coil

4.4.3   Case Study 3: Three Phase to Ground (3Φ-G) Fault

In this case study, a three phase to ground (3Φ-G) fault takes place at the grid side, at t = 3sec, and continues for 50msec. A DC–DC chopper is used, along with a proportional integral (PI) controller, to regulate the chopper duty cycle (as shown in Figure 4.29). The coil can be charged or discharged by regulating the coil voltage value (V_c) and varying the duty cycle, *D,* of the chopper. The DFIG's active power is used as an input to the PI controller.

As stated above, under normal operating conditions, *D* is equal to 0.5, and power does not pass from the coil to the grid, or in the opposite direction (freewheeling mode). During the fault, the PI controller regulates the value of *D* to be in the range of 0.5–1, and the energy within the coil is discharged into the grid (discharging mode). The coil is charged when the PI controller stabilises *D* within the range of 0.5 to 1. The parameters of the PI controller (shown in Figure 4.29) are given in Appendix B.
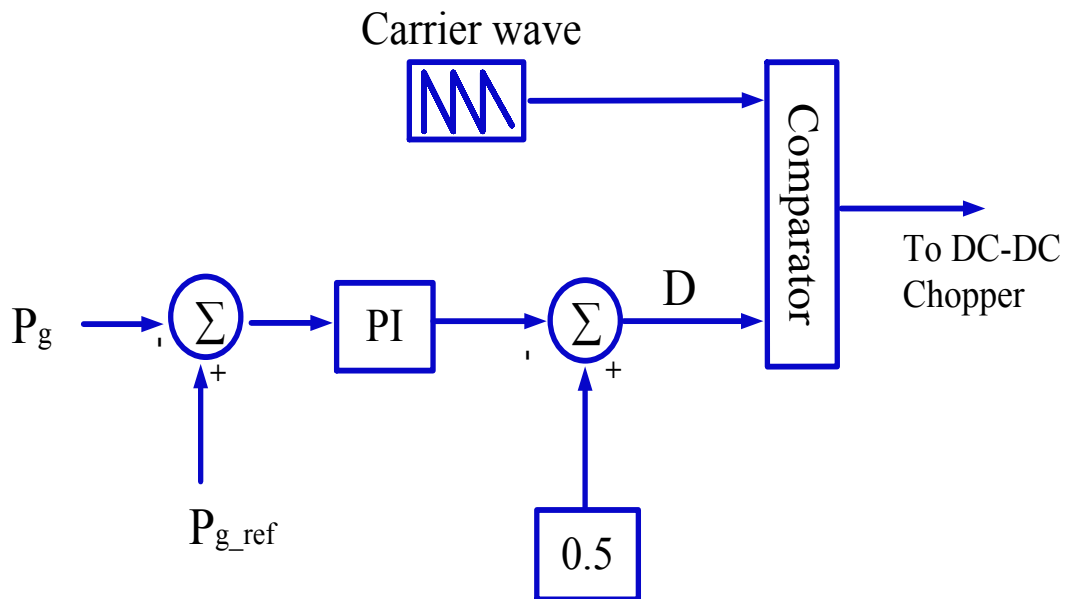
Figure 4.29 Control of the DC–DC chopper

The voltage profile at the PCC is shown in Figure 4.30 (a). It can be seen here that voltage at the PCC drops to 0.19 pu due to the fault. By integrating the coil within the DFIG converters, voltage at the PCC is increased to 0.66 pu. This is due to the reactive power support from the coil. As seen in Figure 4.30 (b), voltage at the PCC violates the LVRT of all mentioned grid codes when the coil is not connected. However, with the proposed topology, the amount of voltage drop is minimised and

reaches a safe level within grid connection requirements (Figure 4.30 (b)).
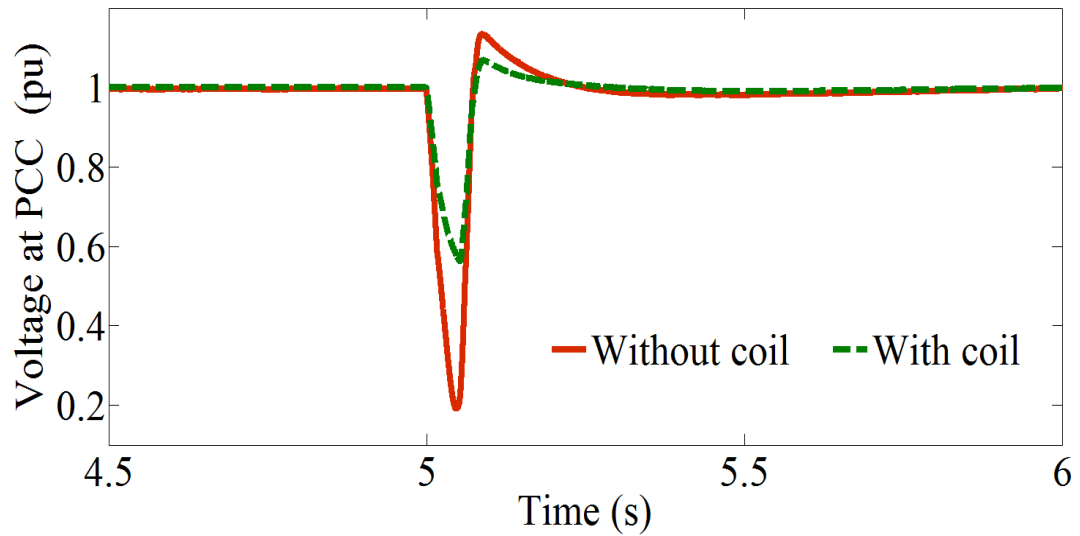
Figure 4.30 (a) Voltage profile at the PCC
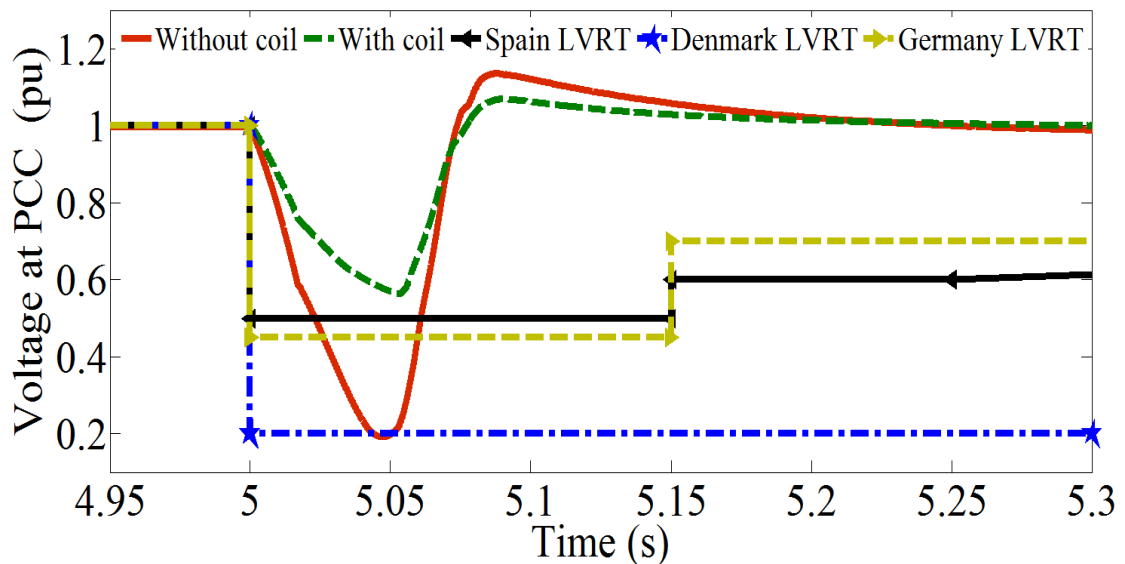
Figure 4.30 (b) PCC voltage compliance with various grid codes

Without the connection of the coil, the fault causes real power at the PCC to drop to -0.76 pu, indicating the DFIG absorbs active power from the grid and runs as a motor (as shown in Figure 4.31). However, when the coil is integrated within the DFIG converters, real power at the PCC is modified to 0.05 pu (as shown in Figure 4.31). Figure 4.32 illustrates the reactive power - with and without the integration of the coil - and shows the amount of surplus reactive power compensated by the coil.
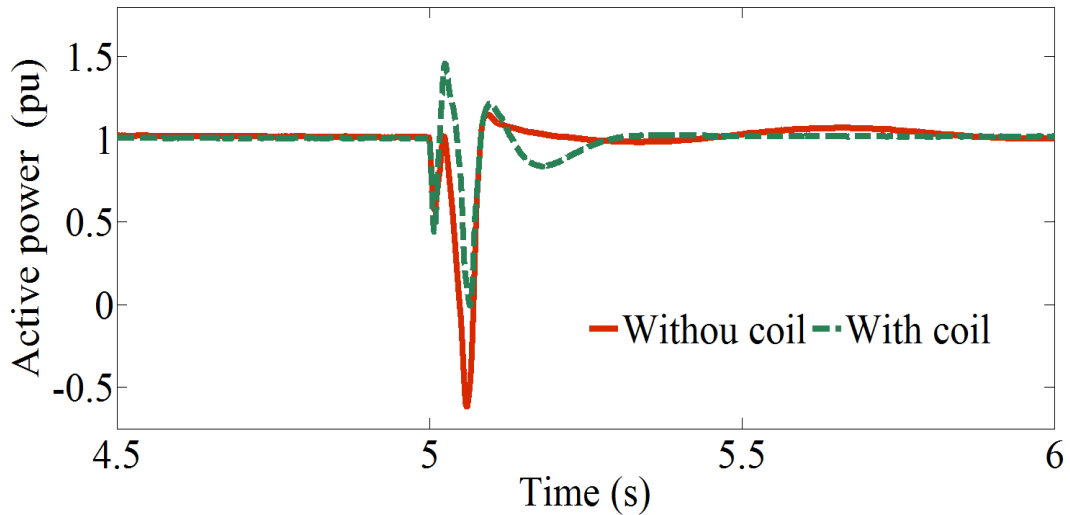
Fig. 4.31 Real power at the PCC
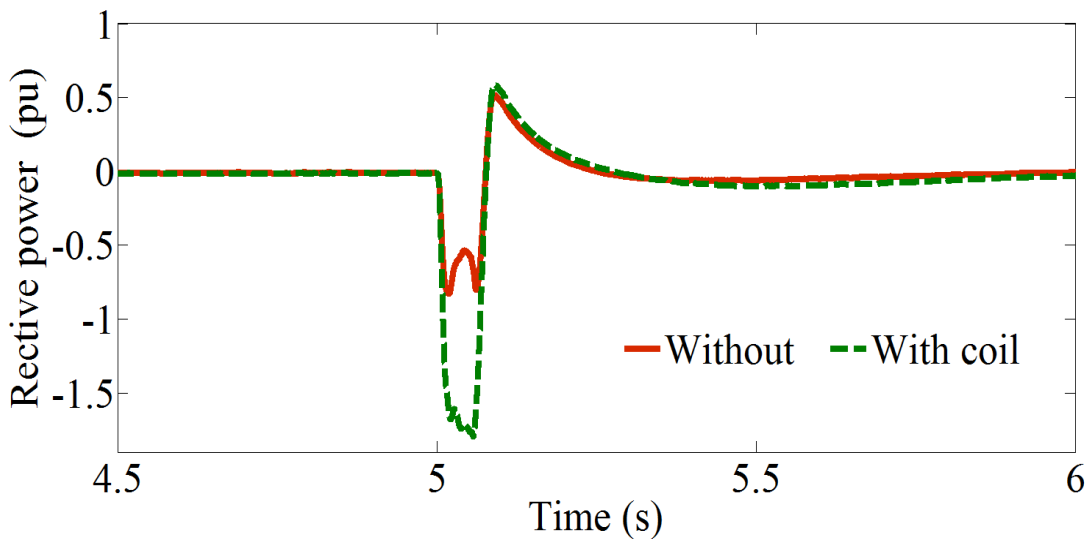
Figure 4.32 Reactive power at the PCC

4.4.4   Case Study 4: Converter Switch Faults

All studies in the literatures consider the impact of grid side faults on the overall performance of a DFIG-based WECS [12]. Few studies, however, have investigated the impact of a converter switch fault on the performance of a DFIG-based WECS, and their proposed solutions are neither efficient nor economical. For example, a STATCOM [21, 25-27]5-8] modulates only reactive power, and a SMES unit [12, 13, 37, 108, 113] is very costly.

In this case study, the proposed coil's ability to mitigate the impact of Fire-through and Misfire, within the voltage source converter (VSC) of the DFIG, is investigated. Fire-through and Misfire are frequent switching faults of the DFIG converter and are produced when the firing circuits malfunction [114]. Fire-through is defined as the

failure to block a valve during a scheduled non-conducting period, and Misfire is defined as the failure to fire a valve during a scheduled conducting period [12]. Some converter malfunctions self-correct if the cause of fault is of a transient nature [115].

Figures 4.33 and 4.34 simulate Fire-through and Misfire faults in IGBT switch number 6 within the GSC and RSC (as shown in Figure 4.35). The faults commence at t=4 sec and clear at t= 4.01sec. As can be seen in Figures 4.33 (a,b), the switching signals from PWM are unsuccessful in blocking the valve for the scheduled non-conducting period in the case of a Fire-through defect. In a Misfire fault, the created switched signals from PWM are unsuccessful in igniting the IGBT valve for the scheduled conducting period (as shown in Figures 4.34 (a,b)).
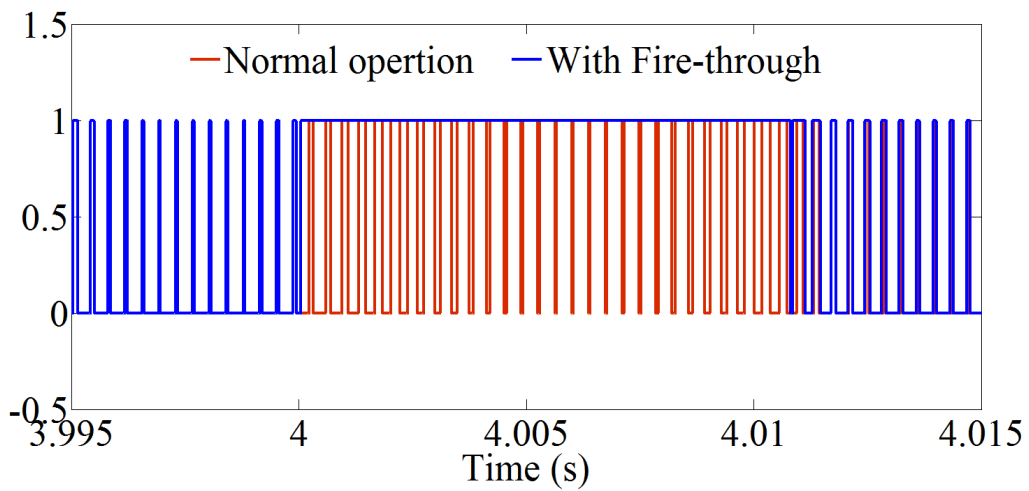
Figure 4.33 (a) Simulation of a Fire-through fault in IGBT-6 of the GSC
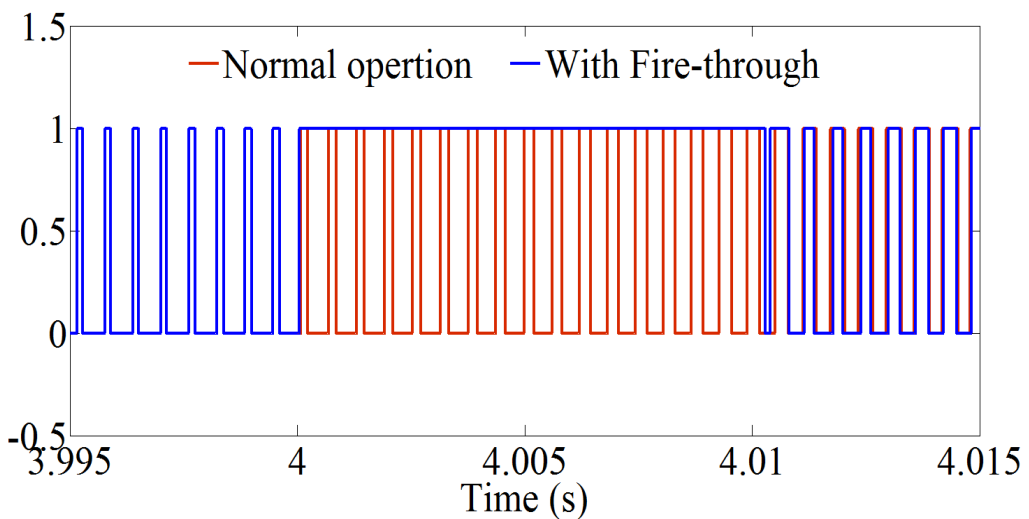
Figure 4.33 (b) Simulation of a Fire-through fault in IGBT-6 of the RSC
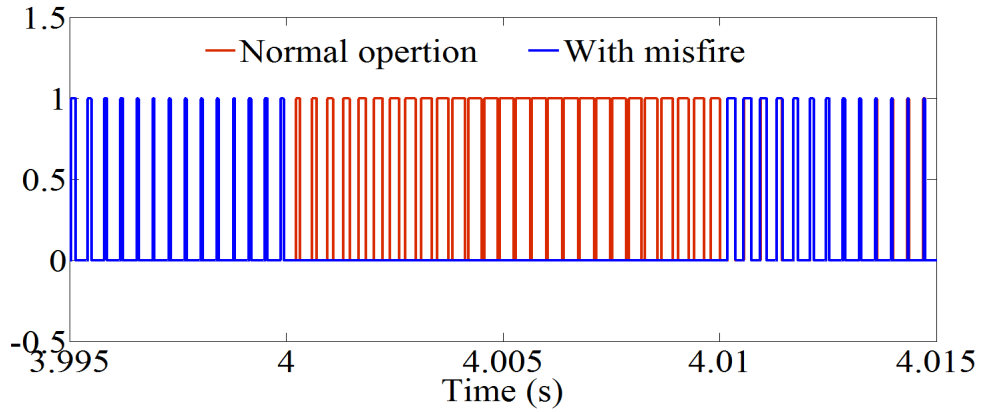
Figure 4.34 (a) Simulation of misfire fault in IGBT-6 of the GSC
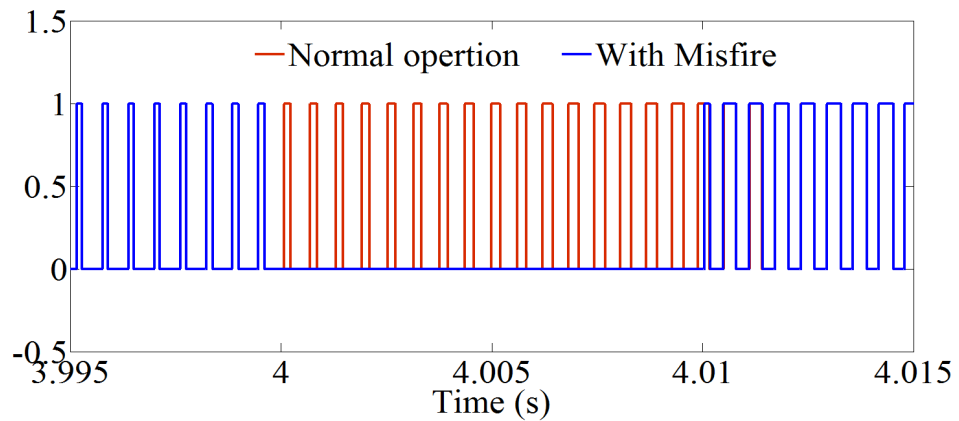
Figure 4.34 (b) Simulation of misfire fault in IGBT-6 of the RSC
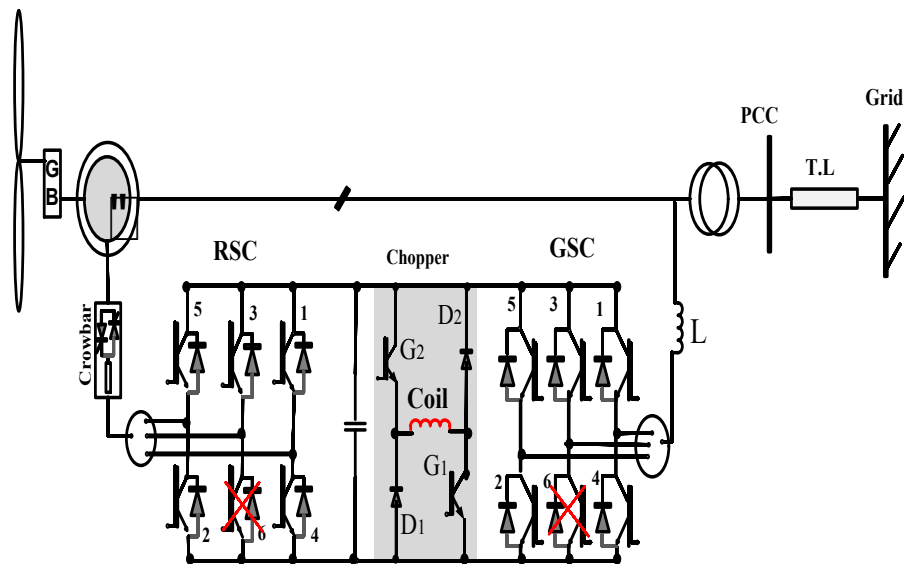
Figure 4.35 System under study for DFIG with Fire-through and Misfire faults

4.4.4.1 Fire-Through and Misfire within the GSC

Intermittent Fire-through and Misfire faults are simulated within the GSC of the studied system in Figure 4.35. The faults occur on switch S6 at t = 8 sec and clear at t = 8.05sec. The model parameters are similar to case study 1. However, the member

functions of the fuzzy set are modified to obtain a better controller performance (as shown in Figures 4.36 to 4.38).
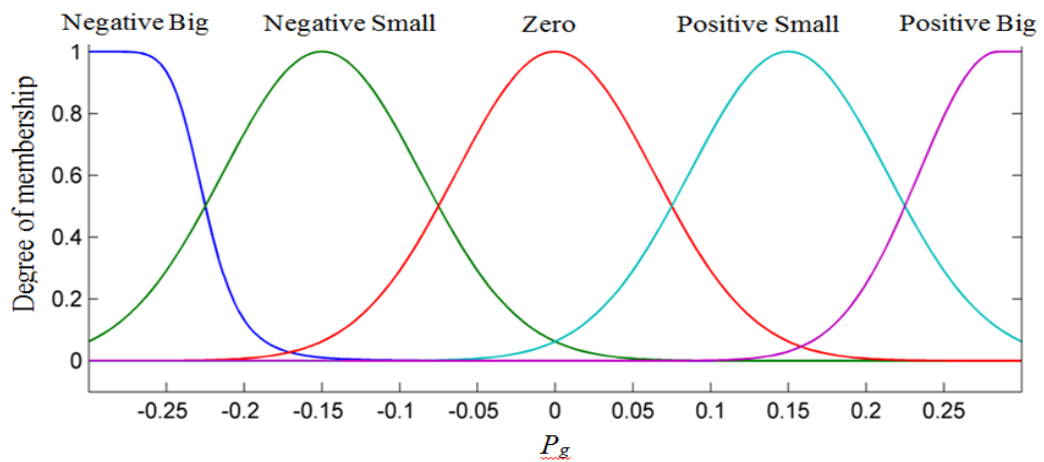
Figure 4.36 Memberships function for P_g (pu)
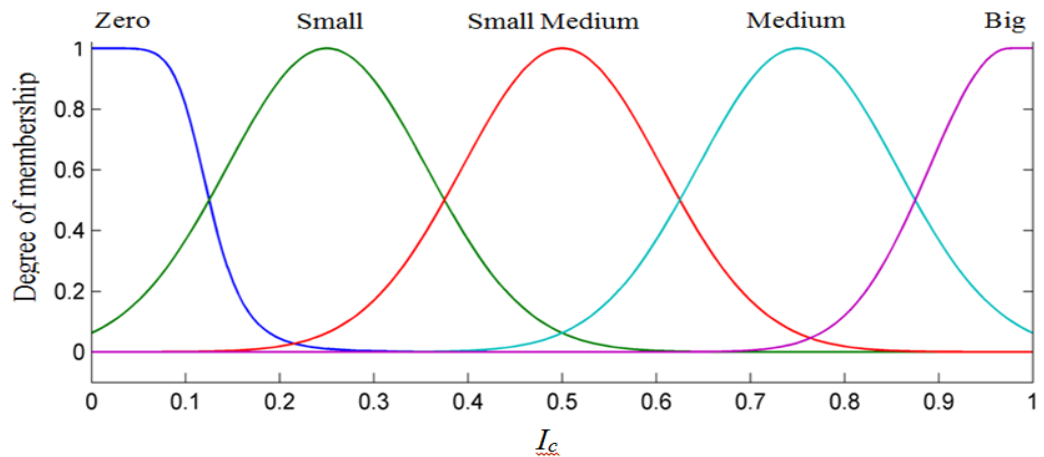
Figure 4.37 Memberships function for I_c (pu)
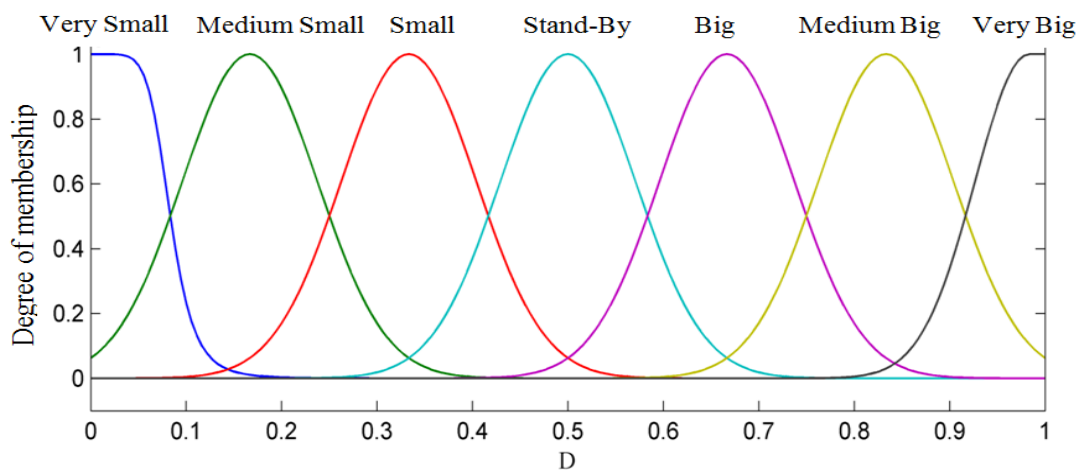
Figure 4.38 Memberships function for the duty cycle (*D*)

Figures 4.39 through 4.43 investigate the dynamic response of the studied system

when a Fire-through fault takes place within the GSC. The voltage profile at the PCC is shown in Figure 4.39 (a), where without the coil, voltage drops to 0.185 pu. By integrating the coil within the DFIG converters, the dropped voltage at the PCC is raised to 0.55 pu due to the reactive power support from the coil. Compared to the Fault Ride Through of Spain and Germany, the voltage at the PCC violates the LVRT limit of the two grid codes when the coil is not connected (as shown in Figure 4.39 (b)). However, with the coil connected, voltage drop reduces and reaches a safe level within grid connection requirements.
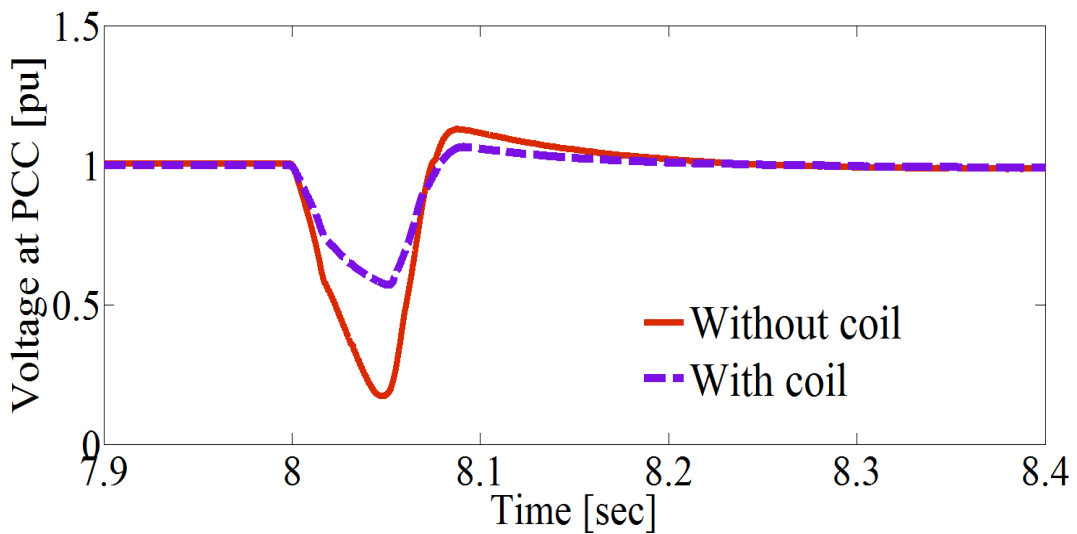
Figure 4.39 (a) Voltage profile at the PCC during fire-through in S6 within the GSC
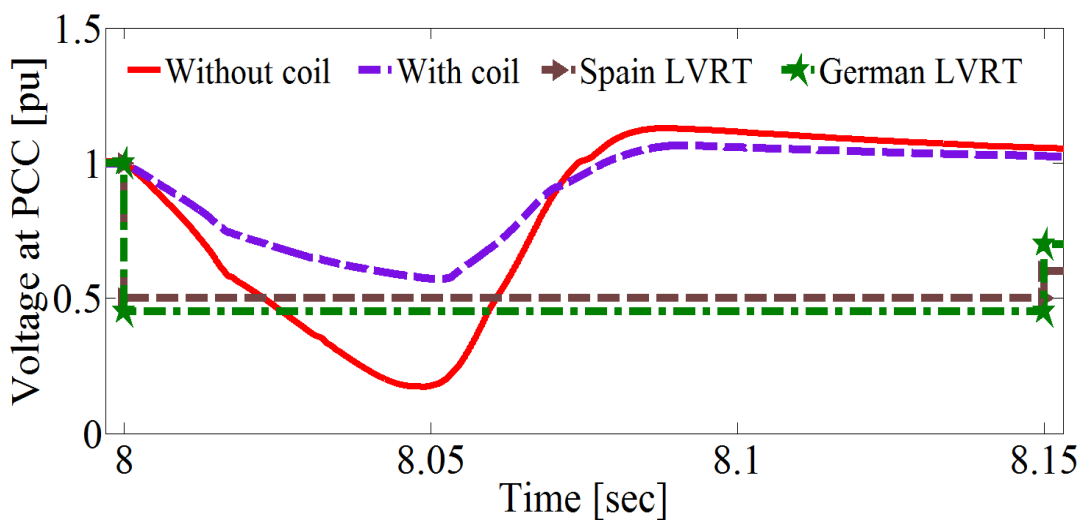
Figure 4.39 (b) PCC voltage compliance with various grid codes

Without the connection of the coil during a Fire-through fault, the real power at the PCC falls to -0.77 pu, and the DFIG acts as an induction motor (as shown in

Figure 4.40). When the coil is integrated within the DFIG converters, it modulates the active power at the PCC to 0.2 pu (as shown in Figure 4.40). The reactive power - with and without the integration of the coil at the PCC - is shown in Figure 4.41. Prior to the fault, the power factor at the PCC is maintained at unity. Upon the fault's occurrence, the machine changes to an induction motor, acquiring about 1.9 pu of reactive power, significantly reducing the power factor at the PCC to approximately ($\frac{0.77}{\sqrt{0.77^2+1.9^2}} = 0.35$). After connection of the proposed coil and controller, the reactive power at the PCC is rectified to -0.9 pu.
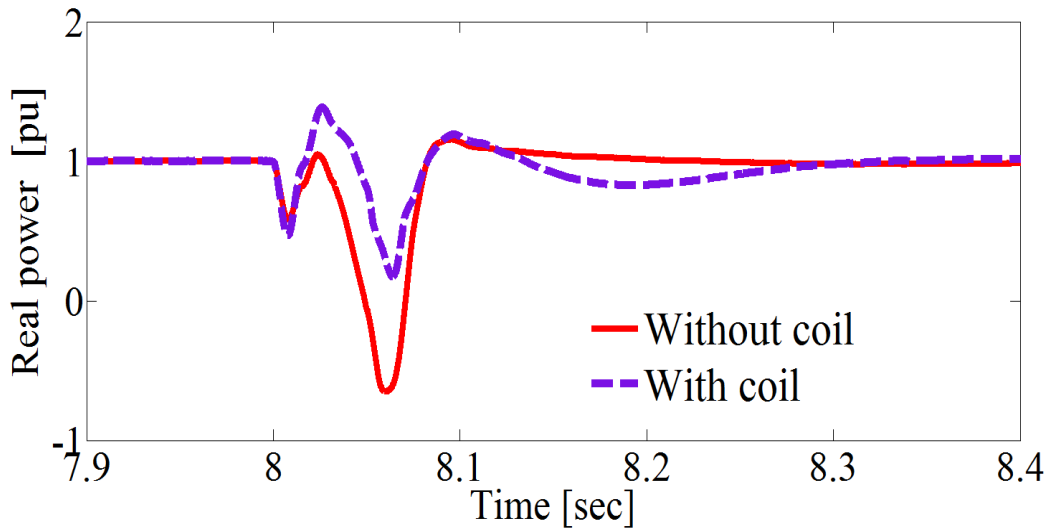
Figure 4.40 Real power at the PCC during fire-through in S6 within the GSC
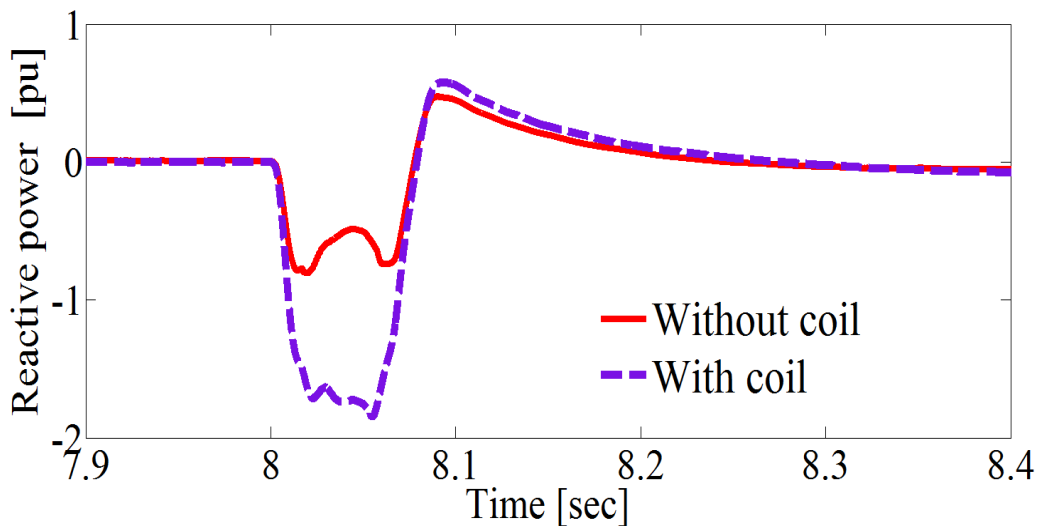
Figure 4.41 Reactive power at the PCC during fire-through in S6 within the GSC

The voltage of the DC-link capacitor during a GSC Fire-through fault is displayed in Figure 4.42. Capacitor voltage drops to zero during the fault, and recovers its nominal level once the fault has cleared.
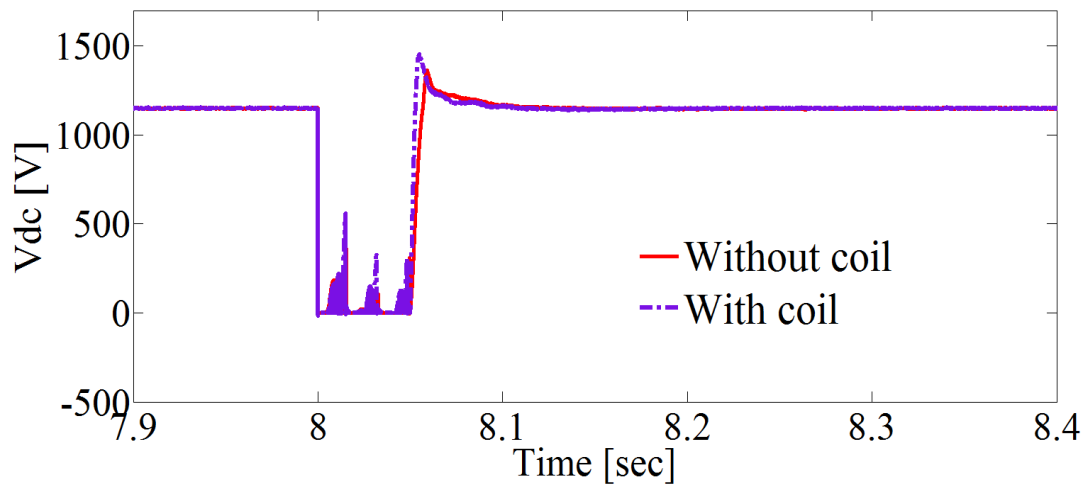
Figure 4.42 DC-link capacitor voltage during in S6 within the GSC

The impacts of a Fire-through fault on converter terminal voltages, as well as voltages across converter switches, can be seen in Figure 4.43 and Figure 4.44 respectively.
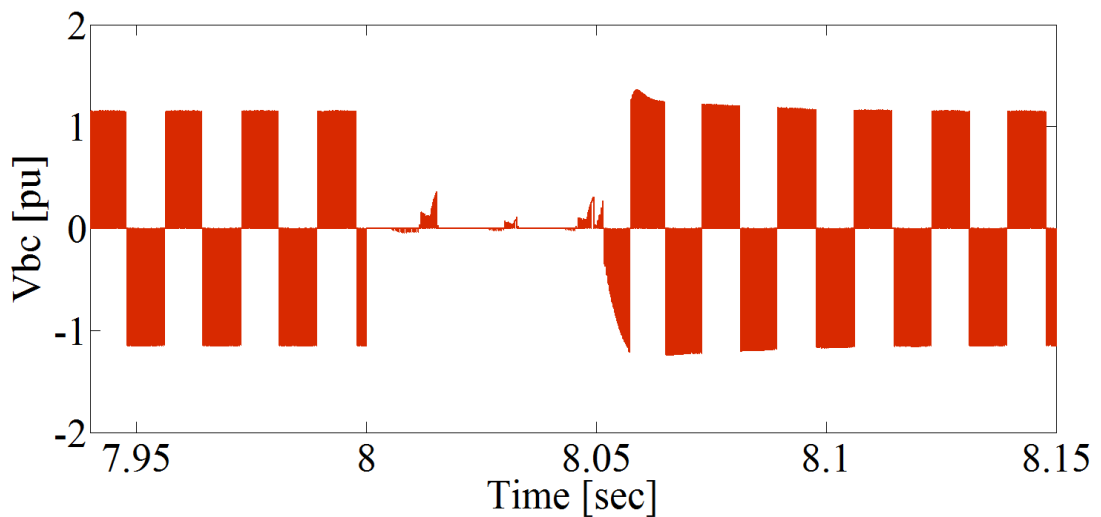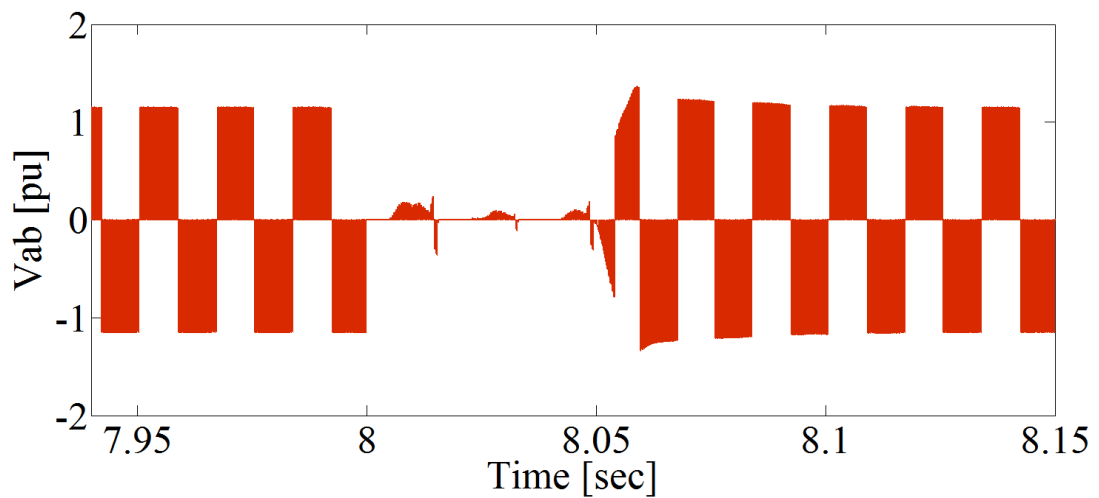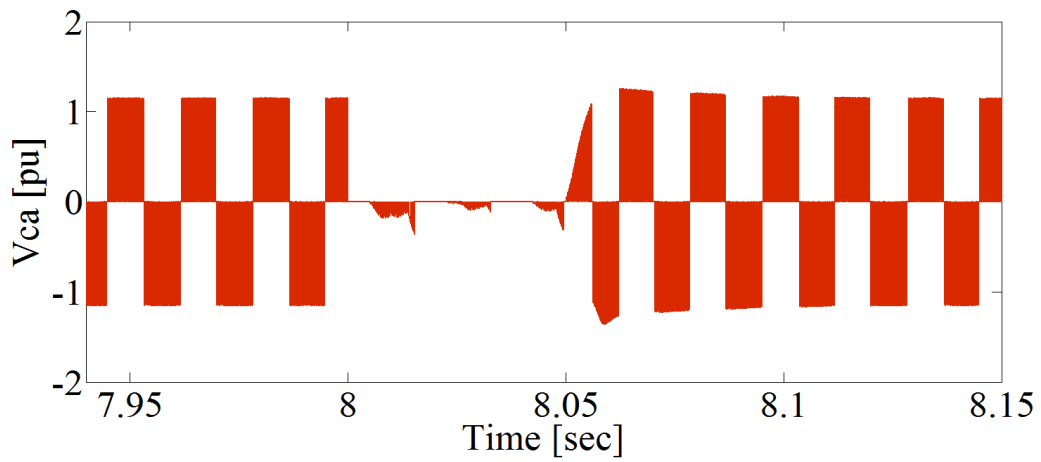
Figure 4.43 Voltage across GSC terminals during fire-through in S6
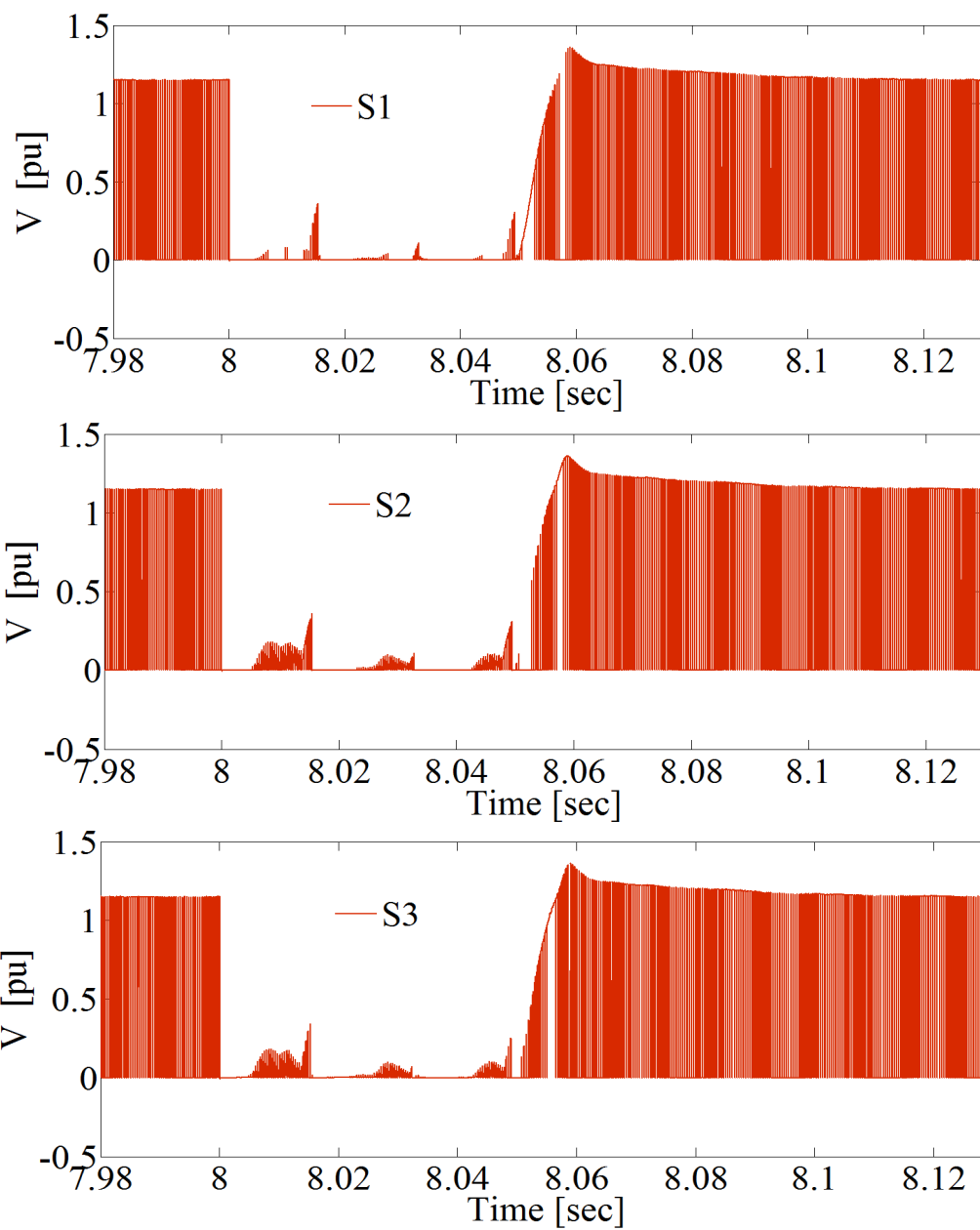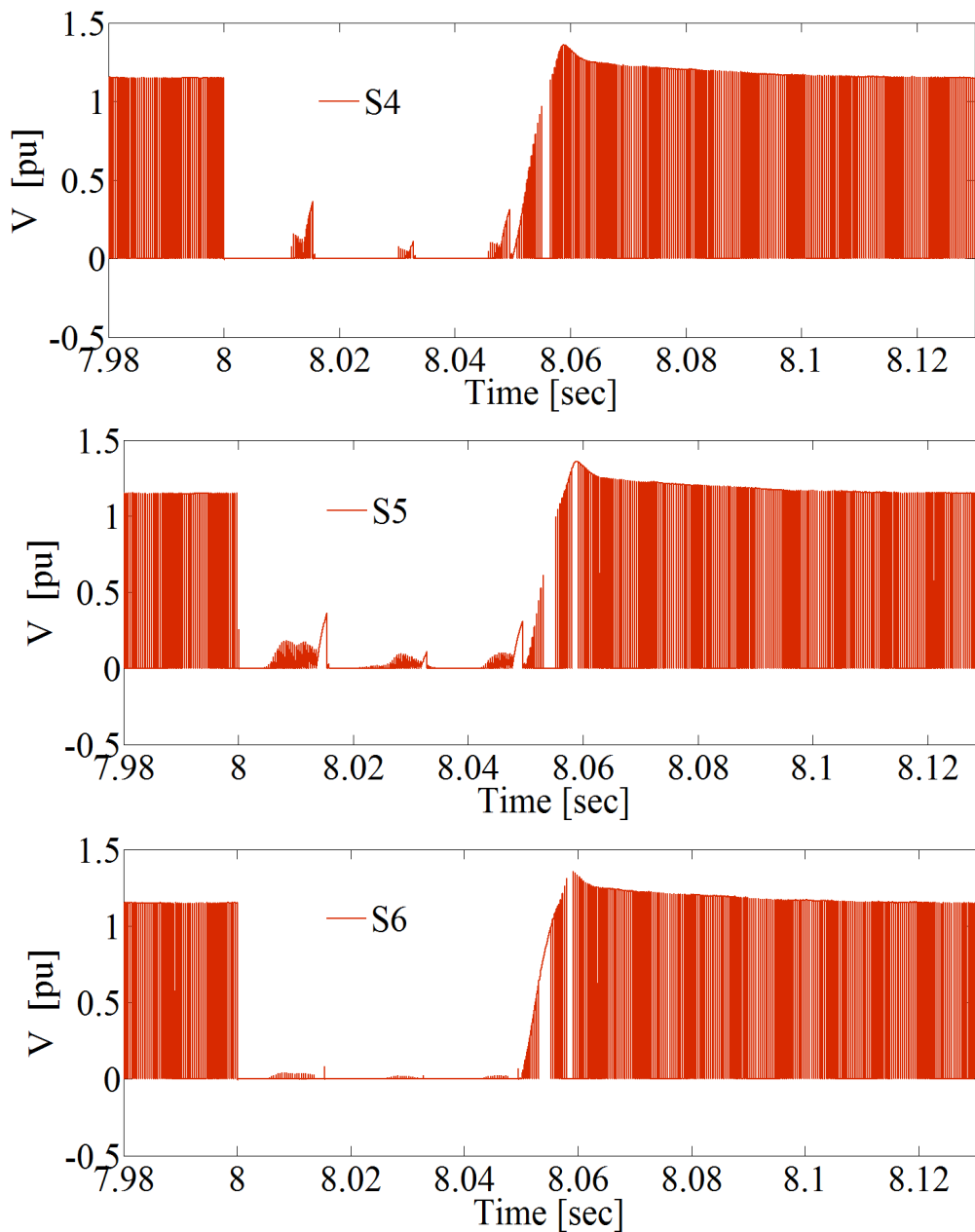
Figure 4.44 Voltage across GSC switches during fire-through in S6

When a misfire is applied to S6 within the GSC at t=8 sec, and cleared at t=8.05sec, the overall performance of the DFIG is not significantly impacted. This is because the dynamic response of the system exhibits slight oscillations during the fault period (as shown in Figures 4.45 (a-e)).
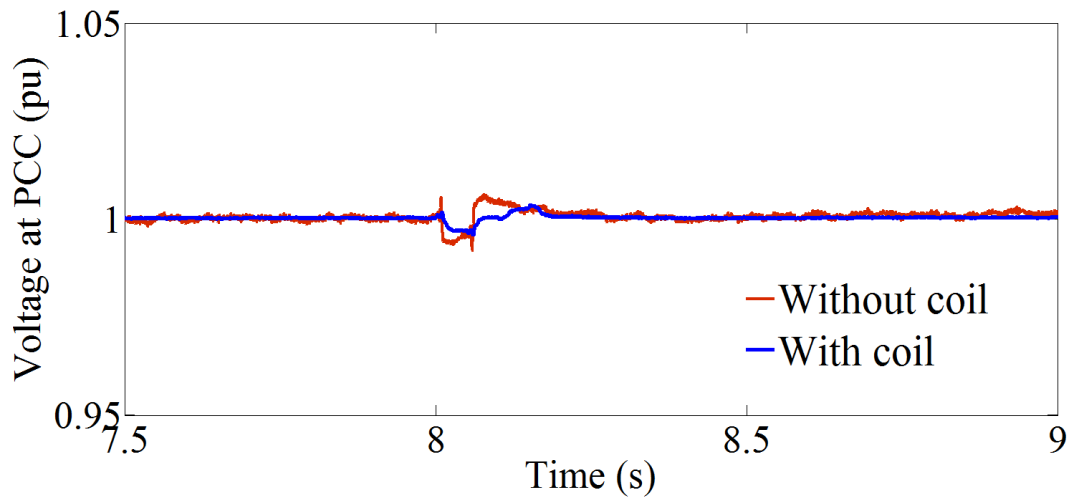
Figure 4.45 (a) Voltage at the PCC during misfire in S6 within the GSC
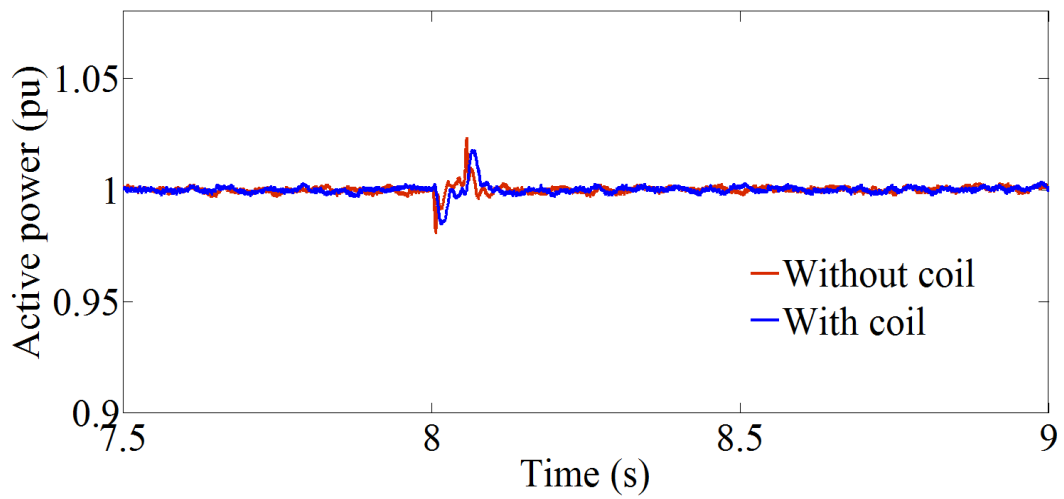
Figure 4.45 (b) Active power at the PCC during misfire in S6 within the GSC
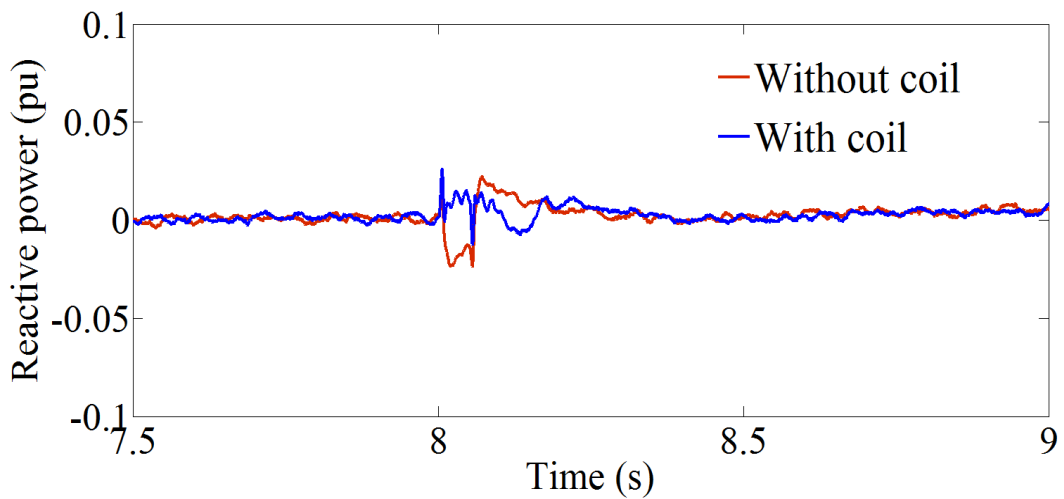
Figure 4.45 (c) Reactive power at the PCC during misfire in S6 within the GSC
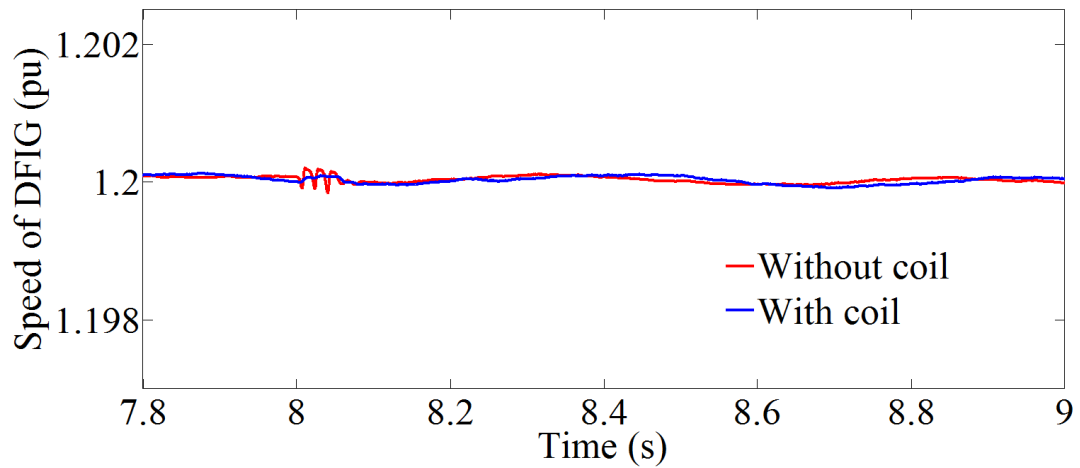
Figure 4.45 (d) DFIG speed during misfire in S6 within the GSC
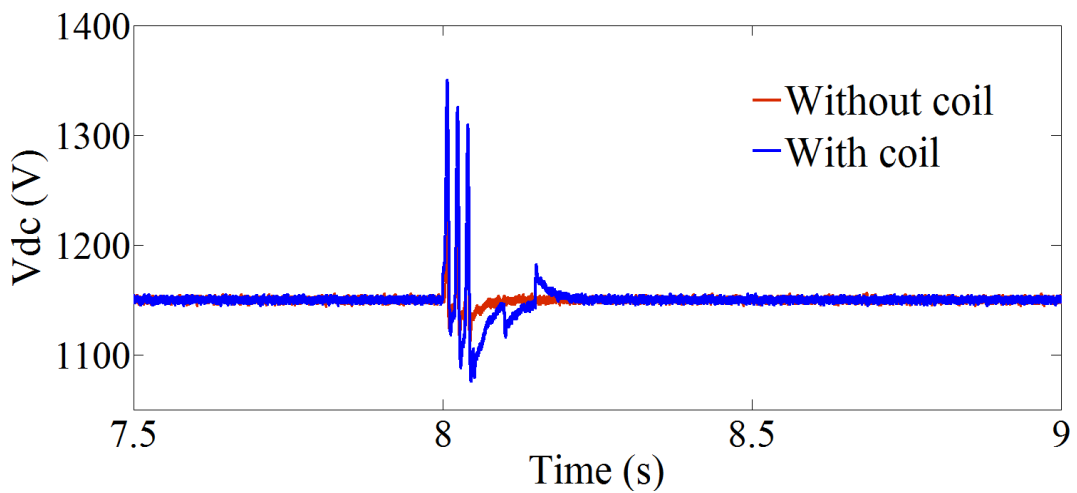
Figure 4.45 (e) DC-link voltage during misfire in S6 within the GSC

During the misfire on switch S6 of the GSC, voltage across both the GSC terminals and switches are only slightly affected (as can be seen in Figures 4.46 and 4.47, respectively).
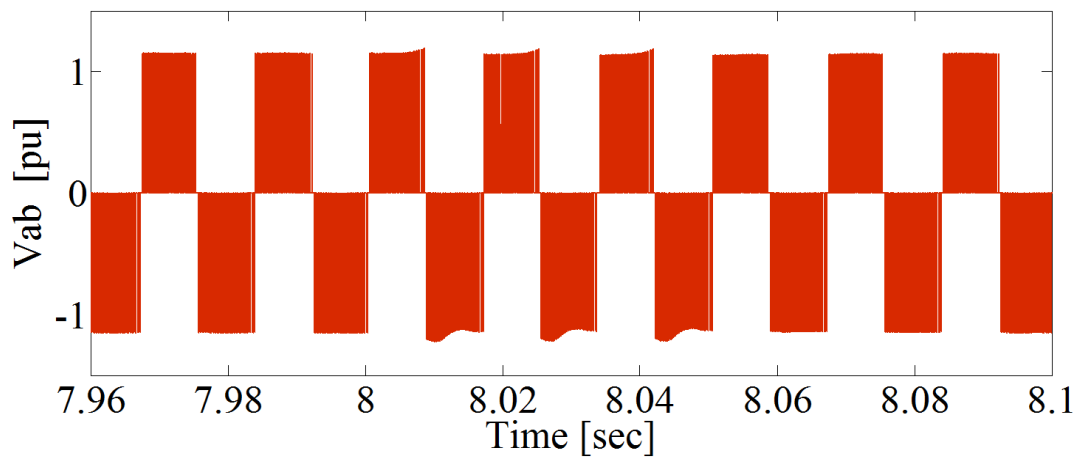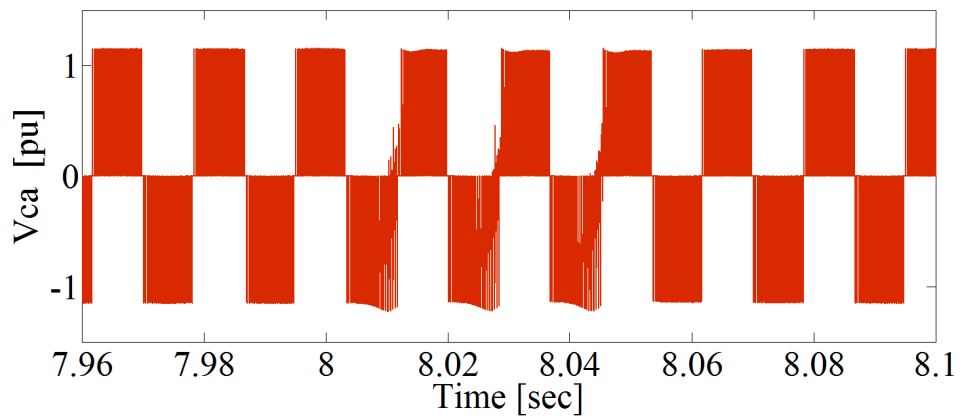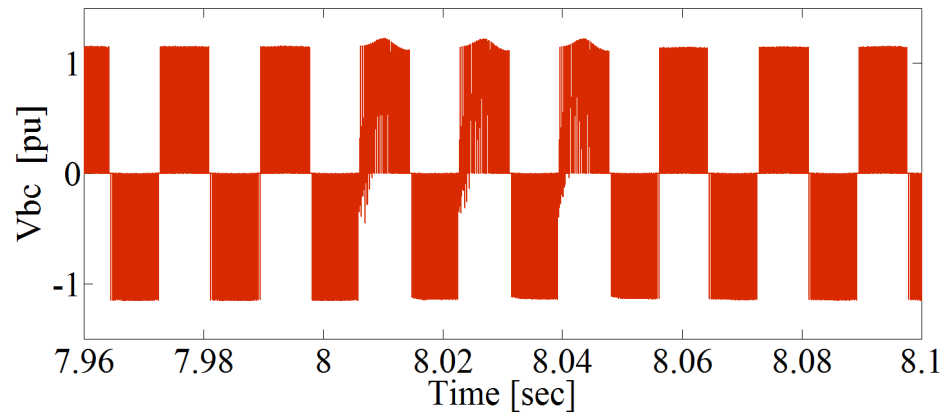
Figure 4.46 Voltage across GSC terminals during misfire in S6
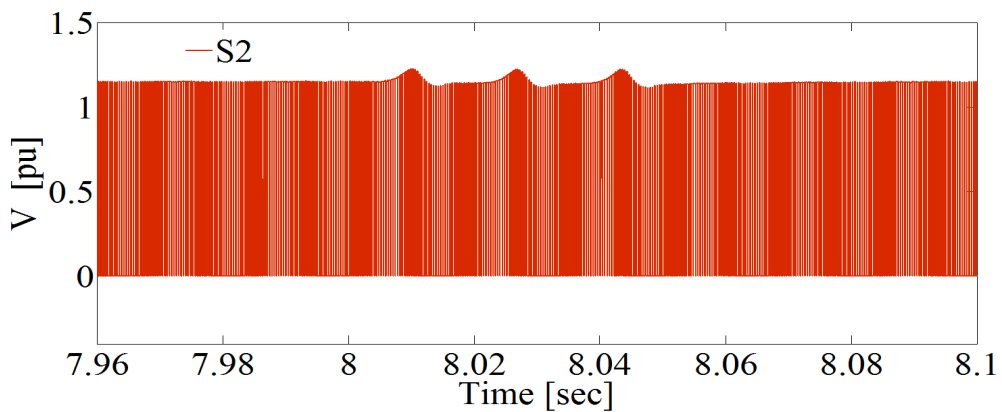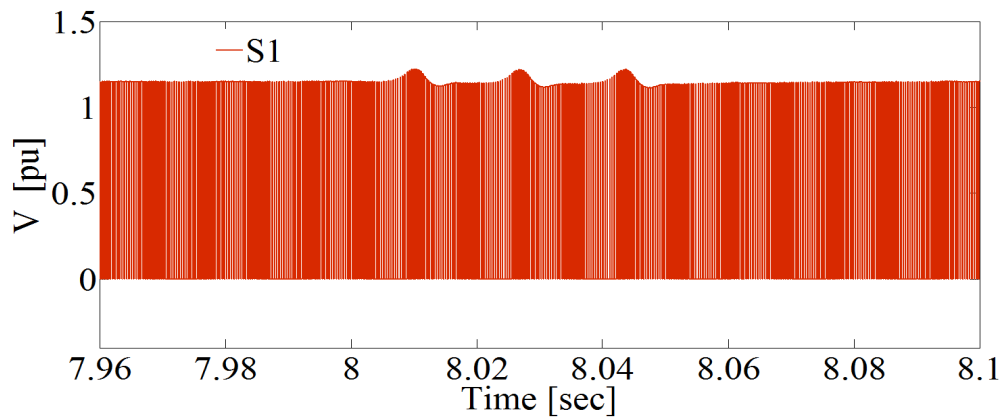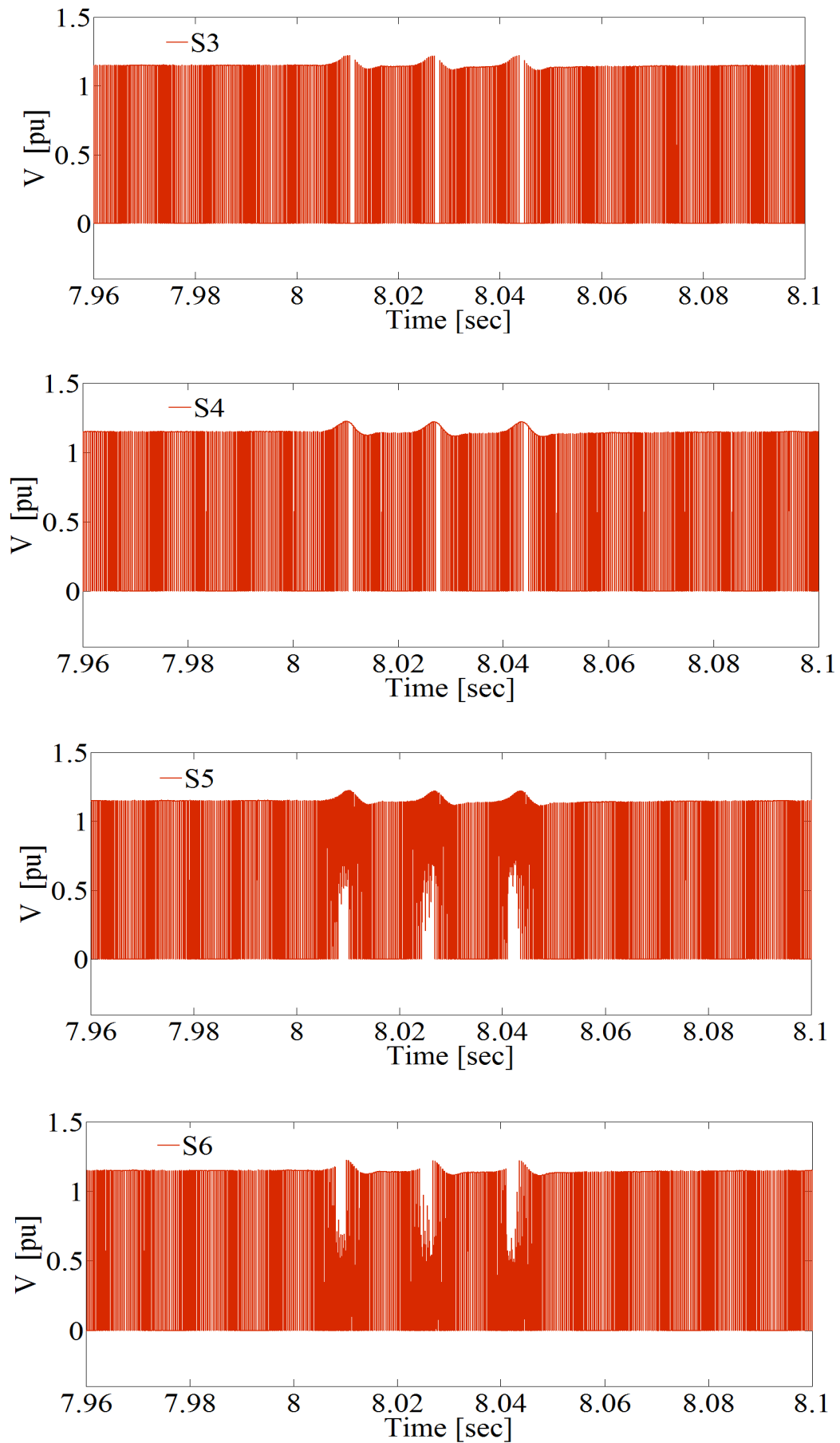
Figure 4.47 Voltage across GSC switches during misfire in S6

The coil's behaviour when fire-through and misfire occur within the GSC is shown in Figures 4.48 (a-d). These figures respectively show voltage across the coil (V_c), coil current (I_c), coil-stored energy (E_c), and duty cycle (D). As in the previous case studies, during normal operating conditions, the duty cycle is maintained at 0.5, and the coil voltage is maintained at zero level (corresponding to maximum coil current and rated stored energy). When the fault occurs, the proposed controller works to adjust the duty cycle to a value less than 0.5 allowing the coil-stored energy to be delivered to the grid. As can be seen in this figure, a small amount of the stored energy within the coil is discharged to the grid during such a disturbance events.
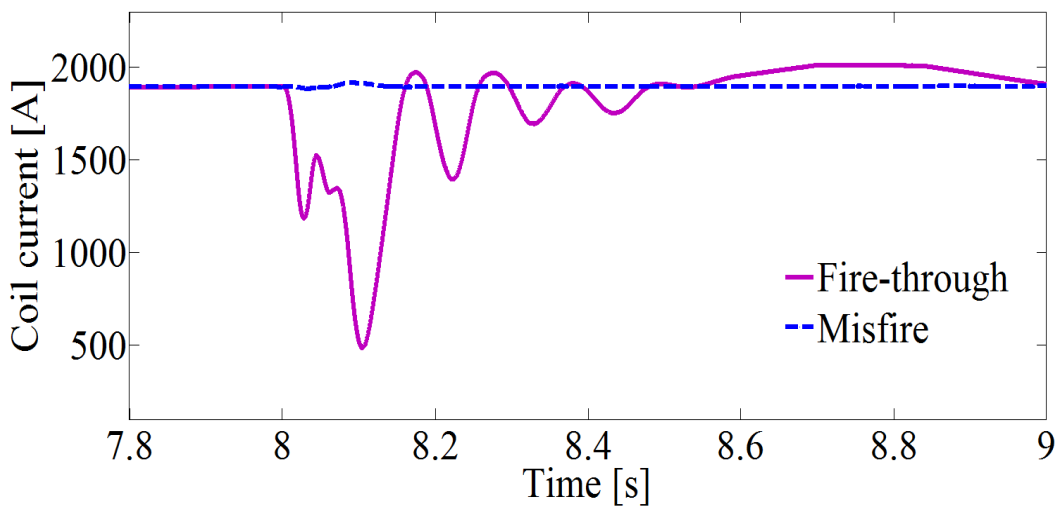
Figure 4.48 (a) Coil current response during fire-through and misfire in S6 within the GSC
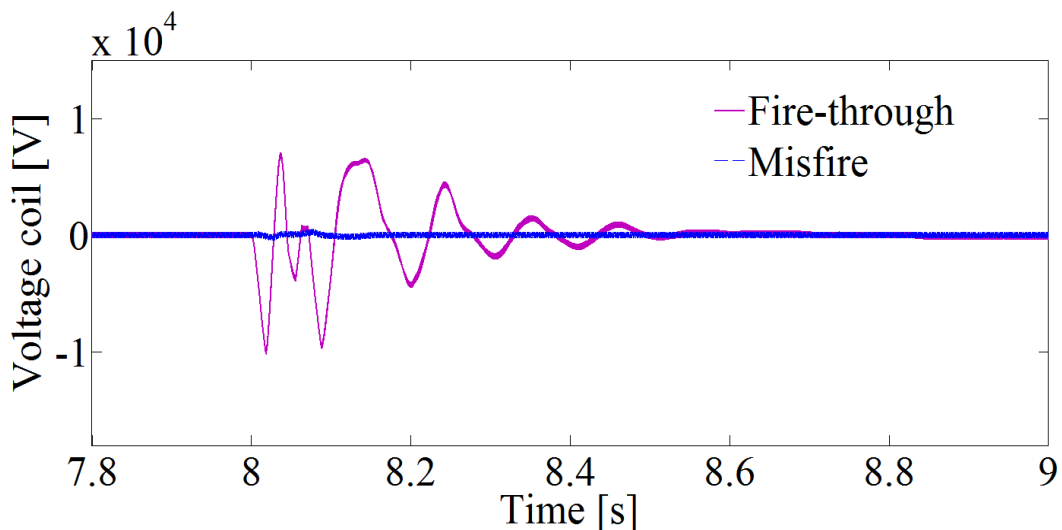
Figure 4.48(b) Voltage across the coil during fire-through and misfire in S6 within the GSC
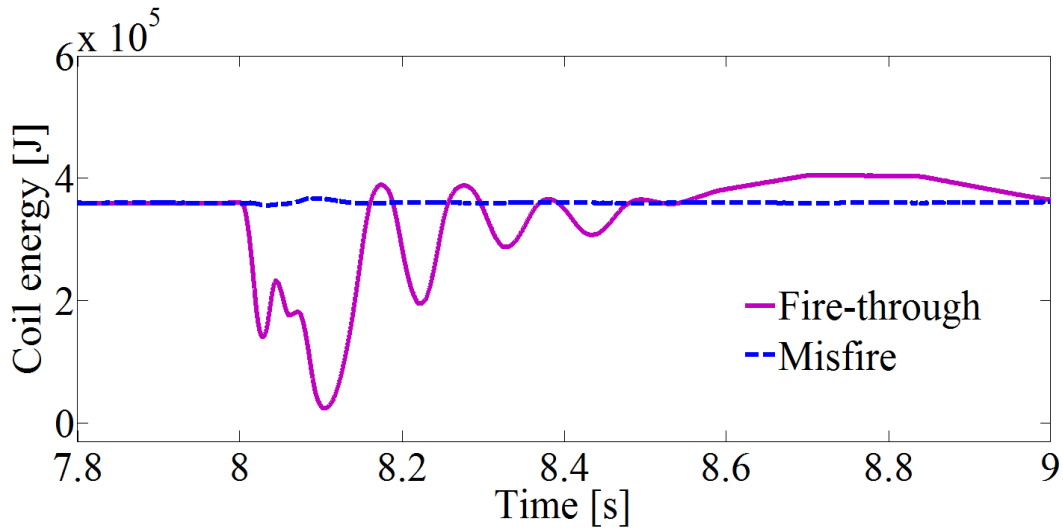
Figure 4.48 (c) Coil energy response during fire-through and misfire in S6 within the GSC
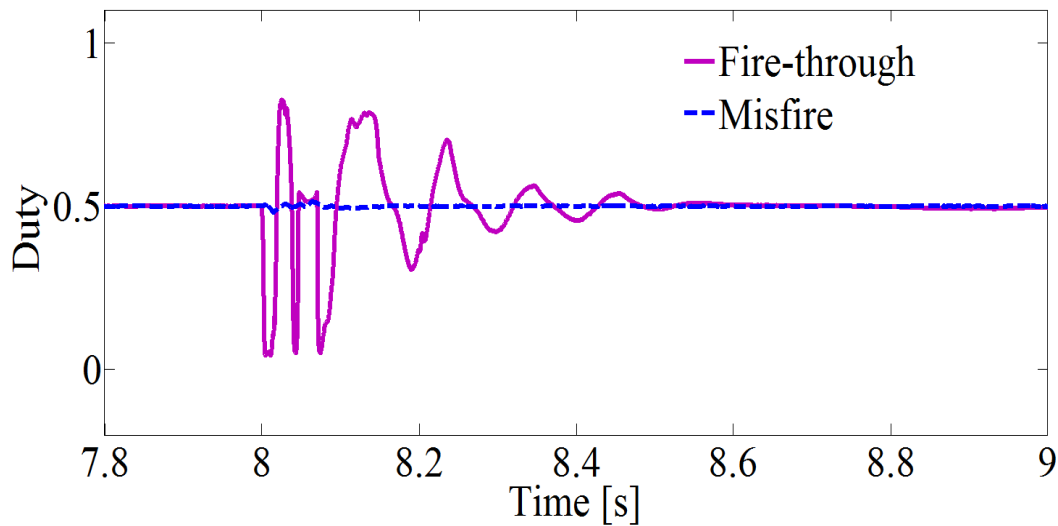
Figure 4.48 (d) Duty cycle during fire-through and misfire in S6 within the GSC

4.4.4.2 Fire-Through and Misfire within the RSC

Intermittent Fire-through and Misfire faults are simulated within the RSC of the studied system in Figure 4.35. The faults occur on switch S6 at t = 8 sec and clear at t = 8.05sec.

Figures 4.49 through 4.52 show the dynamic response of the studied system when fire-through takes place within the RSC. The voltage profile at the point of common coupling (PCC) is shown in Figure 4.49 (a), where without the coil, voltage drops to 0.15 pu. By integrating the coil within the DFIG converters, the dropped voltage at the PCC is raised to 0.59 pu. This is due to the reactive power support from the coil. Compared to the Fault Ride Through of Spain and Germany, when the coil is not connected, the voltage at the PCC violates the LVRT of the two grid codes (as shown

in Figure 4.49 (b)) and calls for the wind turbine to be disconnected from the grid. However, with the coil connected, the voltage drop decreases and reaches a safe level within grid connection requirements.
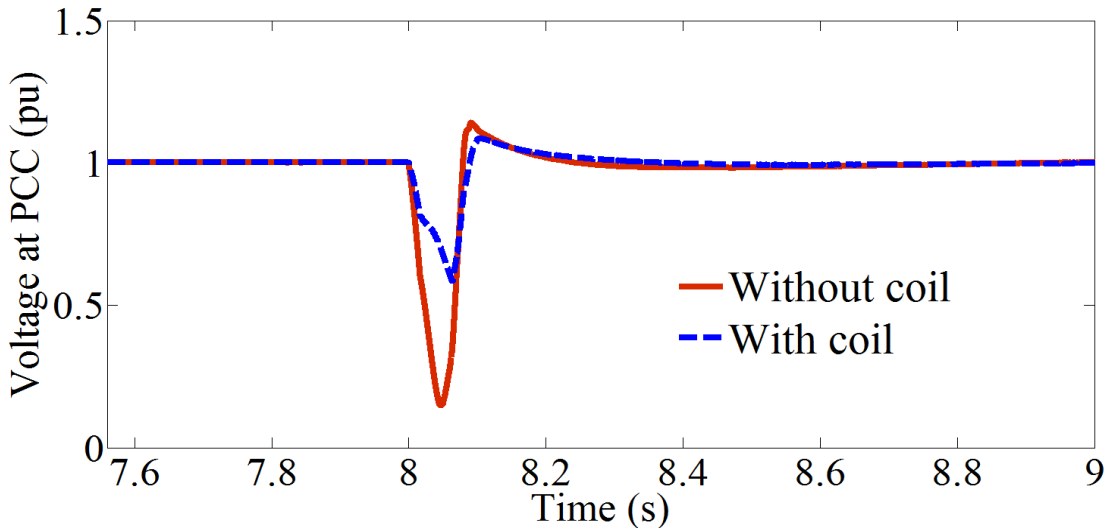
Figure 4.49 (a) Voltage profile at the PCC during fire-through in S6 within the GSC
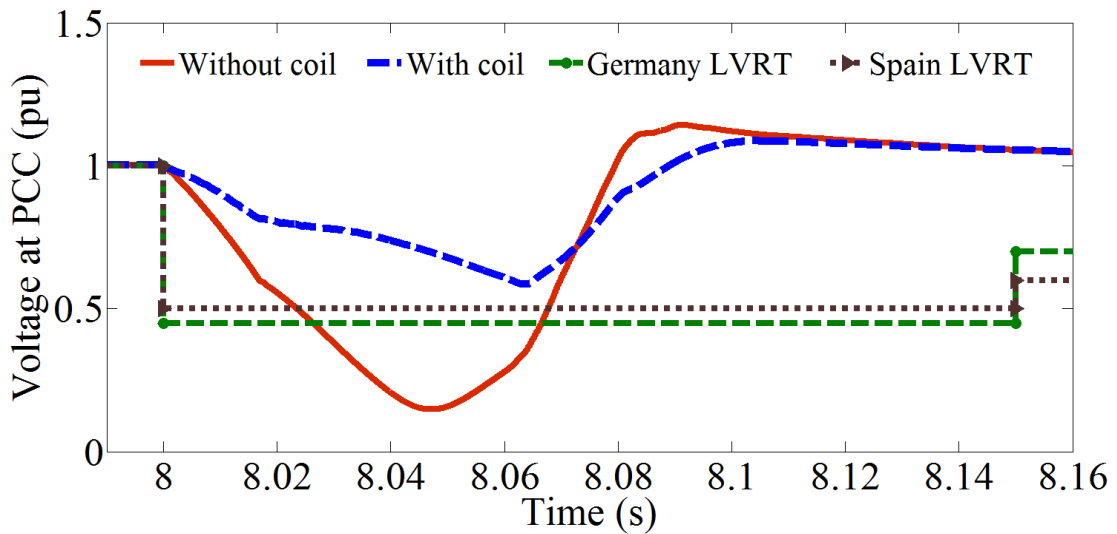
Figure 4.49 (b) PCC voltage compliance with various grid codes

Without the connection of the coil during a Fire-through fault, the active power at the PCC drops to -0.8 pu (as shown in Figure 4.50). When the coil is integrated within the DFIG converters, it can be seen that the absorbed active power at the PCC decreases to -0.2 pu. Figure 4.51 shows the reactive power at the PCC - with and without the integration of the coil - as well as the surplus reactive power compensated by the coil. The DC-link capacitor voltage during a GSC Fire-through fault is displayed in Figure 4.52. Capacitor voltage drops to zero during the fire through within the RSC, and recovers its nominal level once the fault clears.
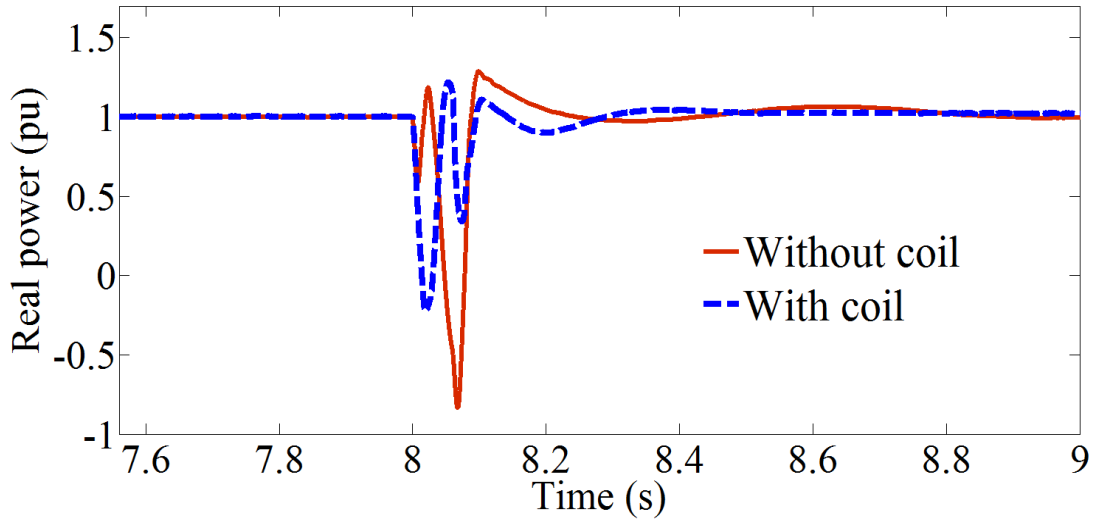
Figure 4.50 Real power at the PCC during fire-through in S6 within the RSC
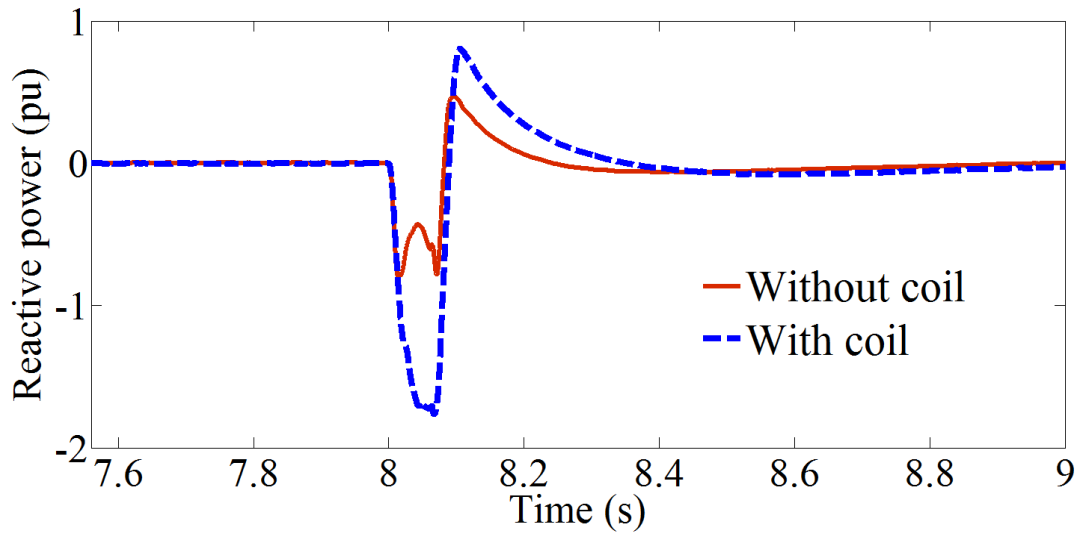
Figure 4.51 Reactive power at the PCC during fire-through in S6 within the RSC
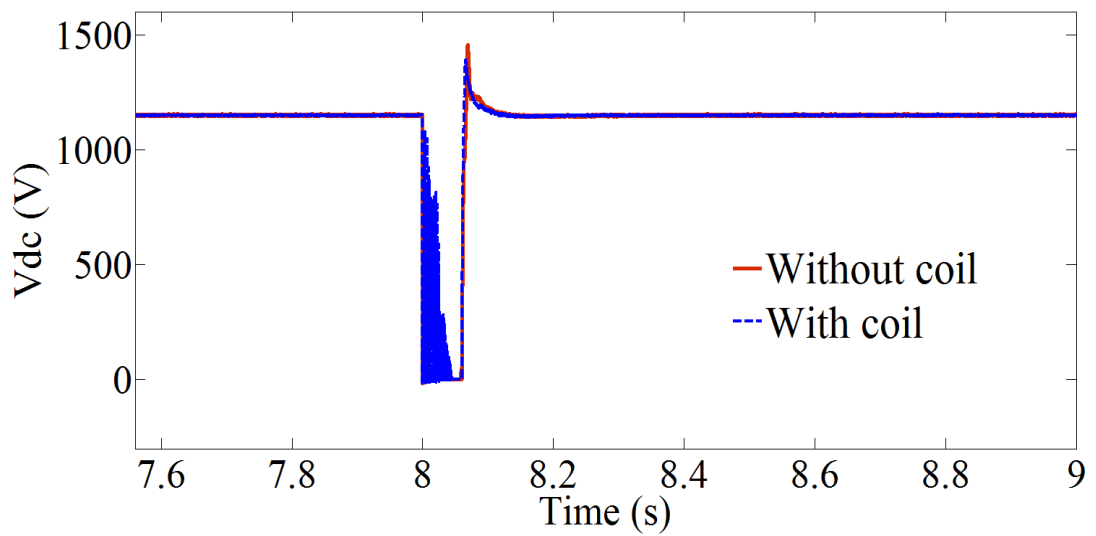
Figure 4.52 DC-link capacitor voltage during fire-through in S6 within the RSC

The impacts of a Fire-through fault on converter terminal voltages, and also voltages across converter switches, can be seen in Figure 4.53 and Figure 4.54 respectively.
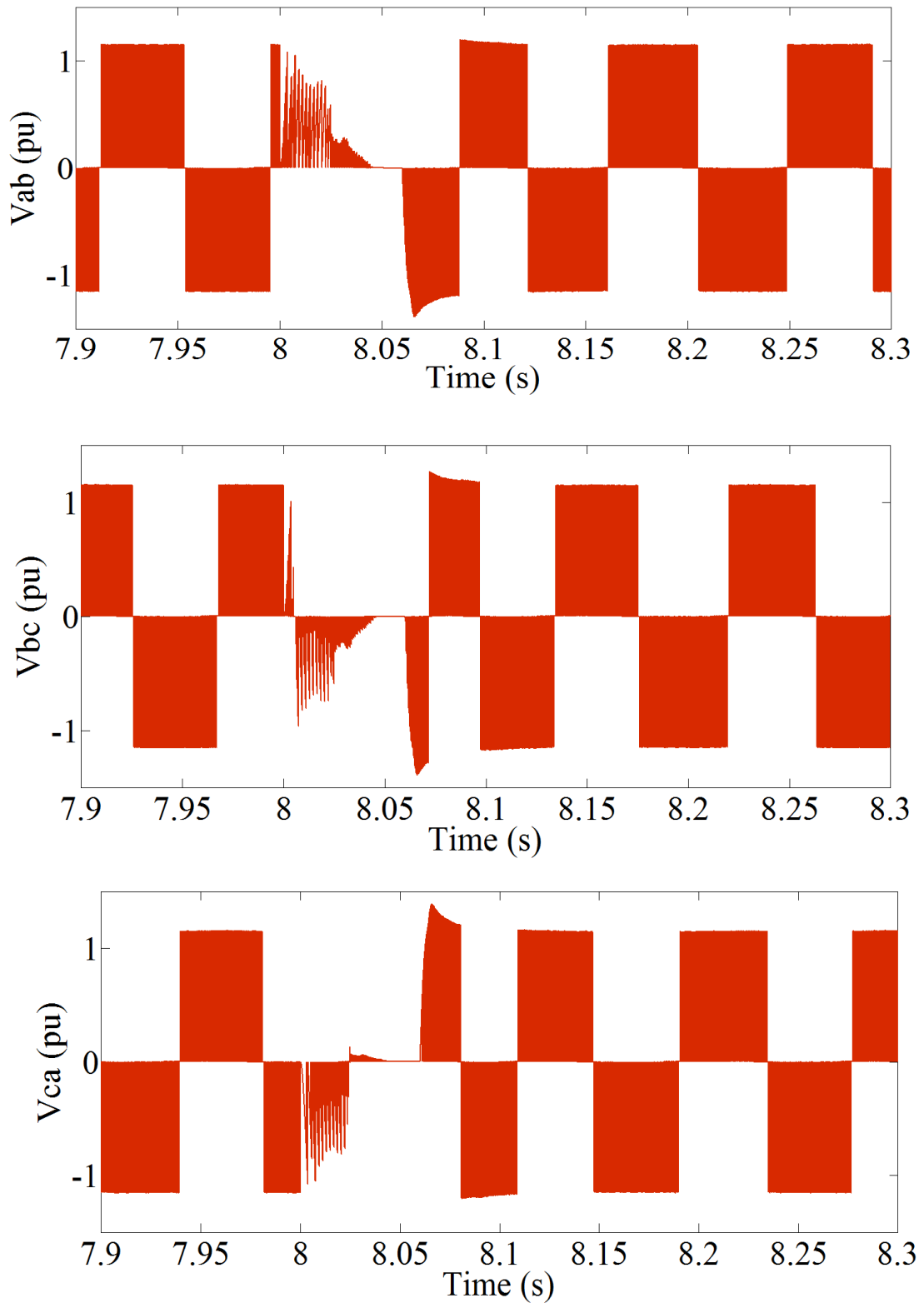
Figure 4.53 Voltage across RSC terminals during fire-through in S6
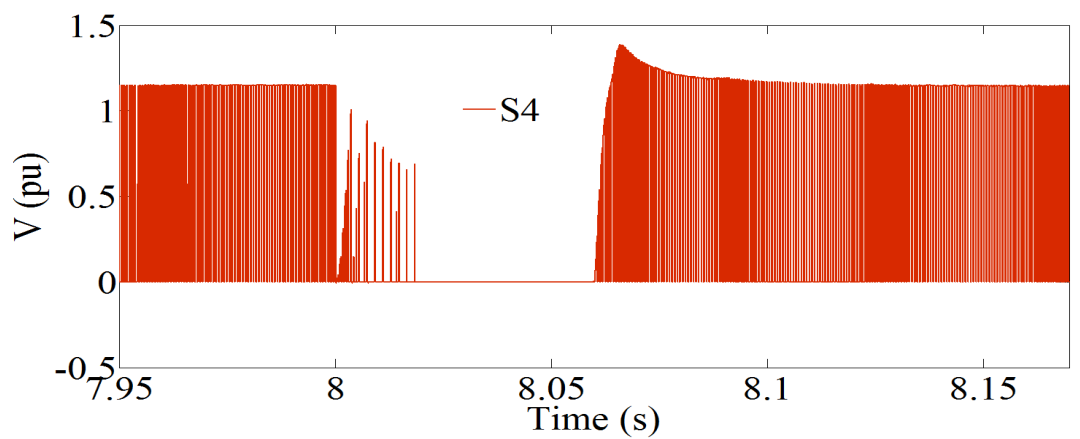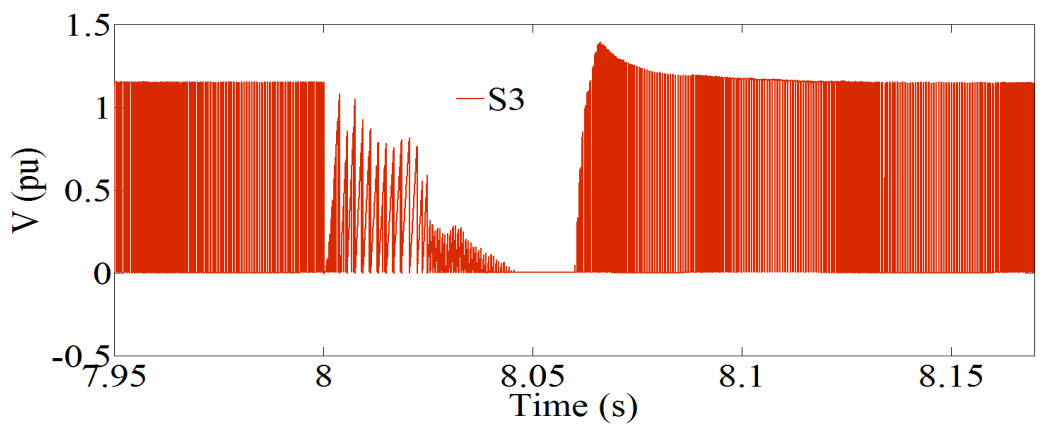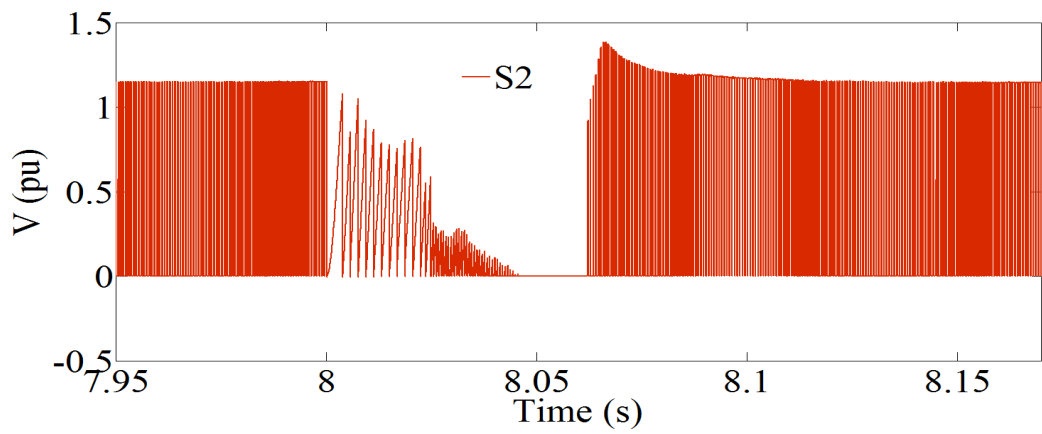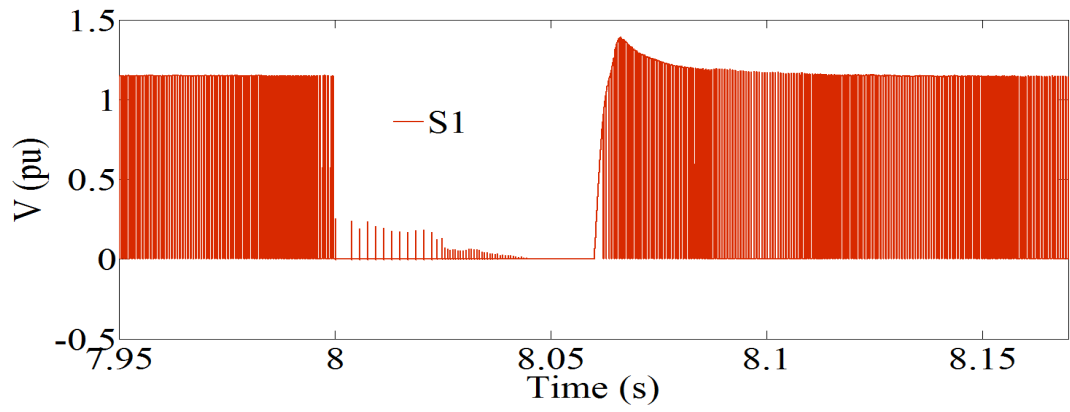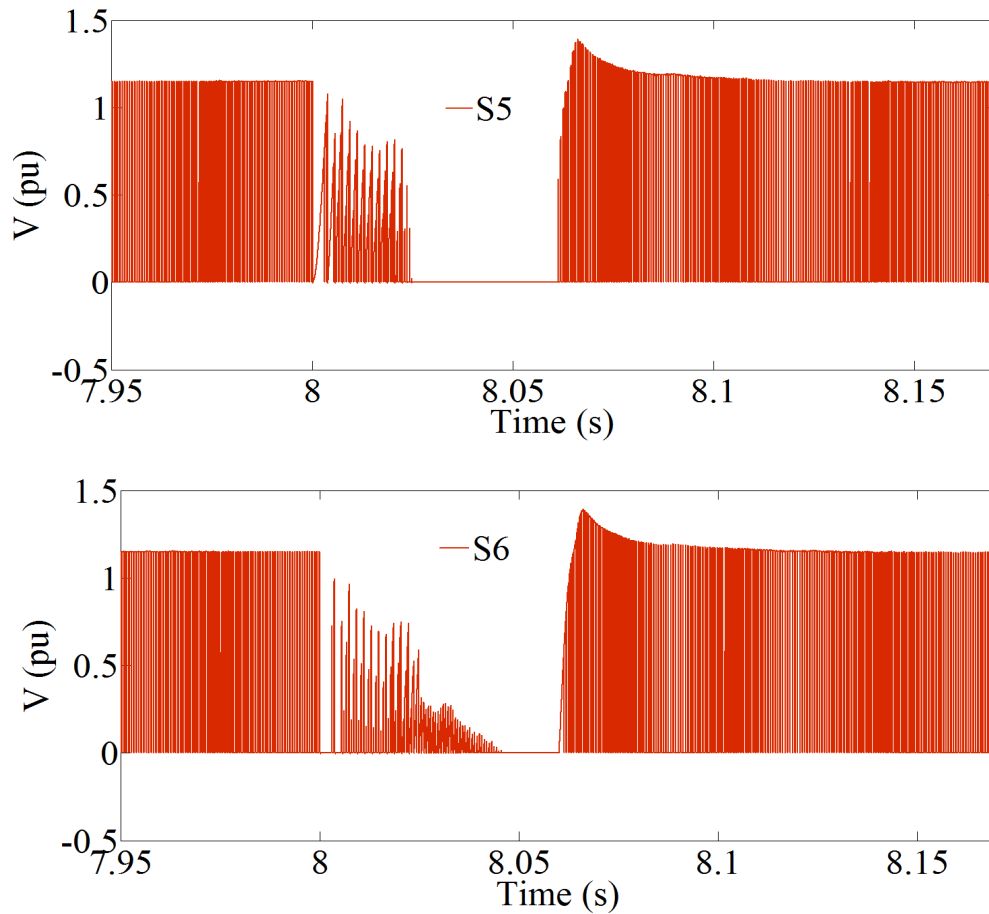
Figure 4.54 Voltage across RSC switches during fire-through in S6

When a misfire is applied to S6 within the RSC at t=8 sec, and cleared at t=8.05sec, the overall performance of the DFIG is not significantly impacted (as shown in Figures 4.55 (a-e)).
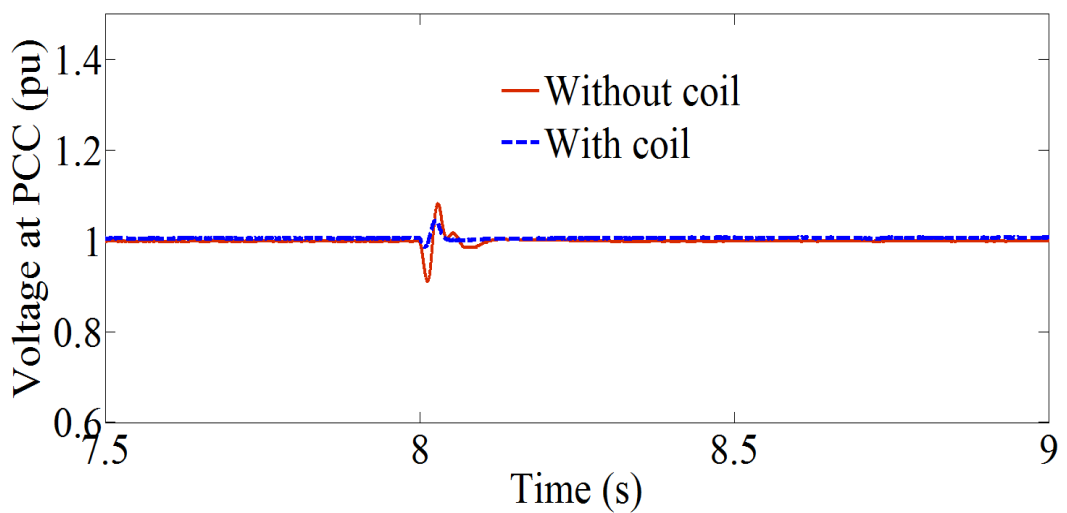
Figure 4.55 (a) Voltage at the PCC during misfire in S6 within the RSC
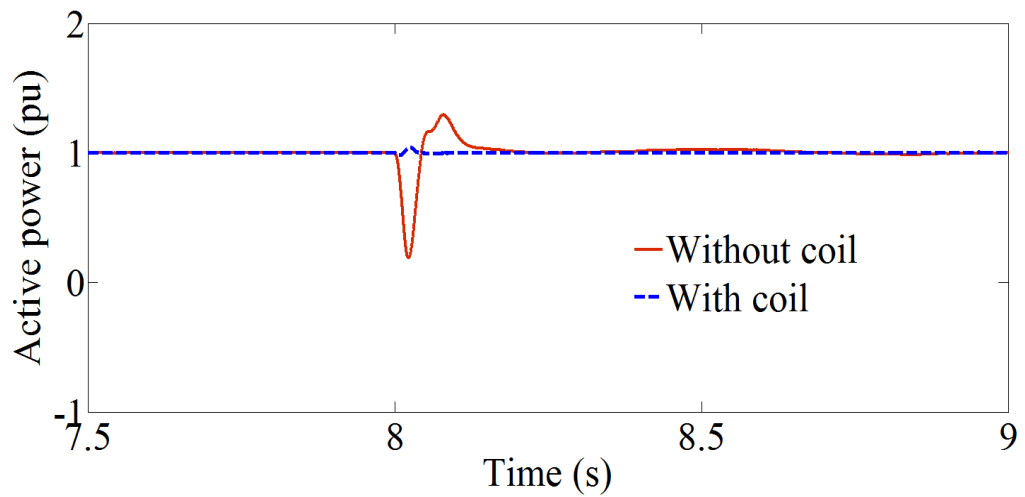
Figure 4.55 (b) Active power at the PCC during misfire in S6 within the RSC
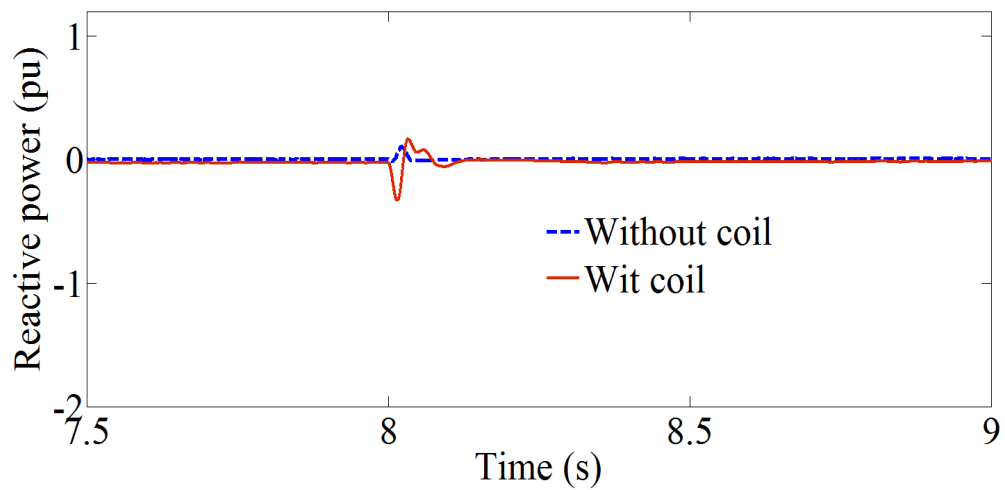
Figure 4.55 (c) Reactive power at the PCC during misfire in S6 within the RSC
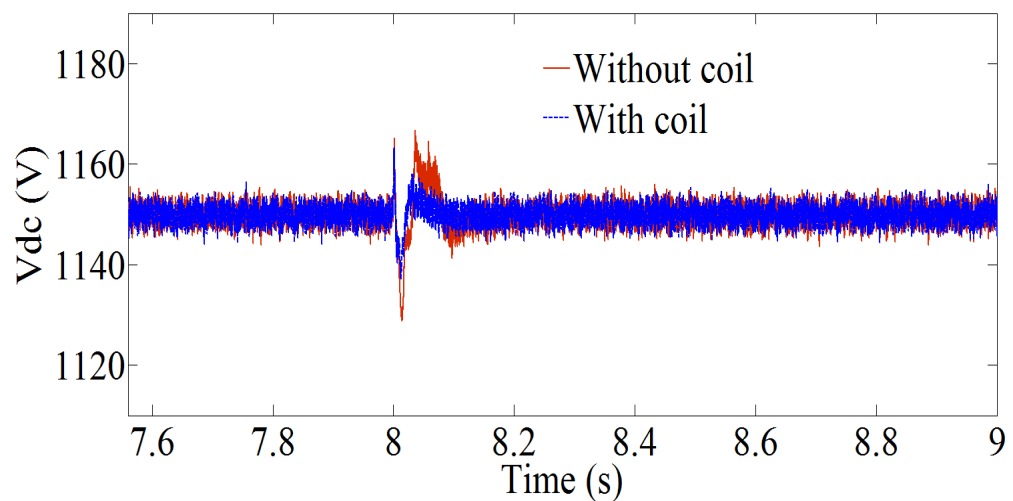
Figure 4.55 (d) DC-link voltage during misfire in S6 within the RSC
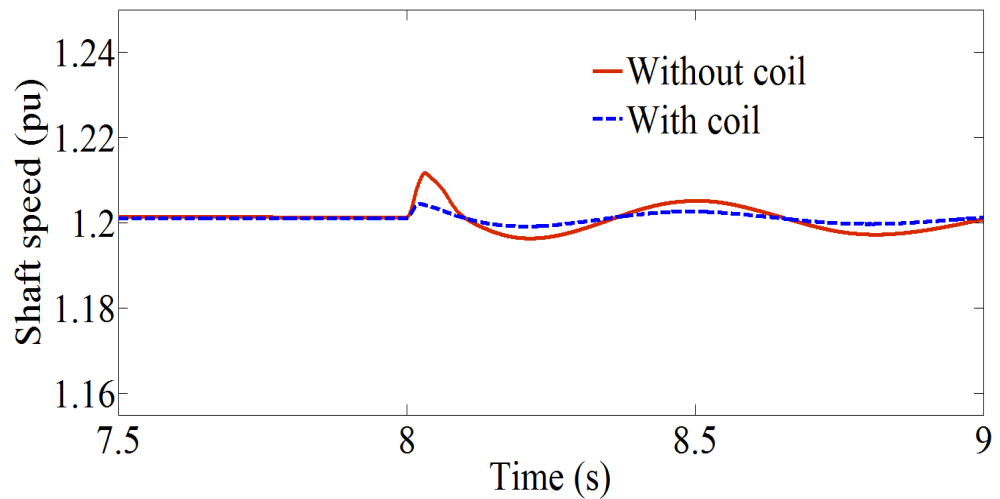
Figure 4.55 (e) DFIG speed during misfire in S6 within the RSC

The impacts of a misfire fault on converter terminal voltages, and also voltages across converter switches, can be seen in Figure 4.56 and Figure 4.57 respectively.
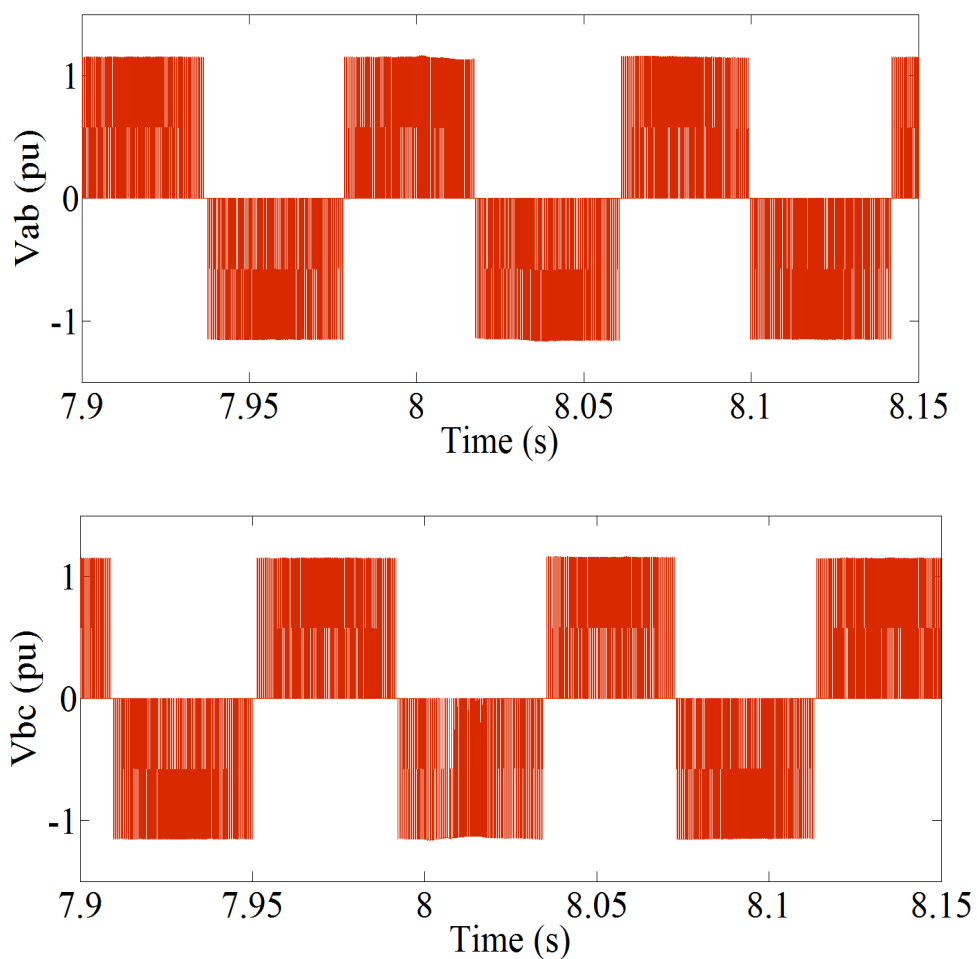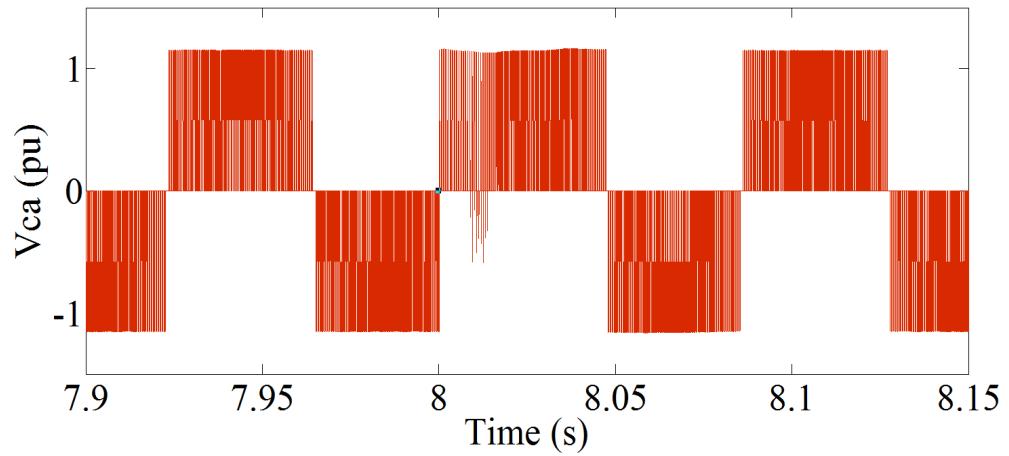
Figure 4.56 Voltage across RSC terminals during misfire in S6
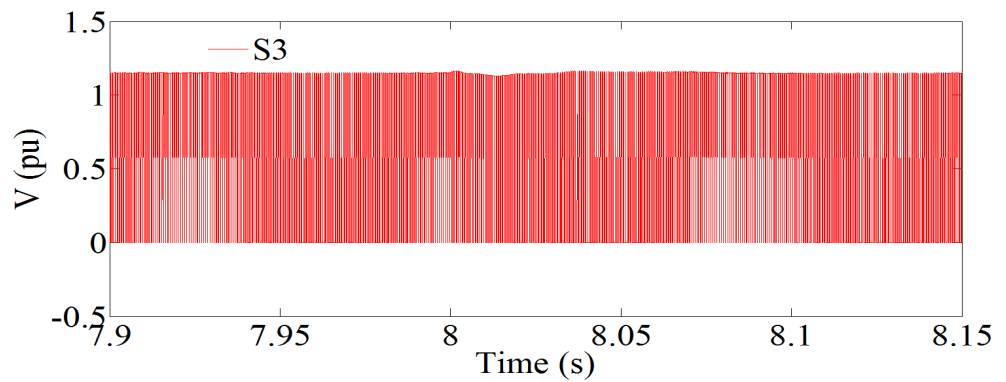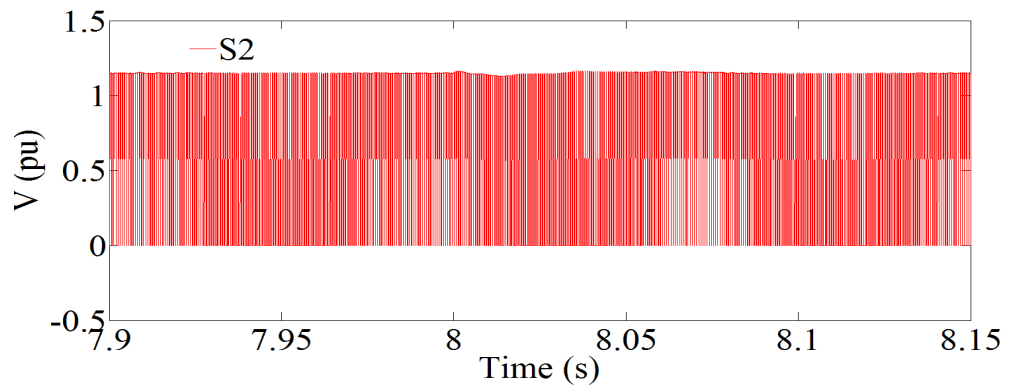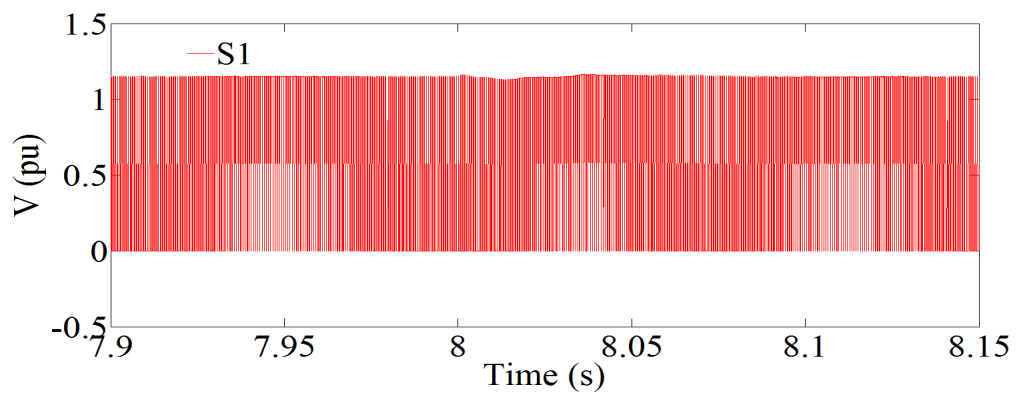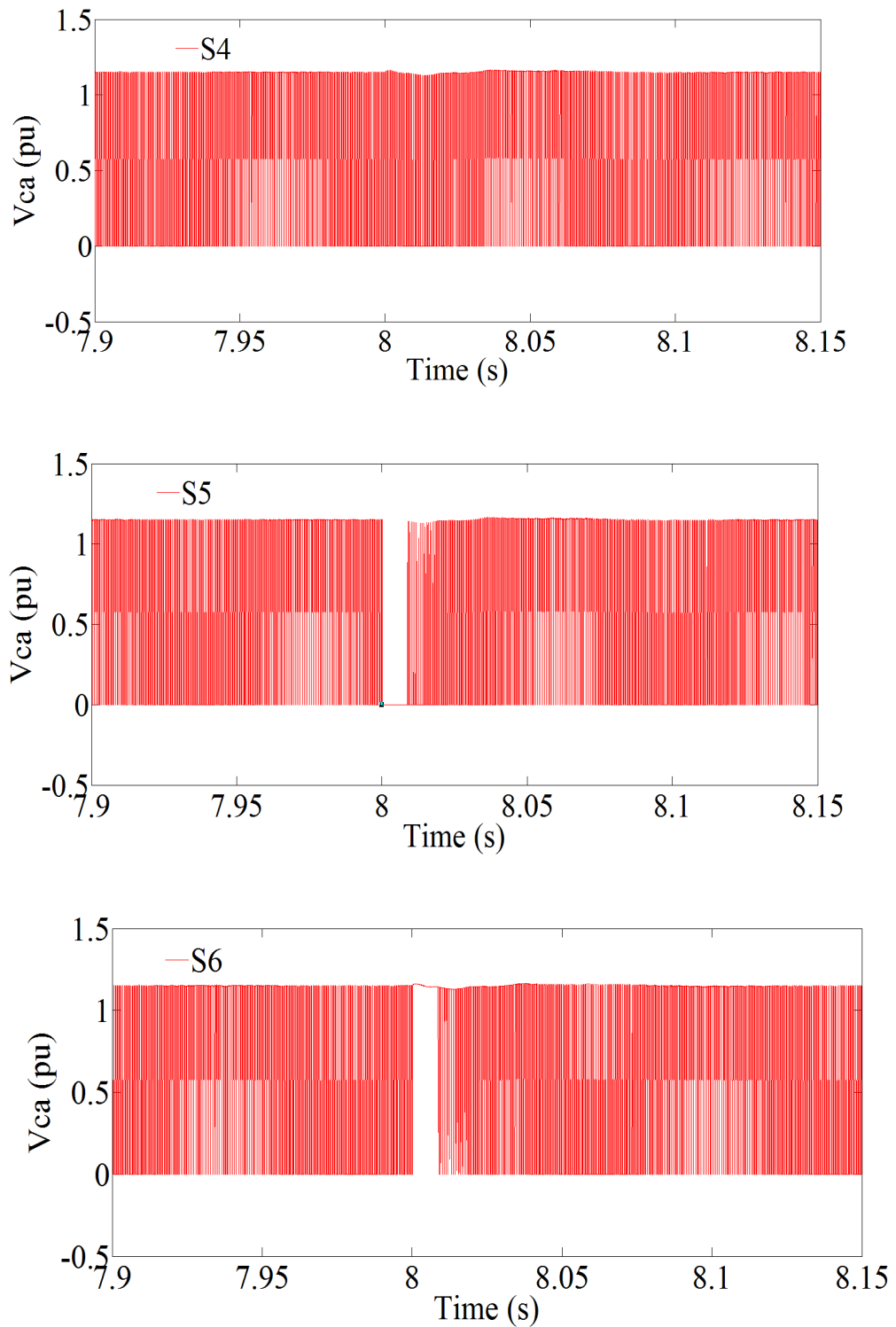
Figure 4.57 Voltage across RSC switches during misfire in S6

The coil's behaviour, when fire-through and misfire occur in S6 within the RSC, is investigated in Figures 4.58 (a-d). These figures respectively show voltage across the coil (V_c), coil current (I_c), coil-stored energy (E_c), and duty cycle (D).
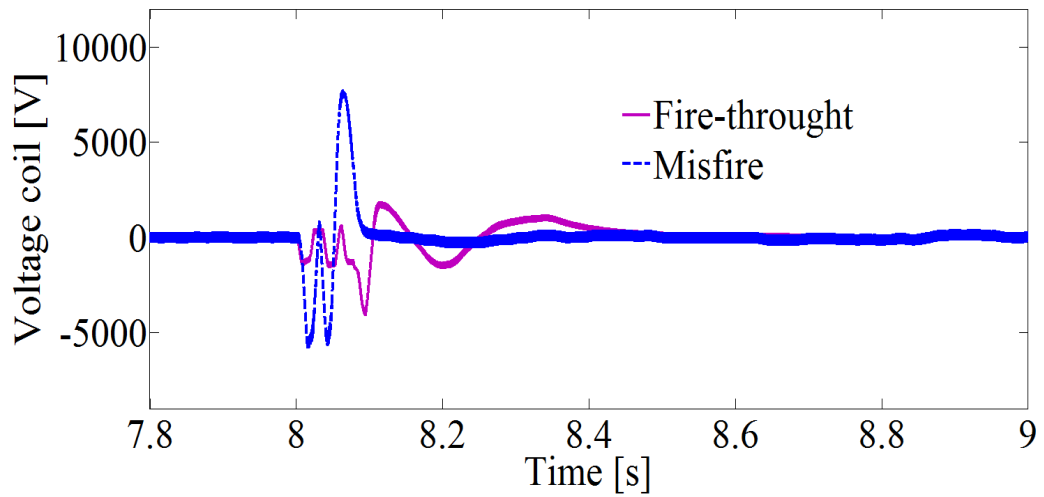
Figure 4.58 (a) Voltage across the coil during misfire in S6 within the RSC
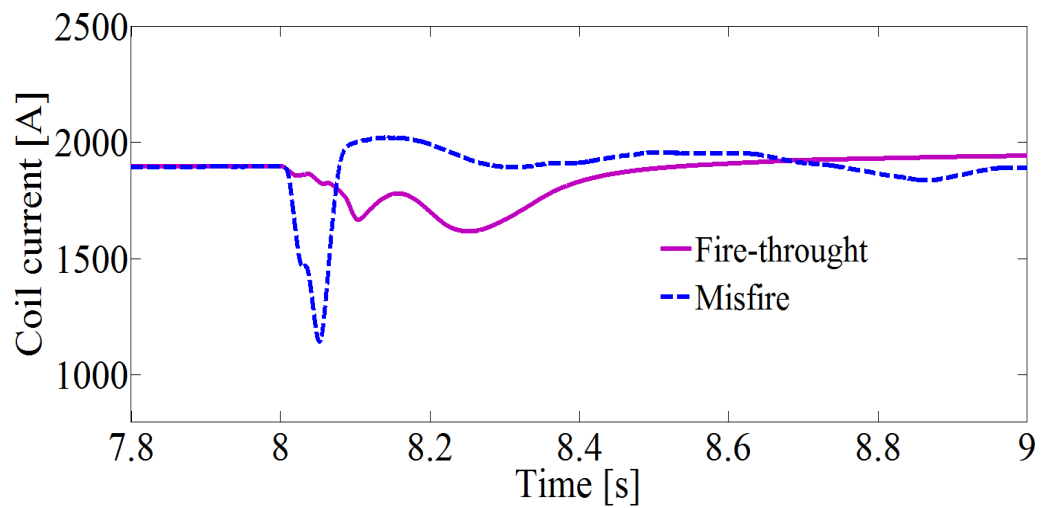
Figure 4.58 (b) Coil current response during misfire in S6 within the RSC
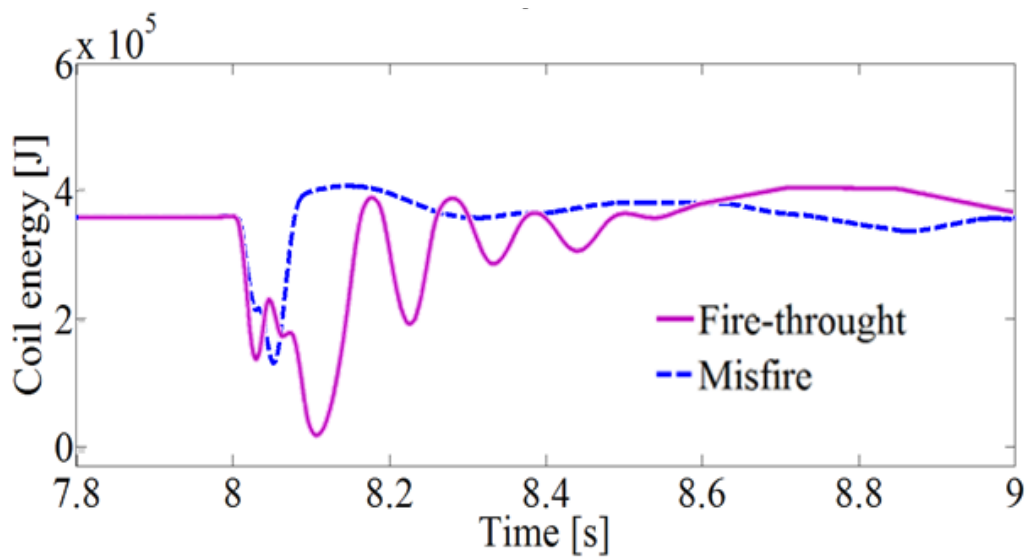
Figure 4.58 (c) Coil energy response during misfire in S6 within the RSC
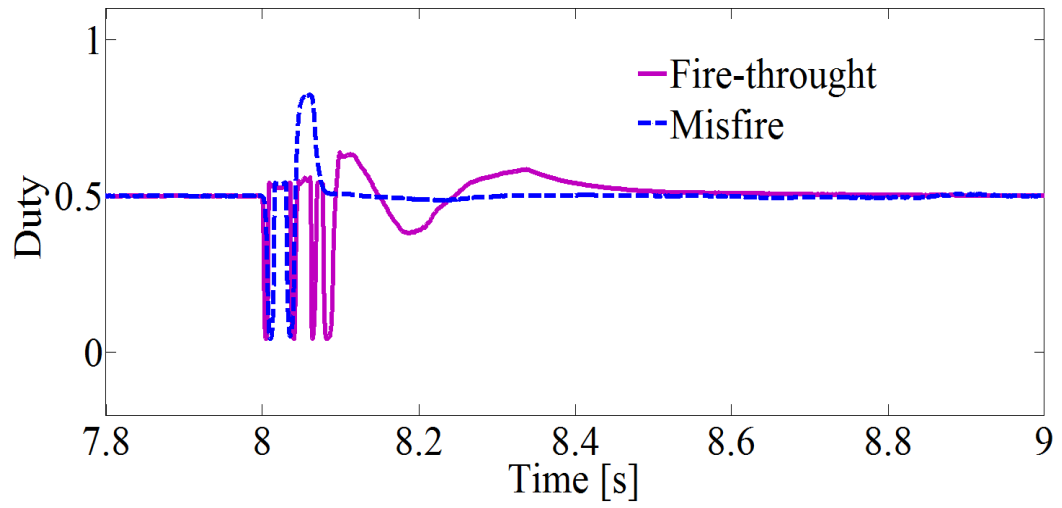
Figure 4.58 (d) Duty cycle during misfire in S6 within the RSC

Chapter Five

Conclusions and Further Work

5.1   Contribution and Significance of Research

This thesis presents a new converter station topology to improve the overall performance of a Doubly Fed Induction Generator-based wind energy conversion system during various disturbance events. The proposed topology relies on reconfiguring the two converters of the Doubly Fed Induction Generator (DFIG) to include a coil that will only be activated during fault conditions. The main idea of including the coil within the converters is to allow the new topology to provide the same (or close to the same) degree of performance as a superconducting magnetic energy storage unit. It will also modulate both active and reactive power during faults - smoothly, rapidly and independently - at the point of common coupling in a four-quadrant operation. The new topology also aims to improve the Fault Ride Through capability of the Doubly Fed Induction Generator enabling the connection of the wind turbine to the grid to meet Transmission Line Operator codes and hence, maintain its connection to the grid during various grid faults.

The contributions, significance and key conclusions of this thesis are highlighted below:

1- The new topology will improve the dynamic performance of a DFIG-based WECS because at the point of common coupling, active power - not just reactive power (as proposed in the literatures) - needs to be compensated.

2- With a proper control scheme to manage the stored energy within a low internal resistance coil (integrated within the DC link of the two converter stations of a DFIG-based WECS), the converter station and coil can provide the same degree of performance during fault conditions as the very costly super conducting magnetic energy storage unit. Both active and reactive powers at the point of common coupling can also be modulated.

3- Simulation results show the coil has no influence on the performance of the DFIG-based WECS during normal operation, and it will only be activated during fault conditions.

4- The robustness of the proposed topology is assessed through extensive simulation analyses on the studied system using SIMULINK/MATLAB software. Externally investigated faults include line to line to ground fault, three phases to ground fault and voltage sag at the grid side. This study also investigates the performance of the studied system - with and without the proposed topology - during converter switch faults, such as fire through and misfire.

5- Simulation results show the new topology can respond quickly, according to the active and reactive power demands of the system, and power fluctuations can be more easily smoothed.

6- Compared with the Fault Ride Through capability of various grid codes (including Spain, Germany, and Denmark), the LVRT of the DFIG with the new topology is much improved. It brings the voltage to a safe level, and the wind turbine's connection to the grid is maintained.

7- A misfire within the converter switches does not have a significant impact on the overall performance of a DFIG-based WECS. However, a fire through fault will have a significant impact on the voltage at the converter terminals, as well as on the active and reactive powers at the point of common coupling.

8- The proposed topology (along with the fuzzy logic controller) has been found effective in improving the performance of the studied system during all investigated faults. The proposed topology is simple and easy to implement within the existing DFIG converters.

9- The effect of fire-through and misfire within the GSC and RSC of the DFIG-based WECS are also studied.

5.2   Future Work

Based on the results of this thesis, the following issues are recommended for future work:

- Re-configuration of the proposed coil controller to be also involved during normal operating conditions to assure best performance of the DFIG-based WECS.

- Optimum coil capacity and the possibility of using high temperature superconductors may require further study.

- The typical configuration of a DFIG includes a DC-DC chopper, which can be facilitated to interface the coil with the DC link. Here, the optimum connection type with the capacitor can be investigated.

REFERENCES

[1]   J. Houghton, *Global warming: the complete briefing*: Cambridge University Press, 2009.

[2]   R. Ayanzadeh, A. S. Z. Mousavi, and S. Setayeshi, "Fossil fuel consumption prediction using emotional learning in Amygdala," in *Electrical Engineering (ICEE), 2011 19th Iranian Conference on*, 2011, pp. 1-6.

[3]   R. R. Bhoyar and S. S. Bharatkar, "Renewable energy integration in to microgrid: Powering rural Maharashtra State of India," in *India Conference (INDICON), 2013 Annual IEEE*, 2013, pp. 1-6.

[4]   H. H. Chen, H.-Y. Kang, and A. H. Lee, "Strategic selection of suitable projects for hybrid solar-wind power generation systems," *Renewable and Sustainable Energy Reviews,* vol. 14, pp. 413-421, 2010.

[5]   M. R. Patel, *Wind and solar power systems: design, analysis, and operation*: CRC press, 2012.

[6]   B. Wu, Y. Lang, N. Zargari, and S. Kouro, *Power conversion and control of wind energy systems* vol. 77: John Wiley & Sons, 2011.

[7]   Q. Ronghai, L. Yingzhen, and W. Jin, "Review of Superconducting Generator Topologies for Direct-Drive Wind Turbines," *Applied Superconductivity, IEEE Transactions on,* vol. 23, pp. 5201108-5201108, 2013.

[8]   E. Hau and H. Von Renouard, *Wind turbines: fundamentals, technologies, application, economics*: Springer Science & Business Media, 2013.

[9]   J. M. Carrasco, L. G. Franquelo, J. T. Bialasiewicz, E. Galvan, R. C. P. Guisado, M. A. M. Prats*, et al.*, "Power-Electronic Systems for the Grid Integration of Renewable Energy Sources: A Survey," *Industrial Electronics, IEEE Transactions on,* vol. 53, pp. 1002-1016, 2006.

[10]   P. W. Carlin, A. S. Laxson, and E. Muljadi, "The history and state of the art of variable-speed wind turbine technology," *Wind Energy,* vol. 6, pp. 129-159, 2003.

[11]   J. Lopez, E. Gubia, E. Olea, J. Ruiz, and L. Marroyo, "Ride Through of Wind Turbines With Doubly Fed Induction Generator Under Symmetrical Voltage Dips," *Industrial Electronics, IEEE Transactions on,* vol. 56, pp. 4246-4254, 2009.

[12]   A. M. Shiddiq Yunus, A. Abu-Siada, and M. A. S. Masoum, "Application of SMES Unit to Improve DFIG Power Dispatch and Dynamic Performance During

Intermittent Misfire and Fire-Through Faults," *Applied Superconductivity, IEEE Transactions on,* vol. 23, pp. 5701712-5701712, 2013.

[13]   A. M. S. Yunus, M. A. S. Masoum, and A. Abu-Siada, "Application of SMES to Enhance the Dynamic Performance of DFIG During Voltage Sag and Swell," *Applied Superconductivity, IEEE Transactions on,* vol. 22, pp. 5702009-5702009, 2012.

[14]   G. Abad, J. Lopez, M. Rodríguez, L. Marroyo, and G. Iwanski, *Doubly fed induction machine: modeling and control for wind energy generation* vol. 85: John Wiley & Sons, 2011.

[15]   J. Morren and S. W. H. de Haan, "Short-Circuit Current of Wind Turbines With Doubly Fed Induction Generator," *Energy Conversion, IEEE Transactions on,* vol. 22, pp. 174-180, 2007.

[16]   G. Pannell, D. J. Atkinson, and B. Zahawi, "Minimum-Threshold Crowbar for a Fault-Ride-Through Grid-Code-Compliant DFIG Wind Turbine," *Energy Conversion, IEEE Transactions on,* vol. 25, pp. 750-759, 2010.

[17]   S. Seman, J. Niiranen, S. Kanerva, A. Arkkio, and J. Saitz, "Performance Study of a Doubly Fed Wind-Power Induction Generator Under Network Disturbances," *Energy Conversion, IEEE Transactions on,* vol. 21, pp. 883-890, 2006.

[18]   M. Tsili and S. Papathanassiou, "A review of grid code technical requirements for wind farms," *IET Renewable Power Generation,* vol. 3, pp. 308-332, 2009.

[19]   Alt, x, M. n, Go, x, O. ksu*, et al.*, "Overview of recent grid codes for wind power integration," in *Optimization of Electrical and Electronic Equipment (OPTIM), 2010 12th International Conference on*, 2010, pp. 1152-1160.

[20]   Z. Shao, T. King-Jet, C. San Shing, N. Trong Duy, and Y. Dai Lin, "Advanced Control of Series Voltage Compensation to Enhance Wind Turbine Ride Through," *Power Electronics, IEEE Transactions on,* vol. 27, pp. 763-772, 2012.

[21]   T. Masaud and P. K. Sen, "A comparative study of the implementation of STATCOM and SVC on DFIG-based wind farm connected to a power system," in *Power and Energy Society General Meeting, 2012 IEEE*, 2012, pp. 1-1.

[22]   W. Li and T. Dinh-Nhon, "Stability improvement of a DFIG-based offshore wind farm fed to a multi-machine power system using a static VAR compensator," in *Industry Applications Society Annual Meeting (IAS), 2012 IEEE*, 2012, pp. 1-7.

[23]   W. Li and T. Dinh-Nhon, "Stability Enhancement of DFIG-Based Offshore Wind Farm Fed to a Multi-Machine System Using a STATCOM," *Power Systems, IEEE Transactions on,* vol. 28, pp. 2882-2889, 2013.

[24] R. M. M. Pereira, C. M. M. Ferreira, and F. P. M. Barbosa, "Comparative study of STATCOM and SVC performance on Dynamic Voltage Collapse of an Electric Power System with Wind Generation," *Latin America Transactions, IEEE (Revista IEEE America Latina),* vol. 12, pp. 138-145, 2014.

[25] A. F. Abdou, H. R. Pota, A. Abu-Siada, and Y. M. Alharbi, "Application of STATCOM-HTS to improve DFIG performance and FRT during IGBT short circuit," in *Power Engineering Conference (AUPEC), 2014 Australasian Universities*, 2014, pp. 1-5.

[26] M. J. Ferdous, Y. Arafat, and M. A. Azam, "Flicker level mitigation of weak grid connected wind turbine with DFIG by injecting optimum reactive power using STATCOM," in *Informatics, Electronics & Vision (ICIEV), 2013 International Conference on*, 2013, pp. 1-5.

[27] M. J. Ghorbanian, F. Goodarzvand, A. Pourdaryaei, and W. N. L. Mahadi, "Mitigating voltage sag by implementing STATCOM on DFIG-based wind farms connected to a power system," in *Engineering Technology and Technopreneuship (ICE2T), 2014 4th International Conference on*, 2014, pp. 131-136.

[28] S. Y. Tamboli and H. T. Jadhav, "Comparison of various techniques for DFIG and STATCOM with HVDC transmission," in *Innovations in Information, Embedded and Communication Systems (ICIIECS), 2015 International Conference on*, 2015, pp. 1-3.

[29] A. O. Ibrahim, N. Thanh Hai, L. Dong-Choon, and K. Su-Chang, "A Fault Ride-Through Technique of DFIG Wind Turbine Systems Using Dynamic Voltage Restorers," *Energy Conversion, IEEE Transactions on,* vol. 26, pp. 871-882, 2011.

[30] C. Wessels, F. Gebhardt, and F. W. Fuchs, "Fault Ride-Through of a DFIG Wind Turbine Using a Dynamic Voltage Restorer During Symmetrical and Asymmetrical Grid Faults," *Power Electronics, IEEE Transactions on,* vol. 26, pp. 807-815, 2011.

[31] S. Alaraifi, A. Moawwad, M. S. El Moursi, and V. Khadkikar, "Voltage Booster Schemes for Fault Ride-Through Enhancement of Variable Speed Wind Turbines," *Sustainable Energy, IEEE Transactions on,* vol. 4, pp. 1071-1081, 2013.

[32] S. I. Gkavanoudis and C. S. Demoulias, "FRT capability of a DFIG in isolated grids with Dynamic Voltage Restorer and Energy Storage," in *Power Electronics for Distributed Generation Systems (PEDG), 2014 IEEE 5th International Symposium on*, 2014, pp. 1-8.

[33] E. El Hawatt, M. S. Hamad, K. H. Ahmed, and I. F. El Arabawy, "Low voltage ride-through capability enhancement of a DFIG wind turbine using a dynamic voltage

restorer with Adaptive Fuzzy PI controller," in *Renewable Energy Research and Applications (ICRERA), 2013 International Conference on*, 2013, pp. 1234-1239.

[34]   A. Abu-Siada and S. Islam, "Application of SMES Unit in Improving the Performance of an AC/DC Power System," *Sustainable Energy, IEEE Transactions on,* vol. 2, pp. 109-121, 2011.

[35]   S. Jing, T. Yuejin, X. Yajun, R. Li, and L. Jingdong, "SMES Based Excitation System for Doubly-Fed Induction Generator in Wind Power Application," *Applied Superconductivity, IEEE Transactions on,* vol. 21, pp. 1105-1108, 2011.

[36]   K. Seung-Tak, K. Byung-Kwan, B. Sun-Ho, and P. Jung-Wook, "Application of SMES and Grid Code Compliance to Wind/Photovoltaic Generation System," *Applied Superconductivity, IEEE Transactions on,* vol. 23, pp. 5000804-5000804, 2013.

[37]   S. Jing, T. Yuejin, Y. Kai, C. Lei, R. Li, L. Jingdong*, et al.*, "SMES Based Dynamic Voltage Restorer for Voltage Fluctuations Compensation," *Applied Superconductivity, IEEE Transactions on,* vol. 20, pp. 1360-1364, 2010.

[38]   I. Ngamroo and T. Karaipoom, "Improving Low-Voltage Ride-Through Performance and Alleviating Power Fluctuation of DFIG Wind Turbine in DC Microgrid by Optimal SMES With Fault Current Limiting Function," *Applied Superconductivity, IEEE Transactions on,* vol. 24, pp. 1-5, 2014.

[39]   G. W. E. Council, "Global wind statistics 2012," *Report. Brussels, Belgium: GWEC,* 2013.

[40]   G. Wind, "Report, Global Wind Energy Council (GWEC)," 2013.

[41]   Y. Lang, N. Zargari, and S. Kouro, *Power conversion and control of wind energy systems* vol. 74: John Wiley & Sons, 2011.

[42]   J. Machowski, J. Bialek, and J. Bumby, *Power system dynamics: stability and control*: John Wiley & Sons, 2011.

[43]   J. F. Manwell, J. G. McGowan, and A. L. Rogers, *Wind energy explained: theory, design and application*: John Wiley & Sons, 2010.

[44]   B. Fox, *Wind power integration: connection and system operational aspects* vol. 50: Iet, 2007.

[45]   M. R. Patel, *Wind and solar power systems: design, analysis, and operation*: CRC press, 2005.

[46]   G. Wenyong, X. Liye, and D. Shaotao, "Enhancing Low-Voltage Ride-Through Capability and Smoothing Output Power of DFIG With a Superconducting Fault-

Current Limiter–Magnetic Energy Storage System," *Energy Conversion, IEEE Transactions on,* vol. 27, pp. 277-295, 2012.

[47]   J. Schachner, *Power connections for offshore wind farms*: na, 2004.

[48]   H. Guo, K. Rudion, and Z. A. Styczynski, "Integration of large offshore wind farms into the power system," in *Science and Technology, 2011 EPU-CRIS International Conference on*, 2011, pp. 1-6.

[49]   O. Anaya-Lara, N. Jenkins, J. Ekanayake, P. Cartwright, and M. Hughes, *Wind energy generation: modelling and control*: John Wiley & Sons, 2011.

[50]   L. Xu and B. R. Andersen, "Grid connection of large offshore wind farms using HVDC," *Wind Energy,* vol. 9, pp. 371-382, 2006.

[51]   P. Bresesti, W. L. Kling, R. L. Hendriks, and R. Vailati, "HVDC Connection of Offshore Wind Farms to the Transmission System," *Energy Conversion, IEEE Transactions on,* vol. 22, pp. 37-43, 2007.

[52]   H. Guo, K. Rudion, C. Heyde, and Z. A. Styczynski, "Stability studies of offshore wind farms," in *Critical Infrastructure (CRIS), 2010 5th International Conference on*, 2010, pp. 1-7.

[53]   P. Kundur, J. Paserba, V. Ajjarapu, G. Andersson, A. Bose, C. Canizares*, et al.*, "Definition and classification of power system stability IEEE/CIGRE joint task force on stability terms and definitions," *Power Systems, IEEE Transactions on,* vol. 19, pp. 1387-1401, 2004.

[54]   S. Yuan-Zhang, L. Jin, L. Guo-jie, and L. Xiong, "A review on the integration of wind farms with variable speed wind turbine systems into power systems," in *Sustainable Power Generation and Supply, 2009. SUPERGEN '09. International Conference on*, 2009, pp. 1-6.

[55]   L. Yazhou, "Studies on wind farm integration into power system [J]," *Automation of Electric Power Systems,* vol. 8, p. 017, 2003.

[56]   A. F. Abdou, A. Abu-Siada, and H. R. Pota, "Application of STATCOM to improve the LVRT of DFIG during RSC fire-through fault," in *Universities Power Engineering Conference (AUPEC), 2012 22nd Australasian*, 2012, pp. 1-6.

[57]   M. Tsili and S. Papathanassiou, "A review of grid code technical requirements for wind farms," *Renewable Power Generation, IET,* vol. 3, pp. 308-332, 2009.

[58]   Alt, x, M. n, Go, O. ksu, R. Teodorescu*, et al.*, "Overview of recent grid codes for wind power integration," in *12th International Conference on Optimization of Electrical and Electronic Equipment (OPTIM), 2010* 2010, pp. 1152-1160.

[59]   K. Ahsanullah and J. Ravishankar, "Fault ride-through of doubly-fed induction generators," in *Power, Signals, Controls and Computation (EPSCICON), 2012 International Conference on*, 2012, pp. 1-6.

[60]   M. Y. Khamaira, A. Abu-Siada, and S. Islam, "DFIG-based WECS fault ride through complying with Australian grid codes," in *Power Engineering Conference (AUPEC), 2014 Australasian Universities*, Perth, Australia, 2014, pp. 1-5.

[61]   M. Mohseni and S. M. Islam, "Transient Control of DFIG-Based Wind Power Plants in Compliance With the Australian Grid Code," *Power Electronics, IEEE Transactions on,* vol. 27, pp. 2813-2824, 2012.

[62]   M. Mohseni, M. A. S. Masoum, and S. M. Islam, "Low voltage ride-through of DFIG wind turbines complying with Western-Power grid code in Australia," in *Power and Energy Society General Meeting, 2011 IEEE*, 2011, pp. 1-8.

[63]   C. Feltes, S. Engelhardt, J. Kretschmann, J. Fortmann, F. Koch, and I. Erlich, "High voltage ride-through of DFIG-based wind turbines," in *Power and Energy Society General Meeting - Conversion and Delivery of Electrical Energy in the 21st Century, 2008 IEEE*, 2008, pp. 1-8.

[64]   Q. Wei, "Dynamic modeling and control of doubly fed induction generators driven by wind turbines," in *Power Systems Conference and Exposition, 2009. PSCE '09. IEEE/PES*, 2009, pp. 1-8.

[65]   M. G. Simoes and F. A. Farret, *Alternative energy systems: design and analysis with induction generators* vol. 13: CRC press, 2011.

[66]   T. Ackermann, *Wind power in power systems* vol. 140: Wiley Online Library, 2005.

[67]   A. Tapia, G. Tapia, J. X. Ostolaza, and J. R. Saenz, "Modeling and control of a wind turbine driven doubly fed induction generator," *Energy Conversion, IEEE Transactions on,* vol. 18, pp. 194-204, 2003.

[68]   L. Yazhou, A. Mullane, G. Lightbody, and R. Yacamini, "Modeling of the wind turbine with a doubly fed induction generator for grid integration studies," *Energy Conversion, IEEE Transactions on,* vol. 21, pp. 257-264, 2006.

[69]   G. R. Slemon, "Modelling of induction machines for electric drives," *Industry Applications, IEEE Transactions on,* vol. 25, pp. 1126-1131, 1989.

[70]   J. G. Slootweg, H. Polinder, and W. L. Kling, "Dynamic modelling of a wind turbine with doubly fed induction generator," in *Power Engineering Society Summer Meeting, 2001*, 2001, pp. 644-649 vol.1.

[71]   L. M. Fernández, J. R. Saenz, and F. Jurado, "Dynamic models of wind farms with fixed speed wind turbines," *Renewable Energy,* vol. 31, pp. 1203-1230, 7// 2006.

[72]   V. Akhmatov, *Analysis of dynamic behaviour of electric power systems with large amount of wind power*: Electric Power Engineering, Ørsted-DTU, Technical University of Denmark, 2003.

[73]   D. Wei, H. Benteng, W. Huifang, Z. Baohui, and S. Jin, "The impact of wind farms on the small signal stability of power system," in *Advanced Power System Automation and Protection (APAP), 2011 International Conference on*, 2011, pp. 74-78.

[74]   Y. Guo, S. H. Hosseini, J. N. Jiang, C. Y. Tang, and R. G. Ramakumar, "Voltage/pitch control for maximisation and regulation of active/reactive powers in wind turbines with uncertainties," *Renewable Power Generation, IET,* vol. 6, pp. 99-109, 2012.

[75]   S. K. Salman and A. L. J. Teo, "Windmill Modeling Consideration and Factors Influencing the Stability of a Grid-Connected Wind Power Based Embedded Generator," *Power Engineering Review, IEEE,* vol. 22, pp. 61-61, 2002.

[76]   L. Ting, M. Barnes, and M. Ozakturk, "Doubly-fed induction generator wind turbine modelling for detailed electromagnetic system studies," *Renewable Power Generation, IET,* vol. 7, pp. 180-189, 2013.

[77]   O. Anaya-Lara, N. Jenkins, and J. Ekanayake, *Wind Energy Generation Systems : Modelling and Control*. Hoboken, NJ, USA: John Wiley & Sons, 2009.

[78]   M. Singh and S. Santoso, *Dynamic models for wind turbines and wind power plants*: National Renewable Energy Laboratory, 2011.

[79]   J. G. Slootweg, S. W. H. De Haan, H. Polinder, and W. L. Kling, "General Model for Representing Variable-Speed Wind Turbines in Power System Dynamics Simulations," *Power Engineering Review, IEEE,* vol. 22, pp. 56-56, 2002.

[80]   J. B. Ekanayake, L. Holdsworth, W. XueGuang, and N. Jenkins, "Dynamic modeling of doubly fed induction generator wind turbines," *Power Systems, IEEE Transactions on,* vol. 18, pp. 803-809, 2003.

[81]   E. Tremblay, S. Atayde, and A. Chandra, "Comparative Study of Control Strategies for the Doubly Fed Induction Generator in Wind Energy Conversion Systems: A DSP-Based Implementation Approach," *Sustainable Energy, IEEE Transactions on,* vol. 2, pp. 288-299, 2011.

[82] H. Jiabing, N. Heng, X. Hailiang, and H. Yikang, "Dynamic Modeling and Improved Control of DFIG Under Distorted Grid Voltage Conditions," *Energy Conversion, IEEE Transactions on,* vol. 26, pp. 163-175, 2011.

[83] M. Sleiman, B. Kedjar, A. Hamadi, K. Al-Haddad, and H. Y. Kanaan, "Modeling, control and simulation of DFIG for maximum power point tracking," in *Control Conference (ASCC), 2013 9th Asian*, 2013, pp. 1-6.

[84] R. Pena, J. C. Clare, and G. M. Asher, "Doubly fed induction generator using back-to-back PWM converters and its application to variable-speed wind-energy generation," *Electric Power Applications, IEE Proceedings -,* vol. 143, pp. 231-241, 1996.

[85] L. Shuhui and T. A. Haskew, "Analysis of Decoupled d-q Vector Control in DFIG Back-to-Back PWM Converter," in *Power Engineering Society General Meeting, 2007. IEEE*, 2007, pp. 1-7.

[86] A. F. A. Abdou, "Performance Improvement of Doubly Fed Induction Generator-based Wind Energy Conversion System during Various Internal Converter Faults," Doctor of Philosophy, School of Engineering and Information Technology, University of New South Wales, University of New South Wales, 2013.

[87] A. D. Hansen, N. A. Cutululis, H. Markou, P. E. Sørensen, and F. Iov, *Grid fault and design-basis for wind turbines-Final report*: Danmarks Tekniske Universitet, Risø Nationallaboratoriet for Bæredygtig Energi, 2010.

[88] M. K. Das, S. Chowdhury, S. P. Chowdhury, and C. T. Gaunt, "Control of a grid connected doubly-fed induction generators for wind energy conversion," in *Universities Power Engineering Conference (UPEC), 2009 Proceedings of the 44th International*, 2009, pp. 1-5.

[89] I. Erlich, J. Kretschmann, J. Fortmann, S. Mueller-Engelhardt, and H. Wrede, "Modeling of Wind Turbines Based on Doubly-Fed Induction Generators for Power System Stability Studies," *Power Systems, IEEE Transactions on,* vol. 22, pp. 909-919, 2007.

[90] T. Lei, M. Ozakturk, and M. Barnes, "Modelling and analysis of DFIG wind turbine system in PSCAD/EMTDC," in *Power Electronics, Machines and Drives (PEMD 2012), 6th IET International Conference on*, 2012, pp. 1-6.

[91] H. Jadhav and R. Roy, "A comprehensive review on the grid integration of doubly fed induction generator," *International Journal of Electrical Power & Energy Systems,* vol. 49, pp. 8-18, 2013.

[92]   P. Ling, B. Francois, and L. Yongdong, "Improved Crowbar Control Strategy of DFIG Based Wind Turbines for Grid Fault Ride-Through," in *Applied Power Electronics Conference and Exposition, 2009. APEC 2009. Twenty-Fourth Annual IEEE*, 2009, pp. 1932-1938.

[93]   L. Changling, H. Banakar, B. Shen, and O. Boon-Teck, "Strategies to Smooth Wind Power Fluctuations of Wind Turbine Generator," *Energy Conversion, IEEE Transactions on,* vol. 22, pp. 341-349, 2007.

[94]   Q. Wei, G. K. Venayagamoorthy, and R. G. Harley, "Real-Time Implementation of a STATCOM on a Wind Farm Equipped With Doubly Fed Induction Generators," *Industry Applications, IEEE Transactions on,* vol. 45, pp. 98-107, 2009.

[95]   T. M. Masaud and P. K. Sen, "Study of the implementation of STATCOM on DFIG-based wind farm connected to a power system," in *Innovative Smart Grid Technologies (ISGT), 2012 IEEE PES*, 2012, pp. 1-7.

[96]   S. Uong and I. Ngamroo, "Coordinated control of DFIG wind turbine and SVC for robust power system stabilization," in *Electrical Engineering/Electronics, Computer, Telecommunications and Information Technology (ECTI-CON), 2015 12th International Conference on*, 2015, pp. 1-6.

[97]   H. Zhou, H. Wei, X. Qiu, J. Xu, X. Wei, and S. Wang, "Improvement of Transient Voltage Stability of the Wind Farm Using SVC and TCSC," in *Power and Energy Engineering Conference (APPEEC), 2011 Asia-Pacific*, 2011, pp. 1-4.

[98]   A. F. Abdou, A. Abu-Siada, and H. R. Pota, "Application of SVC on stabilizing torsional oscillations and improving transient stability," in *Power and Energy Society General Meeting, 2012 IEEE*, 2012, pp. 1-5.

[99]   C. Wessels, F. Gebhardt, and F. W. Fuchs, "Dynamic voltage restorer to allow LVRT for a DFIG wind turbine," in *Industrial Electronics (ISIE), 2010 IEEE International Symposium on*, 2010, pp. 803-808.

[100]   W. Li and V. Quang-Son, "Power Flow Control and Stability Improvement of Connecting an Offshore Wind Farm to a One-Machine Infinite-Bus System Using a Static Synchronous Series Compensator," *Sustainable Energy, IEEE Transactions on,* vol. 4, pp. 358-369, 2013.

[101]   P. Bhatt, "Short term active power support from DFIG with coordinated control of SSSC and SMES in restructured power system," in *Power and Energy Engineering Conference (APPEEC), 2014 IEEE PES Asia-Pacific*, 2014, pp. 1-6.

[102] W. Li, L. Hao-Wen, and W. Cheng-Tai, "Stability Analysis of an Integrated Offshore Wind and Seashore Wave Farm Fed to a Power Grid Using a Unified Power Flow Controller," *Power Systems, IEEE Transactions on,* vol. 28, pp. 2211-2221, 2013.

[103] Y. M. Alharbi, A. M. S. Yunus, and A. Abu-Siada, "Application of UPFC to improve the LVRT capability of wind turbine generator," in *Universities Power Engineering Conference (AUPEC), 2012 22nd Australasian*, 2012, pp. 1-4.

[104] M. Ferdosian, H. Abdi, and A. Bazaei, "Improved dynamic performance of wind energy conversion system by UPFC," in *Industrial Technology (ICIT), 2013 IEEE International Conference on*, 2013, pp. 545-550.

[105] M. T. Hagh, A. Lafzi, and A. R. Milani, "Dynamic and stability improvement of a wind farm connected to grid using UPFC," in *Industrial Technology, 2008. ICIT 2008. IEEE International Conference on*, 2008, pp. 1-5.

[106] L. Piyasinghe, M. Zhixin, J. Khazaei, and F. Lingling, "Impedance Model-Based SSR Analysis for TCSC Compensated Type-3 Wind Energy Delivery Systems," *Sustainable Energy, IEEE Transactions on,* vol. 6, pp. 179-187, 2015.

[107] M. Y. Khamaira, A. Abu-Siada, S. Islam, and M. A. S. Masoum, "Application of SMES unit to improve the overall Performance of DFIG- based WECS " in *Power and Energy Society General Meeting, 2014 IEEE*, 2014, pp. 1-5.

[108] M. Y. Khamaira, A. M. Shiddiq Yunus, and A. Abu-Siada, "Improvement of DFIG-based WECS performance using SMES unit," in *Power Engineering Conference (AUPEC), 2013 Australasian Universities*, Hobart, TAS, Australia, 2013, pp. 1-5.

[109] A. K. Gaurav, "Comparison between conventional PID and fuzzy logic controller for liquid flow control: Performance evaluation of fuzzy logic and PID controller by using MATLAB/Simulink," *International Journal of Innovative Technology and Exploring Engineering (IJITEE) ISSN,* pp. 2278-3075, 2012.

[110] L. Reznik, *Fuzzy controllers handbook: how to design them, how they work*: Newnes, 1997.

[111] "IEEE Recommended Practice for Monitoring Electric Power Quality," *IEEE Std 1159-2009 (Revision of IEEE Std 1159-1995),* pp. c1-81, 2009.

[112] Y. Kumsuwan and Y. Sillapawicharn, "An application of improved synchronous reference frame-based voltage sag detection in voltage sag compensation system," in *Power Electronics and Applications (EPE), 2013 15th European Conference on*, 2013, pp. 1-8.

[113] M. Y. Khamaira, A. Abu-Siada, S. Islam, and M. A. S. Masoum, "Application of SMES unit to improve the overall performance of DFIG-based WECS," in *PES General Meeting | Conference & Exposition, 2014 IEEE*, Washington, 2014, pp. 1-5.

[114] J. Arrillaga, *High voltage direct current transmission*: Iet, 1998.

[115] K. Padiyar, *HVDC power transmission systems: technology and system interactions*: New Age International, 1990.

"Every reasonable effort has been made to acknowledge the owners of copyright material. I would be pleased to hear from any copyright owner who has been omitted or incorrectly acknowledged"

APPENDICES

Appendix A

Table A-1 Drive train parameters of the simulated DFIG

Drive Train Parameters	Value
Wind Turbine Inertia Constant, H (s)	4.32
Shaft Spring Constant (p.u. of Mechanical Torque/Rad)	80.27
Shaft Mutual Damping(p.u. of Mechanical Torque/pu dw)	1.5
Turbine Initial Speed (p.u.)	1.2
Initial Output Torque (p.u.)	0.8

Table A-2 Converter parameters of the simulated DFIG

Converters Parameters	Value
Grid-side converter maximum current (pu of generator nominal current)	0.8
Grid Side Coupling Inductor, (L,R) (p.u.)	[0.3 0.003]
Nominal DC bus Voltage (V)	1150
DC Bus Capacitor (F)	10000e-6
Line Filter Capacitor, (Q=50) (VAr)	120e3

Table A-3 Generator parameters of the simulated DFIG

Generator Parameters	Value
Mutual Inductance, L_m (p.u.)	2.9
Stator Leakage Inductance, $L_{\sigma s}$ (p.u.)	0.18
Rotor Leakage Inductance, $L_{\sigma r}$ (p.u.)	0.16
Stator Resistance, R_s (p.u.)	0.023
Rotor Resistance, R_r (p.u.)	0.016
Inertia constant (s)	0.685
Friction factor	0.01
Number of pair poles, p	3

Table A-4 Parameters of the DFIG

Parameters	Value
Rated Power	9 MW (6 x1.5) MW)
Stator Voltage	575 V
Frequency	60 Hz
R_S	0.023 pu
R_R	0.016 pu
V_{DC}	1150 V

Table A-5 Parameters of the transmission line

Parameters	Value
R_1, R_0 (Ω/km)	0.1153, 0.413
L_1, L_0 (H/km)	1.05×10^{-3}, 3.32×10^{-3}
C_1, C_0 (F/km)	11.33×10^{-9}, 5.01×10^{-9}

Table A-6 Parameters of the proposed coil

Parameters	Value
L_{coil}	0.2 H
I_{coil}	2000 A

Appendix B

Table B-1 Parameters of PI controller

K_p	0.5
K_i	1